APATITE BASED MICROCARRIERS FOR BONE TISSUE ENGINEERING APPLICATIONS

FENG YONG YAO, JASON

NATIONAL UNIVERSITY OF SINGAPORE

2015

APATITE BASED MICROCARRIERS FOR BONE TISSUE ENGINEERING APPLICATIONS

FENG YONG YAO, JASON

B.Eng.(Hons), National University of Singapore

A THESIS SUBMITTED FOR THE DEGREE OF MASTER OF ENGINEERING

DEPARTMENT OF MECHANICAL ENGINEERING
NATIONAL UNIVERSITY OF SINGAPORE

2015

Declaration

I hereby declare that this thesis is my original work and it has been written by me in its entirety. I have duly acknowledged all the sources of information, which have been used in the thesis.

This thesis has also not been submitted for any degree in any university previously.

FENG YONG YAO, JASON

5 JANUARY, 2015

Abstract

The use of bioceramics, either alone or with other biomaterials has grown in its various biomedical applications over the past 40 years. In the fields of orthopaedics and dental surgery bioceramics have been extensively used as biomaterials in prosthetic implants as well as bone graft substitutes. Recently, the role of bioceramics has been featured in the field of regenerative medicine, specifically in the niche of bone tissue engineering. Within this domain, apatite based biomaterials can serve as substrates and scaffolds for bone regeneration. One of the strategies proposed is the incorporation of *in-vitro* cultured cells which are seeded on the scaffolds to create a more functional tissue. However, the conventional method of culturing sufficient cells on the scaffold can be inefficient and impractical. Use of microcarriers can overcome these issues, but their applicability in bone tissue engineering has not been considered.

The purpose of this report is to describe and evaluate the development of a novel apatite based microcarrier. These microcarriers had been fabricated using a unique drip casting method. In this method, 0.03 g/ml alginate solutioni was mixed with 40 wt.% apatite, and the resultant solution was extruded drop-wise through a drop-on-demand device into a 0.5M caclcium chloride cross-linking solution. The apatite-alginate beads were then washed, dried and subjected to a multi-stage sintering profile to 1150°C, to obtain the apatite microcarriers. These microcarriers featured a substantially spherical macromorphology of 200 – 300 μm, with a rough surface morphology and open porous structure. Chemical characterisation confirmed a phase-pure

apatite composition without impurities. An *in-vitro* biological study was also conducted to evaluate the microcarriers' cytocompatibility as well as osteogenic potency. Results demonstrated that the microcarriers were a highly viable platform for *in-vitro* cell expansion, in which proliferation and viability were significantly higher when compared with Cytodex® 3. Expressions of alkaline phosphatase (ALP), type I collagen (COL1) and osteocalcin (OC) were significantly higher over monolayer tissue culture plate controls. A preliminary *in-vivo* study was also conducted on a mouse model to assess ectopic bone formation. Over a two-month period, immature bone formation was observed, with indications of active bone remodelling.

In conclusion, these findings would suggest that the apatite microcarriers possessed excellent biocompatibility for bone implant applications, and when seeded with stem cells, produced osteo-regenerative properties. Ultimately, this report aims to evaluate the apatite microcarriers as a viable biomaterial for bone tissue engineering, intended as a single-step cell expansion and *in-situ* osteogenic differentiation platform to be implemented as a non-invasive, injectable bone graft substitute for the repair and regeneration of bone defects.

Acknowledgements

I would like to express my sincere appreciation to A/Prof Dr Thian Eng San, Dr. Jerry Chan, and Dr. Wilson Wang for their invaluable guidance, support, advice and assistance to this project.

I would like to thank Dr. Mark Chong and Dr. Zhang Zhiyong for their supervision and assistance throughout the whole project and answering of all the queries.

I would like to also thank Dr. Lim Poon Nian for her assistance in carrying out the synthesis and characterisation successfully and other various assistance given.

Lastly, I would like to thank everyone that has helped me out in any other ways throughout the whole study.

Publications, Conferences and Awards

Journals:

1) Feng J, Chong M, Chan J, Zhang ZY, Teoh SH, Thian ES. A scalable approach to obtain mesenchymal stem cells with osteogenic potency on apatite microcarriers. Journal of Biomaterials Applications. 2013, 29:93-103
2) Feng J, Thian ES. Applications of nanobioceramics to healthcare technology. Nanotechnology Reviews. 2013, 2:679-97.

Conferences Proceedings:

1) Feng J, Chong M, Chan J, Zhang ZY, Teoh SH, Thian ES. Fabrication, Characterization and *In-Vitro* Evaluation of Apatite-Based Microbeads. Ceramic Transactions 247. 2014
2) Feng J, Chong M, Chan J, Zhang ZY, Teoh SH, Thian ES. Apatite-based microcarriers for bone tissue engineering. Key Engineering Materials 529-530. 2013

Conferences (Oral):

1) Feng J, Chong M, Chan J, Zhang ZY, Teoh SH, Thian ES. Cell-loaded ceramic based microbeads for direct bone implant science. 10th Pacific Rim Conference on Ceramic and Glass Technology, San Diego, USA, 2nd June 2013 – 7th June 2013
2) Thian ES, Feng J, Chong M, Chan J, Zhang ZY, Teoh SH. Apatite-based microcarriers for bone tissue engineering. 24th International Symposium on Ceramics in Medicine, Fukuoka, Japan, 21st October – 24th October 2012

Conferences (Poster):

1) Thian ES, Feng J, Chong M, Chan J, Zhang ZY, Teoh SH. Apatite microbeads as a means for stem cell expansion, 3rd Tissue Engineering and Regenerative Medicine World Congress, Vienna, Austria, 5th September – 8th September 2012
2) Feng J, Chong M, Chan J, Zhang ZY, Teoh SH, Thian ES. Apatite microcarriers as a potential bone tissue engineering solution. 1st International Conference of Young Researchers on Advanced Materials, Singapore, 1st July – 6th July 2012

Awards

1) Best Poster Presenter Award (First Runner-Up) at the 1st International Conference of Young Researchers on Advanced Materials, Singapore, 1st July – 6th July 2012

Table of Contents

Lists of Figures

Lists of Tables

Lists of Symbols

ACP	Amorphous calcium phosphate
Alg	Alginate
ALP	Alkaline phosphatase
ANOVA	Analysis of variance
BCP	Biphasic calcium phosphates
ANOVA	Analysis of variance
Ca	Calcium
COL 1	Type I Collagen
DI	Deionised
DMEM	Dulbecco's modified Eagle medium
D10	Dulbecco's modified Eagle medium supplemented-GlutaMAX with 10 % foetal bovine serum and 1 % penicillin-streptomycin
EDS	Energy dispersive x-ray spectroscopy
ECM	Extracellular matrix

FDA	Fluorescein diacetate
FESEM	Field emission scanning electron microscope
FTIR	Fourier transform infrared spectroscope
HA	Hydroxyapatite
hfMSC	Human foetal mesenchymal stem cell
OC	Osteocalcin
OP	Osteopontin
ON	Osteonectin
PBS	Phosphate buffered saline
PI	Propidium iodide
TCP	Tricalcium phosphate
TEM	Transmission electron microscope
XPS	X-ray photoelectron spectroscopy
XRD	X-ray diffraction

CHAPTER 1

Introduction

1.1 Background

Bone is the a load bearing structure of all vertebrates. It is a composite material comprising of mineral and organic phases organised in a complex hierarchical structure, starting from the nanoscale up, and functions to serve vital mechanical, anabolic and metabolic roles. Bone defects, injuries and degeneration can occur either through trauma or disease, or a combination of both. These conditions are frequently encountered in clinical practice and while conventional methods exist to treat these conditions, complete bone regeneration cannot be consistently assured, which can lead to complications such as bone non-union and development of post-traumatic osteoarthritis. Moreover, bone-related injuries and diseases may be chronic in nature, which can certainly cause a considerable strain on healthcare resources due to the long-term care required for treatment and rehabilitation. Furthermore, as the population in Singapore (or even worldwide) continues to age, the prevalence of osteoporosis among the elderly would make them more susceptible to bone fractures.

Currently, the use of bone grafts, obtained from either autogenic or allogeneic sources is the preferred strategy for healing of bone defects. Bone grafting remains a major need in the global world, which can amount to a demand of more than $2.5 billion a year[1]. In the United States alone, approximately half of the 3 million musculoskeletal procedures performed annually require

bone grafting with either an autograft or allograft[2]. Around the world, bone grafting involving autografts and allografts account for nearly 2.2 million orthopaedic procedures performed annually[3]. While the use of autografts is considered as the gold standard for bone defect repairs, this is severely limited by donor-site morbidity and availability[1, 4, 5]. In the case of allogeneic grafts, challenges imposed include host compatibility, as well as risks of disease transmission[5]. As a result, research and development of viable, biocompatible, effective and efficacious bone graft substitutes continue to be an area of intense interest.

Several synthetic scaffolds and bone filler biomaterials have been developed to serve as substitutes for bone grafts, but these products vary in success. Bone graft substitutes featuring macrometer-sized scaffolds such as polycaprolactone (PCL) or collagen-based materials are currently available, but these scaffolds may not possess the appropriate mechanical properties of high compressive moduli and high fracture toughness. While the surfaces of these materials can be functionalised with various biomolecules, incorporating the correct microstructural properties (pore size, porosity, roughness, hydrophobicity, etc.) remain highly complex and can be expensive and time-consuming. Furthermore, these scaffolds may not conform well to the defect site and offer limited flexibility in surgical manipulation, which poses a problem in irregularly shaped defects. Bone filler materials that feature ceramic granules such as coralline hydroxyapatite, calcium phosphate or bioglass have been developed to serve as a less invasive flexible solution for filling bone defects. Nevertheless, synthetic bone filler materials currently

available lack deliberate design of morphology and surface characteristics, which fully replicates the microenvironment of the natural bone. These solutions remain inferior to their autogenic counterparts and do not sufficiently improve healing rates and ensure long-term success.

It would be ideal if bone fractures can be repaired and healed, where functionality of the bone tissues can be restored in a safe, consistent and rapid manner by an off-the-shelf product that is cost-effective and easily implemented by the orthopaedic surgeon. The concept of using stem cells accomplishes this need, regenerating damaged bone tissues, while stimulating the body's own repair mechanisms to assist with the healing process. Stem cells have garnered much attention in this regard since they have the ability to differentiate while maintaining self-renewal. There are already extensive clinical trials being conducted to proof its use, and the potential is highly promising. However, one major obstacle in translating this technology from bench to bedside is the sheer number of hfMSCs required for successful transplantation. A dose of 3 - 5 x 10^7 cells/patient is needed to treat patients with advanced multiple sclerosis [6]whilst 5.7 - 7.5 x 10^8 cells/kg is required for the treatment of osteogenesis imperfecta [7]. The conventional technique to achieve such cell numbers involves the expansion of cells on monolayer tissue culture flasks. Given that a standard T175 flask is able to yield only 3.5 - 5 x 10^6 MSCs at confluence, considerable resources have to be spent on cell medium, flasks and incubators, making such a method neither efficient nor economically feasible. Furthermore, these cells have to undergo repeated passaging which is considered to be labour intensive and time consuming, but

more importantly, diminishes the capacity for MSCs to retain their stemness. The repeated destruction of extra-cellular matrix (ECM) through multiple trypsinisation is also likely to decrease intra-cellular signalling responsible for cell viability, proliferation and differentiation[8]. To overcome this, the use of microbeads has been proposed. This involves the use of micrometre-sized spherical particles where cells are seeded upon, and allowed to proliferate under gentle dynamic flow conditions. Microbeads have been developed for such applications and cell yield up to 10^8 cells/ml can be achieved [9]. However, these microbeads are either polymer or glass based materials, making them unsuitable as long-term bone graft substitutes.

1.2 Objectives

In order to overcome the above mentioned challenges, development of a tissue engineered bone graft substitute, which aims to deliver a single-step, non-invasive, injectable strategy, which incorporates the properties of osteoinduction, osteoconduction and enhances osteogenicity is proposed. This can be accomplished through the use of phase-pure porous apatite microcarriers, which possess the appropriate physicochemical and microstructural properties that enable for in-situ proliferation, differentiation and *in-vivo* phenotypic maintenance of MSCs.

The specific objectives can be summarised as such:

- Develop suitable novel apatite-based porous microcarriers as cell carriers.

- Establish the apatite-based porous microcarriers as an efficient tool for obtaining high yield mesenchymal stem cells (MSCs) isolation and expansion *in-vitro*.
- Establish the apatite-based porous microcarriers as an efficient platform for driving directed differentiation of MSCs into osteogenesis *in-vitro.*
- Evaluate the efficacy of the MSC-loaded apatite-based porous microcarriers to generate ectopic bone formation *in-vivo.*

1.3 Scope

Chapter 1 establishes the background and motivation of this dissertation, which demonstrates the need for bone tissue engineering, and the development of novel biomaterials. It is proposed that the use of phase-pure porous apatite microcarriers will be a superior alternative over conventional monolayer culture techniques. This is hypothesised to enhance bone regeneration when used as a bone graft substitute. Chapter 2 summarises the relevant literature regarding bone, bone tissue engineering and bioceramics, in which key design considerations are highlighted in the development of a bone tissue engineered biomaterial. Chapter 3 presents a detailed study on the fabrication of the apatite microcarriers, which includes the characterisation of its physicochemical properties, as well as optimisation of the various parameters for the fabrication of an apatite microcarrier that is relevant for its intended application. Chapter 4 details the evaluation of the apatite microcarriers *in-vitro*, to assess its cytocompatibility and effects on the osteogenic potency on mesenchymal stem cells, so as it establish its efficacy as a microcarrier for *in-*

vitro cell culture. Chapter 5 further evaluates the apatite microcarriers as implantable bone graft substitutes, through an *in-vivo* study on ectopic bone formation in a mouse model. Properties of biocompatibility, osteogenicity and neo-vascularisation are investigated. Chapter 6 gives an overall conclusion of the present work. Chapter 7 provides an outlook of the possible future work and development of the apatite microcarriers so as to increase its relevance towards various dental and orthopaedic applications, and gain clinical acceptance.

CHAPTER 2
Literature Review

2.1 Bone biology

In order to develop engineering considerations for the bone tissue engineered construct, it is necessary to understand the biology of bone. The bone is the major load-bearing organ of all vertebrates. In addition to providing mechanical stability, it is vital in the process of haematopoiesis, and functioning as the main repository for adult mesenchymal stem cells as well as hematopoietic stem cells. Furthermore, it plays several metabolic functions including mineral storage, growth factor storage, and maintaining acid-base balance. Bone has also been implicated as fulfilling the endocrine role of maintaining glucose and phosphate homeostasis by producing hormones such as FGF23 and osteocalcin which influence phosphate disposal and glucose utilisation respectively[10].

2.1.1 Physicochemical characteristics of bone

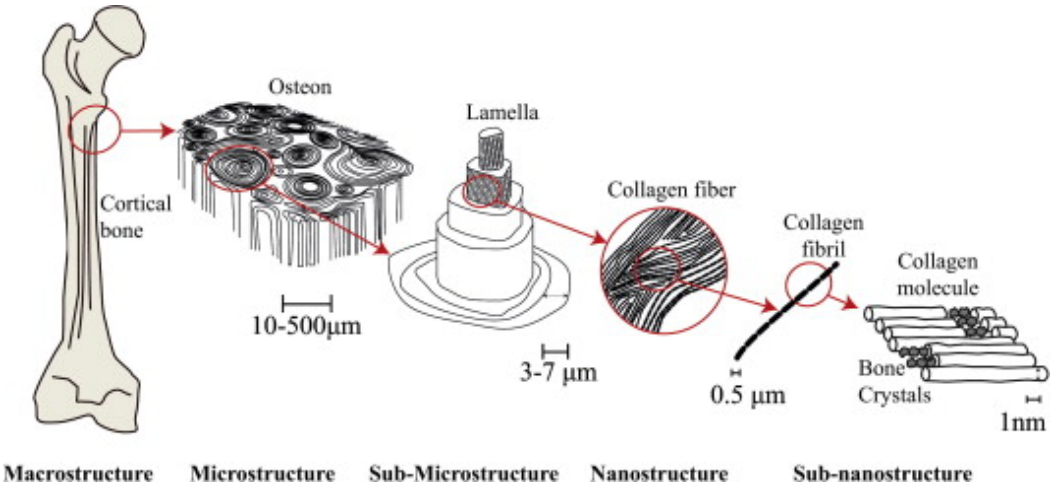

Figure 2.1. Hierarchical nature of bone*[11]*.

Chemically, bone is composed of an organic phase consisting of mainly collagen (35% dry weight) and a mineral phase of carbonated apatite (65% dry weight). These phases are organised in a highly hierarchical structure (Figure 2.1). At the macroscale level, bone can be described an organ consisting of two kinds of osseous tissue: cortical bone and trabecular bone. Cortical bone covers the outer surface of the bone and is a dense and compact tissue, which sustains major loading forces. It is thickest at the middle of the shaft and becomes thinner at both ends of the bone. At the proximal and distal ends of the bone, where cortical bone is the thinnest, bone transitions into a less dense and more porous structure, or trabecular bone. This is to facilitate load transfer during articulation[12]. Trabecular bone has an average density of 0.2 g/cm3 and porosity as high as 90%, with 1 mm spacing between the trabecular columns. In comparison, cortical bone is much denser at 1.80 g/cm3, with a porosity of 3-12% with no visible macropores. Microscopically, both cortical and trabecular bone are made up of Haversian systems (osteons) which are layers of compact bone stacked in concentric layers around a Haversian canal which contains the bone's blood vessels and nerves. These concentric layers, or lamellae, have a nanoarchitechture consisting of bundles of collagen fibres interspaced with apatite crystals[11]. These lamellae are stacked in an alternating fibre orientation at 45° to the vertical axis. Collectively, the nano-, micro-, and macro-scale architecture of bone is responsible for its unique rigidity, viscoelasticity and toughness. In addition to contributing to its mechanical properties, the microstructure of bone forms a unique microenvironment for the bone cells. The four main mature cells that

contribute to synthesis and remodelling of the bone matrix are osteoblasts, osteoclasts, osteocytes and periosteal cells. Stem cells such as mesenchymal stem cells and hematopoietic stem cells are found in the bone marrow situated within the central intramedullary cavity of the bone shaft and between the trabecular spaces. These cells are responsible for the dynamic nature of the bone; constantly remodelling itself in response to external loading conditions, a feature which has to be taken into account when designing a tissue engineered construct and will be covered in Section 2.2.2. From an engineering viewpoint, the bone can be regarded as a polymer-ceramic composite in which the lamellar polymer fibre structure is interspaced with a ceramic. Each parameter such as bone composition (porosity, mineralisation) as well as structural organisation (nano, microarchitecture, fibre orientation) has profound effects on the overall mechanical property of the bone.

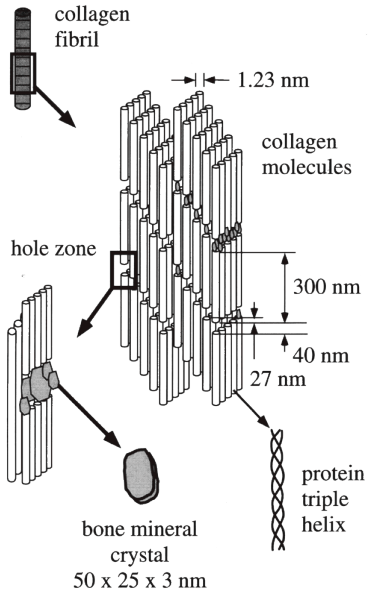

Figure 2.2. A schematic diagram illustrating the assembly of collagen fibrils and fibres and bone mineral crystals. The well known 67 nm periodic pattern results from the presence of adjacent hole (40 nm) and overlap (27 nm) regions of the assembled molecules*[11]*.

Type I collagen, which is the most abundant form of collagen in the bone, is a fibrillar heterotrimer collagen consisting of two identical polypeptide α1 chains and one α2 chain arranged in a right-handed triple-helical structure, stabilised by covalent crosslinks. Each collagen molecule is 300 nm in length and approximately 1 nm thick (Figure 2.2), and several molecules of collagen are stacked to form fibrils of 50 – 500 nm thick. The fibrils then stack together again to form bundles, which constitute to the collagen fibre of 3 – 7 μm thick. Collagen has an elastic modulus of 1 – 2 GPa and ultimate tensile strength of 50 – 1,000 MPa. This contrasts with hydroxyapatite, which exists as nano crystals within the fibrillar structure of collagen. It has an elastic modulus of approximately 130 GPa, and an ultimate tensile strength of 100 MPa. The combination of these two materials with dissimilar properties in a composite structure allows for bone to have a wide range of mechanical properties that is tuned specifically to the intended function, and responds preferentially to the type of loading applied, and is able to withstand high impact forces (Table 2.1).

Table 2.1 Mechanical properties of cortical bone and trabecular bone[13].

Property	**Cortical bone**	**Trabecular bone**
Compressive strength (MPa)	100 – 230	2 – 12
Tensile strength (MPa)	50 – 150	10 – 20
Strain to failure (%)	1 – 3	5 – 7
Fracture toughness (MPa)	2 – 12	-
Elastic modulus (GPa)	7 – 30	0.5 – 0.05

Due to the hierarchical nature of bone, it is therefore necessary to highlight the differences in mechanical properties across the different levels of organisation

(Table 2.2). From this it is evident that changes to the microstructure of bone will result in differing macrostructural properties although the composition of bone may be the same.

Table 2.2. Elastic modulus of bone according to different levels of organisation[14].

Level of organisation	Elastic modulus (MPa)
Macrostructural	14 – 20
Microstructural	5.4
Submicrostructural	22

2.1.2 Fracture healing mechanism

Understanding the pathophysiological process of bone healing would enable considerations to be made for the *in-vivo* response of the bone tissue engineered construct. For biocompatibility of the biomaterial to be ensured, a systematic approach to design the engineered construct is required such that the biomaterial enables a seamless integration throughout the healing process; from the initial inflammatory response, to repair and remodelling phases, such that the engineered construct achieves it intended effect by ensuring appropriate host-tissue response, while avoiding undesirable consequences such as fibrotic encapsulation, osteolysis or systemic inflammation.

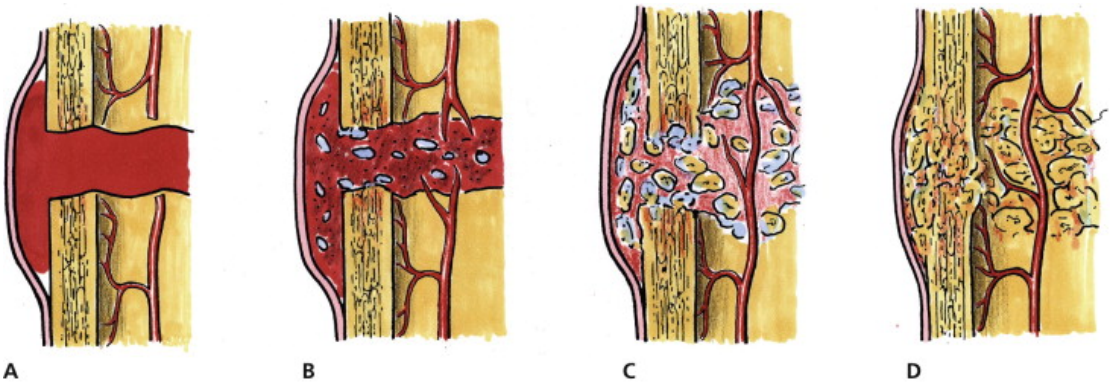

Figure 2.3. The fracture healing process. The fracture hematoma (A) is transformed into granulation tissue first, followed by migration and differentiation of MSCs and fibroblasts into osteoblasts and chondrocytes respectively (B). Mineralisation of the callus occurs, forming woven bone (C). Restoration of the cylindrical shape occurs through remodelling of the bony callus to lamellar bone (D)*[15]*

Bone healing is governed by the biomechanics of the fracture site as well as availability of blood to the healing site. Healing is characterised by three phases: inflammatory, repair and remodelling (Figure 2.3). In each phase, an orchestrated sequence of events overlaps one another (Figure 2.4). Thus, facilitation and enhancement of these events will lead to faster recovery times, as well as decreased incidence in non-union.

Following injury and/or trauma, the rupture of blood vessels causes blood to fill the area, and damage to tissues and cells results in a release of proinflammatory factors, which initiate the inflammatory cascade. Within the facture gap, fibrinogen from blood plasma is converted to fibrin, which results in an insoluble mass of blood clot known as hematoma which contains the damaged tissue, inflammatory cells, as well as proinflammatory and anti-inflammatory cytokines, which serve the signal the recruitment of more inflammatory cells. Neutrophils, mainly polymorphonuclear neutrophils (PMNs) are the first cells to reach the site and these short-lived cells serve to recruit macrophages, which act to clear the injury site of debris and any foreign bodies. Presence of PMNs impede the progression of the healing phases into the bone repair phase. Persistence of PMNs can be an indication of delayed fracture healing. As such, biomaterials that modulate the response of PMNs and which prevent overactivity of PMNs can be beneficial towards

enhanced bone healing rates. Macrophages, on the other hand, have been identified as essential towards MSC recruitment and osteogenesis. Lymphocyte migration to the healing site occurs towards the end of the inflammatory phase, and they function to regulate the immune response at the site. The proinflammatory cytokines, IL-1, IL-6, TNF, RANK ligand, as well as the TGF-β superfamily that includes BMP-2, BMP-4, BMP-5 and BMP-6, are released during the initial inflammatory phase and are identified to be key osteoinductive factors, essential towards the subsequent phase of bone repair through the signalling MSC migration, proliferation and differentiation. In addition, growth factors such as angiopoetin-1 (ANG-1) and vascular endothelial growth factor (VEGF) released in response to the hypoxic conditions created by the hematoma function to stimulate blood vessel formation through angiogenesis by signalling the endothelial cells from the surrounding intact periosteal vessels to grow in the direction of the hematoma. Revascularisation of the healing site following fracture has been established as an essential step in healing; functioning to bring essential nutrients and cells to the healing site, while removing debris and waste.

The repair phase is characterised by the recruitment of MSCs to the healing site, differentiation into osteoblasts, production and mineralisation of extracellular matrix (ECM). Depending on the biomechanics of the healing site, repair proceeds via two mechanisms: intramembranous ossification and endochondral ossification. Where there is little perturbation to the healing site, the predominant mechanism is intramembranous ossification. If the fracture surfaces are in contact with one another and in compression, Haversian

systems develop across the gaps and mature bone is laid over these systems via the formation of a basic multicellular units (BMUs) consisting of both osteoclasts and osteoblasts which function to resorb bone and form bone respectively[16]. Where a gap between the fractures is present, woven (immature) bone is first laid down and vascularised from the periosteum and medulla, before being bridged by osteon formation. This process is a relatively long one, where complete repair can take up to 3 years[17]. Endochondral ossification is the main mechanism in healing sites where stability is low and interframentary movement is high. In this process, high movement of the hematoma stimulates the development of a granulation tissue consisting of leukocytes, macrophages, and fibroblasts. A fibrous soft fibrous callus formation grows in the direction of the fracture gap. This is driven by chondrocytes derived from fibroblasts which are exposed to the hypoxic environment in the hematoma[18]. Once the fracture gap is filled with soft callus, calcification of the callus occurs as the chondrocytes become hypertrophic and undergo apoptosis. At this stage, interfragmentary movement is markedly decreased, which paves the way for blood vessel invasion and migration of MSCs and monocytes to the callus. The monocytes form multi-nuclear units similar to osteoclasts, which resorb the cartilage, while MSCs undergo osteogenesis to differentiate into osteoblasts, which replace the resorbed cartilage with woven bone. The subsequent bony bridging further increases stability to the healing site, which in turn promotes intramembranous ossification, which supplements the repair phase. Complete mineralisation of

the soft callus marks the end of the repair phase. At the same time as repair activity diminishes, the remodelling phase is initiated (Figure 2.4).

This is the phase whereby resorption of the periosteal callus occurs by osteoclast activity at the surface of the bone. At the same time, woven bone is converted gradually to lamellar bone such that it is laid in the direction of applied stress. Bone remodelling proceeds in five distinct phases:

1. Resting state: The surface of the bone is lined with inactive cells. Former osteoblasts are trapped as osteocytes within the mineralized matrix.

2. Activation: Hormonal or physical stimuli signal mononuclear monocytes and macrophages to migrate to the remodelling site and differentiate into osteoclasts. Sites with microfractures or microdamage may exhibit a certain predisposition for remodelling.

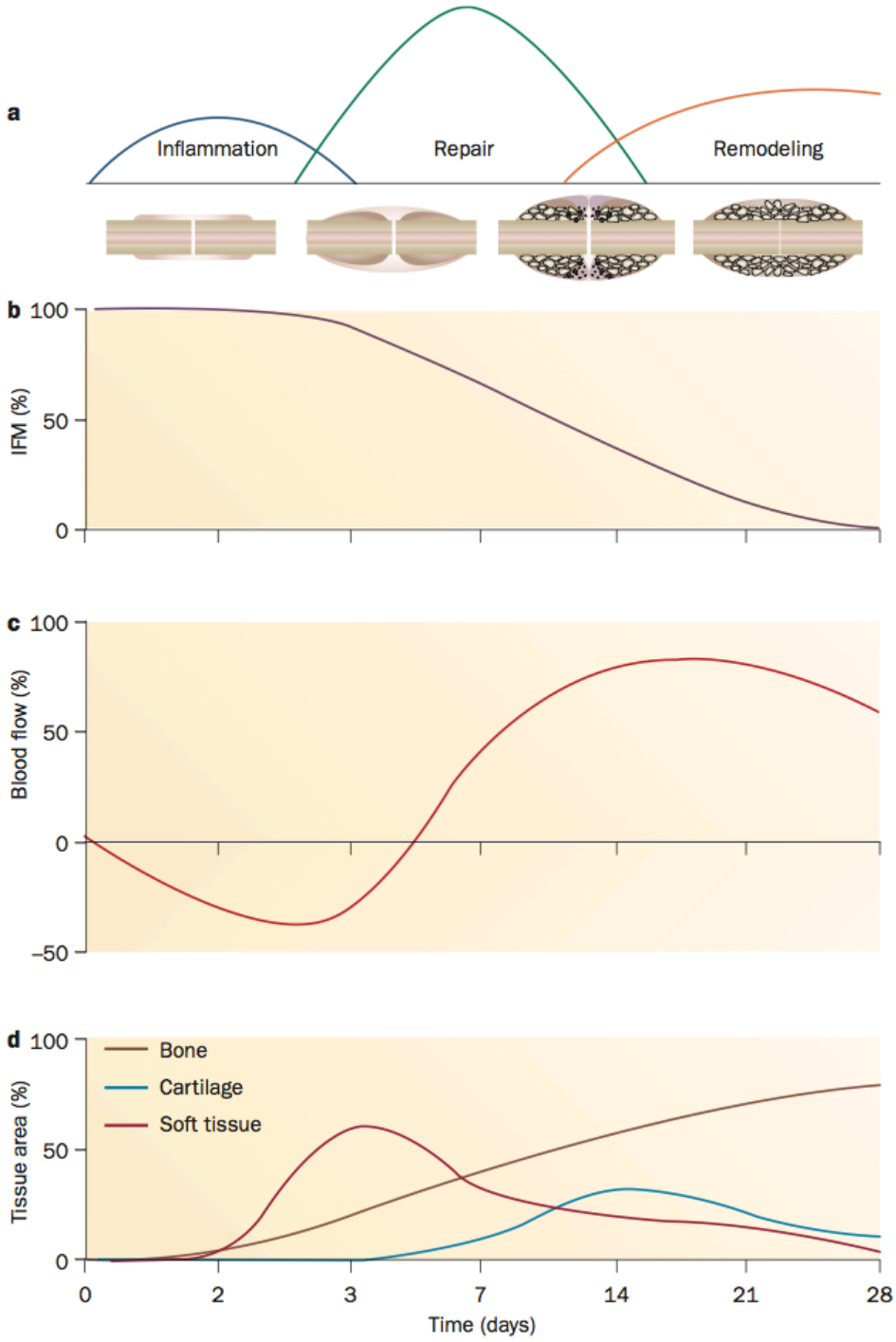

Figure 2.4. Sequence of events following fracture in a rat model. a) Fracture healing can be divided into three overlapping phases: inflammation, repair and remodelling. b) IFM varies over the course of fracture healing. c) Blood flow is represented as percentage change from pre-fracture levels. d) Tissue composition varies throughout fracture repair. Abbreviations: IFM, interfragmentary movement[19].

3. Resorption: Osteoclasts begin to remove the organic and mineral components of bone and form a cavity of characteristic shape and dimensions called a Howship's lacuna in trabecular bone and a cutting cone in cortical bone. When the cavity reaches a depth of about 60 μm from the surface in trabecular bone and about 100 μm in cortical bone, resorption at that location ceases.

4. Reversal: Osteoclasts die and mononuclear macrophage-like cells smooth the resorbed surface by depositing a cement-like substance that will bind new bone to old. Pre-osteoblasts begin to appear. This phase is characterized by factors that stimulate osteoblast precursors to proliferate, including IGF-2 and TGF-β.

5. Formation: Differentiated osteoblasts fill in the resorption cavity and begin forming new osteon in a two-stage process. First, they deposit osteoid (mostly collagen type I). The rate of matrix apposition is initially very rapid and the osteoblasts are columnar and densely packed. Mineralisation of the osteoid commences when the cavity has been filled to 20 μm. With the onset of mineral apposition, the rate of mineralization exceeds the rate of matrix apposition and continues, with a substantially lower rate, even after the termination of matrix synthesis, until the bone surface returns to its original resting state.

The remodelling process is long term and occurs until the bone approaches its original geometry, strength and stiffness, optimised to the external mechanical

stimuli[20]. During this phase, vascularisation within the callus is also reduced to match that of the original site[21].

In summary, the bone healing process is defined by three phases: inflammation, repair and remodelling. Non-union and delayed healing of bone is due to a failure in any one of the three phases. A biomaterial or bone tissue engineered construct which has properties which can initiate, facilitate and modulate through the different healing phases will have immense benefits of stimulating, enhancing and maintaining the body's own regenerative capacity in bridging the bone defects. These materials can achieve such an effect by employing different strategies. The 'diamond concept' has been proposed by Giannoudis *et al.*, in which growth factors, osteoconductive scaffolds, MSCs and mechanical environment are the four main factors that should be considered in the treatment of fractures[22]. Indeed, the use of bone morphogenetic proteins (BMP-2 and BMP-7), released by cells during the inflammatory phase, have been extensively studied to deliver an osteoinductive effect and are in clinical use currently[23-28], and these have been incorporated into scaffolds for the treatment of critical-sized defects[29-31]. Other inflammatory cytokines such as VEGF and PDGF have also been studied to achieve revascularisation and angiogenesis in tissue engineered scaffolds[32-34]. In consideration of osteoconductivity, bioceramics play a fundamental role in the development of bone tissue engineered scaffolds because of their excellent biocompatibility with bone tissue, as well as their physicochemical properties which allow scaffold to achieve mechanical properties close to natural bone[35]. Various parameters that affect the micro-

and macro-structure of these materials can be designed using current engineering techniques, and these will be crucial towards ensuring an appropriate microenvironment for cell-ingrowth as well as blood vessel formation. MSCs, in addition to their ability to undergo osteogenesis, are key to the entire bone healing process, functioning to modulate the transition between phases, and synthesising new bone. As such, various biochemical and surface topological cues have to be arranged in a spatio-temporal manner which mimics the *in-vivo* microenvironment of these cells for the most optimal results to be achieved[36]. Finally, the biomaterial or bone tissue engineered construct has to allow for appropriate transmission of mechanical stimulation, as the concept of mechanotransduction is crucial towards the understanding of bone remodelling.

2.1.3 Stress shielding and bone mechanotransduction

In the early 20th century, metallic orthopaedic implants used in total hip arthoplasty faced problems of stress shielding, whereby reduction in bone mass is observed around the area where the implant is placed. This is caused by the mismatch in stiffness of the implant material and the surrounding bone, resulting in removal of stresses experienced by the bone. This led to the discovery of Wolff's law, which states that the bone will remodel itself in accordance to the experienced stress field; increased loading results in denser bone in the direction of the applied stress, while greater bone resorption occurs in areas experiencing less loading. This underscores the importance of mechanical stimulation in the development of orthopaedic implants such that

consideration of the material's elastic modulus and stress field influences at the implant site forms an important facet in material selection.

Wolff's law is implicated in the bone remodelling process, which occurs throughout an individual's lifetime. This process involves the conversion of mechanical stimuli into biochemical signals in a process known as mechanotransduction. Osteocytes are the main cells that sense changes in the applied mechanical stresses.

The matrix around osteocytes and processes is not calcified and they interconnect with one another to establish a three-dimensional network. This network extends towards the periosteum, making contact with the bone lining cells. Such a network creates a highly sensitive mechano-sensing tissue that confers dynamic properties to bone[37]. Its close proximity to the MSCs and the periosteum allows contact with osteoblasts and osteoclasts, while water and small molecules can penetrate their network of lacunae (space occupied by the body of the osteocyte) and canaliculi (channels that allow the processes of osteocytes to come in contact).

The microenvironment that is created from this network is instrumental in bone mechanotransduction. During increased mechanical strain, excessive stimulation of osteocytes increases the release of osteoblastic factors and induces bone growth. The transfer of signals via the gap junctions of the lacuno-canalicular network is believed to induce recruitment of osteoblasts. As extra bone is produced, the basal mechanical loads in bone are restored and bone growth ceases. Conversely, during mechanical unloading, as in the case

of stress shielding, decrease in osteocyte stimulation leads to osteocyte apoptosis, which in turn signals for an increase in osteoclastic activity. The resultant increase in bone resorption occurs and bone density decreases until the new norm in mechanical loading is achieved[38]. In addition to mechanical strain, it has been noted that fluid shear stresses in the lacuno-canalicular network manifests from external loading conditions also play a role in underlying the mechanism of Wolff's law. Reich *et al.* has reported that osteoblasts express increased amounts of Expressions of cyclic adenosine monophosphate (cAMP); a known mediator of bone formation, by osteoblasts was shown to increase when cultured at shear rates as low as 10 s^{-1}. Increase in viscosity, which results in increased fluid shear stress, corresponded to a proportional increase in cAMP[39]. Nitric oxide (NO) and prostaglandins E_2 and I_2 (PGE_2 and PGI_2) have also been shown to be expressed in greater amounts by both osteoblasts and osteocytes when subjected to fluid shear stress[40-42]. NO is a free radical known to promote vascularisation and angiogenesis, inhibit osteoclastic activity and stimulate osteoblastic proliferation, while PGE_2 and PGI_2 are involved with bone mechanotransduction as well as bone formation.

From this, it is clear that the immediate microenvironment around the cell plays an important role in which the cell senses changes. This is achieved by cell-surface receptors (integrins) that mediate both cell attachment and serve as link between the matrix and the cytoskeleton. In such a mechanism, physical stimulus applied to the bone matrix gets transmitted to the cells via integrins, which then induce changes to the organization of the cytoskeleton,

which leads to gene upregulation or downregulation. Similarly, biomaterials not only serve to create a scaffold for tissue structure, but also transmit information to the attached cells. Specifically, the mechanical strain causes a change in clustering of integrins and their associated intracellular protein configuration leads to cytoskeleton polymerisation/ depolymerisation and reorganisation, thus changing the morphological structure of the cell[43]. This has been demonstrated by Rhee *et al.*, in which differences to matrix rigidity or exogenous tension determines rate of fibroblast migration through strength of matrix-ligand binding and density[44].

2.1.4 Cellular Response

The degree to which attached osteoblasts respond to physical simulation can be influenced by the strength of adhesion to the biomaterial. The strength of adhesion is in turn governed by the biomaterial's surface morphology and chemistry[45]. Depending on the microenvironment and material surface characteristics, cells can respond to the tension created through rearrangement of their cytoskeletal network[46]. Cytoskeletal network organisation has been implicated in osteoblast proliferation and differentiation, whereby MSCs undergo distinct cytoskeletal changes during osteogenic differentiation (fibroblastic to round, spindle-shape). Clearly, cell-matrix interactions play a fundamental role during osteogenesis. Osteoblasts adhere preferentially to matrix components through focal adhesion contacts, and this adhesion is primarily mediated by integrins and cadherin which form connections with both the cytoskeleton and ECM[47]. Indeed, FAK signalling through integrin engagement has been identified as playing a critical role in regulating ECM-

induced osteogenic differentiation among MSCs[48]. As such, engineering a biomaterial that has physicochemical cues that induce integrin binding and clustering in a spatially specific manner can be a potential way to guide bone regeneration.

2.2 Bone Tissue Engineering

Traditionally, orthopaedic surgeries for the treatment of bone diseases, repair of bone defects due to trauma or tumour removal involved the use of autografts, which is often considered as the 'gold standard' of treatment. However, the limited availability of bone tissue and donor site morbidity represent major limitations with autografts[49, 50]. The use of allografts and xenografts circumvent this problem, but they present significant risks of adverse immune reaction, tissue rejection as well as viral or bacterial infection[51]. Furthermore, there were persistent issues of insufficient revascularisation and remodelling, which are speculated to contribute to 25% of allograft failures and 30 – 60% of post-operative complications.

In light of this, there have been extensive research and development into naturally derived and synthetic bone graft substitutes over the last 30 years. This forms the basis for development of a subset of biomaterials, whereby specific set of considerations were established in order to achieve a biomaterial that would ensure adequate biocompatibility with the surrounding bone tissue, while fulfilling its intended goal of restoring function to the damaged or replaced tissue.

Initially, metallic prostheses were chosen as implant biomaterials, where primary concerns were focused on withstanding mechanical loads and ensuring structural integrity. However, it soon became evident that metallic implants faced long-term issues of insufficient integration with the host tissue, resulting in complications such as aseptic loosening, implant migration, and osteolysis. In addition, the tribology of these materials when used in articulating surfaces also resulted in unintended host response. These metals while in bulk, insoluble forms were harmless, elicited strong local and systemic immunological response when exposed to wear and tear due to the release of metal ions and debris into the system. This prompted thorough deliberations into the actual definition of 'biocompatibility' where it became widely accepted that the biomaterial should elicit a favourable host-tissue response, while preventing any adverse immunologic effects.

Better appreciation of the bone biology and fracture healing process (See Section 2.1.2) made the issue of biocompatibility even more relevant in the paradigm of host-implant integration. The 'diamond concept' of an ideal bone substitute material was introduced, whereby properties of osteoinduction, osteogenesis and osteoconduction should be incorporated into a three-dimensional structure that mimics the *in-vivo* microenvironment and contains appropriate mechanical properties that sustains loading, promotes revascularisation and allows for mechanical and fluidic stimulation.

From this, the concept of bone tissue engineering emerged. Fundamentally, the development of functional, biological solutions to repair or replace

damaged tissues and organs is the goal of tissue engineering. This involves the interplay between cells, scaffolds and biomolecules that would generate a favourable response when implanted into the patients, thus restoring functions lost or impaired due to injuries or disease. This chapter will focus on the key design considerations of a tissue engineered construct, which encompasses an overview of the types of the various scientific disciplines that are required. Particular attention will be devoted to a review on the use of bioceramics, which play an indispensible role in majority of bone graft substitutes as well as bone tissue engineered constructs. This is because of their unique physicochemical properties, which can produce an osteoconductive effect. Bioceramics, when used in conjunction with synthetic polymers or other naturally derived materials, have the potential to create a truly biomimetic biomaterial ideal for bone tissue engineering applications.

2.2.1 Biocompatibility

Biocompatibility is the most fundamental requirement that has to be fulfilled by all biomaterials. Defined as "the ability of a biomaterial to perform its desired function with respect to a medical therapy, without eliciting any undesirable local or systemic effects in the recipient or beneficiary of that therapy, but generating the most appropriate beneficial cellular or tissue response in that specific situation, and optimising the clinically relevant performance of that therapy"[52], it entails a deliberate and meticulous method of appreciating the specific physiological environment that the biomaterial is being implanted to, the function that it intends to replace or restore, and the physio-biological processes that enable seamless acceptance

into the body. This “living in the problem” paradigm spurred intense research and development of key design considerations that demands an interdisciplinary approach, which would engineer a biomaterial with characteristics that direct host response along its intended path. Broadly, three strategies were undertaken to achieve this: bioinert, bioactive and bioresorbable. Bioinert biomaterials were developed due to insufficient understanding of the host tissue response and are no longer considered as a material with good biocompatibility. Bioactive biomaterials represent the next generation of biomaterials, able to initiate, promote or maintain a certain host tissue response, which is believed to be beneficial towards repairing or replacing tissue function. Within the strategy of incorporating bioactivity, bioresorbable biomaterials are materials that become resorbed into the body either by dissolution or metabolic processes, which are favourable in specific cases where complete tissue regeneration and restructuring is expected. These materials serve as temporary scaffolds for cell adhesion, guiding tissue formation while performing biochemical and biomechanical functions before the regenerative process is complete. For example, bioresorbable VICRYL™ (polyclactin 910) sutures made of a mixture of 90% glycolide and 10% L-lactide are used in various applications requiring soft tissue ligation. These sutures serve the function of stitching tissues together and is resorbed into the body once the incision heals over, reducing the formation of scar tissue[53].

Within the context of bone tissue engineering, the concept of incorporating bioactivity, whether through bioresorbable or long-term implants, can be further sub-divided into three properties of action: osteoinduction,

osteogenicity, and osteoconduction. No single material, apart from autografts, has been able to incorporate all three properties of action, and all current bone graft substitutes employ a combination of cell, growth factor and material based approaches to achieve these properties. A summary of bone graft substitutes currently available has been provided in Table 2.3.

Table 2.3. Summary of bone graft substitutes currently available[54].

Class	Description	Examples	Properties of action
Autograft	Used alone	AlloFuse, Accell 100, Puros	Osteoconductive, osteoinductive, osteogenic
Decellularised Allograft	Alone or combination with other materials	Allergo, Orthoblast, Grafton	Osteoconductive, osteoinductive
Growth factor based	Natural or recombinant	BMP, TGF-β, PDGF, FGF, VEGF	Osteoinductive
Cell based	Cells used to generate new bone	MSCs, ESCs, iPSCs, periosteal cells, osteoblasts	Osteogenic
Ceramic based	Includes calcium phosphates, calcium sulfate, bioactive glass	Osteograf, Osteoset, NovaBone	Osteoconductive
Polymer based	Includes degradable and nondegradable polymers used alone and in combination with other materials	Cortoss, OPLA, Immix	Osteoconductive
Naturally derived	Type I collagen mixed with calcium phosphates	Integra Mozaik, MasterGraft INFUSE (with addition of rhBMP-2)	Osteoconductive, Osteoinductive (with addition of rhBMP-2)

These three approaches to bone graft substitutes can be further elaborated as such:

1. Cellularised therapies

These are usually osteoblasts or their derived progenitors. Such cells are usually isolated, grown and differentiated down the osteogenic lineage *in-vitro*

before being implanted into the healing site. These cells can either be of allogeneic or autogenic sources and they contribute directly to the synthesis of new bone ECM (i.e. osteogenicity).

2. Growth factor incorporation

Growth factors are signalling biomolecules that stimulate cellular migration, proliferation, and differentiation. These are obtained either from natural or recombinant sources, and when applied in bone tissue engineering applications, deliver an osteoinductive effect by attracting MSCs, promoting osteogenic differentiation, and bone mineralisation. Examples of these growth factors include BMP-2, BMP-7, as well as TGF-β. Other growth factors such as fibroblast growth factor (FGF), platelet-derived growth factors (PDGF) and vascular endothelial growth factor (VEGF) are also used as these growth factors deliver the stimulatory effect of inducing vascularisation and angiogenesis[55]. Growth factors are highly potent biomolecules that have to be tightly regulated during their release into the host tissue. Use of growth factors in orthopaedic therapies is still limited because of their prohibitively high costs, and possible side effects or tumorgenesis[56, 57].

3. Biomaterials as scaffolds

Biomaterials underlie the bone tissue engineering approach. They function to provide a three-dimensional structure that guides cell migration, proliferation and differentiation. They form the base substrate for which cellular therapies and growth factors can be incorporated. While some tissue engineering applications can feature scaffold free strategies, the need for scaffolds is

essential in bone graft substitutes, because the construct is required to bridge gaps in defects and sustain mechanical loading while the bone healing process is underway. The types of biomaterials used as scaffold include metals such as cobalt-chromium-molybdenum, stainless steel and titanium, polymers such as polycaprolactone (PCL), poly lactic-co-glycolic acid (PLGA), and poly (l-lactic acid) (PLLA), and ceramics such as zirconia, calcium phosphates and bioglass. Another class of biomaterials is derived from natural origins, and these include demineralised bone matrix, collagens, chitosan and silk[58].

2.2.2 Design considerations: Mechanical properties, degradation profile, surface characteristics, porosity and pore size

Through an in-depth appreciation of the bone biology and the healing process (Section 2.1), a general agreement on the design considerations can be established. Since the biomaterial is expected to undertake mechanical functions, it should have mechanical properties which resemble that of the natural bone. Structurally, they should not undergo massive deformation under normal loading conditions, but should demonstrate visco-elastic strain characteristics to allow for proper mechanotransduction. Figure 2.5 illustrates the stiffness to strength relationship of commonly used biomaterials and where they stand with respect to tissues in the body.

While metals and alloys possess high stiffness and strength, they can result in issues related to stress-shielding due to the mismatch in stiffness compare to the host tissue, and have limited biocompatibility. Polymers may have stiffness and strength resembling that of soft tissues and trabecular bone, but possess undesirable effects of undergoing permanent deformation with

sustained loading. Bioceramics, which represent the bulk of currently available bone graft substitutes, are favoured because they are highly biocompatible with the host tissue, and have high stiffness and compression strength. However, they fail easily through brittle facture during tensile loading and are difficult to manipulate to form complex shapes. Use of bioceramics has been traditionally restricted to granule forms and coatings. Increasingly, with the development of new fabrication technology, composites featuring combination of both polymers (natural or synthetic) and bioceramics are being developed, offering unique opportunities of customising the material's properties to match that of the host tissue.

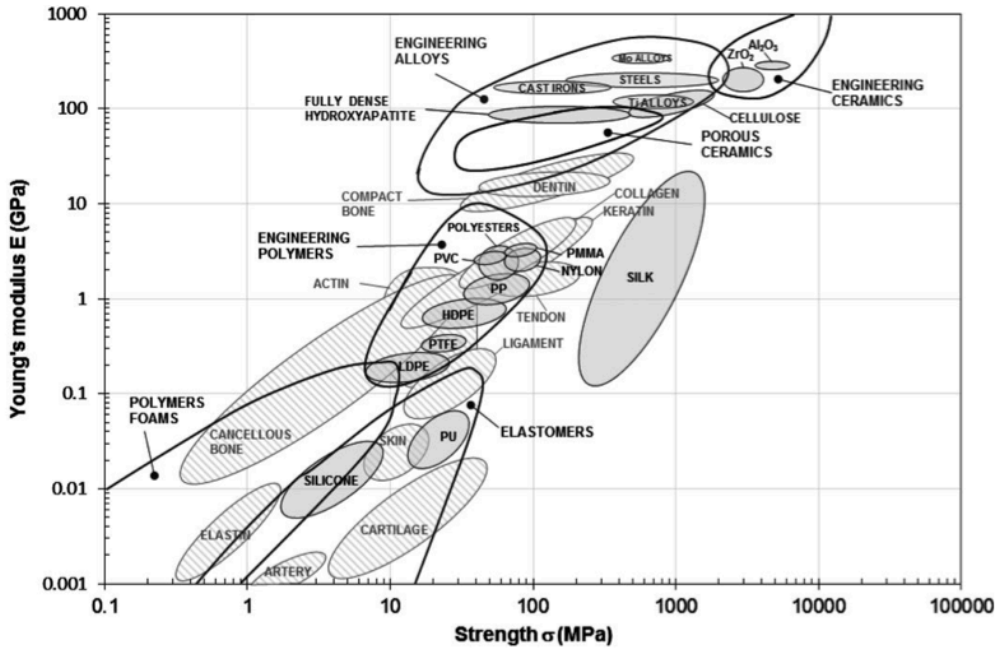

Figure 2.5. Ashby map illustrating the comparison of Young's modulus (Stiffness) to strength of various biomaterials. Note that stiffness and strength of metals and their alloys are generally several orders of magnitude higher than that of other materials and biological tissue[59].

In bone tissue engineering, the degradation and resorption characteristics of the biomaterial should be designed to progress in tandem with the healing process, sustaining mechanical loads while new tissue grows over. This is to maintain a stable microenvironment for cell proliferation and vascularisation of the construct. This should be designed with the type of bone that the biomaterial intends to replace. In trabecular bone, it should degrade within 6 – 12 months, while in cortical bone, 6 – 12 months, to allow the remodelling phase to proceed. For example, by mixing calcium phosphates of an insoluble phase of hydroxyapatite (HA) with a highly soluble phase of amorphous tricalcium phosphate (TCP) in the creation of biphasic calcium phosphates (BCP) it is possible to tailor the degradation characteristics of the biomaterial ranging from weeks to years. Ultimately, the purpose here would be to select and develop a biomaterial for the specific bone tissue engineering application. As such, biomaterials featuring a composite of different materials that complement one another are increasingly favoured over traditional biomaterials.

Upon introduction into the biological environment, proteins and other biomolecules from the surrounding serum are adsorbed onto the biomaterial's surface. It is this protein layer that interacts with the cell, rather than the actual biomaterial. Specific control of this layer chemically as well as spatially would allow for direct manipulation of cellular responses. For instance, the bioactivity of certain bioceramics such as calcium phosphates and bioglasses can be attributed to the dissolution-reprecipitation mechanism, whereby an ion exchange process occurs, resulting in the creation of an apatite layer. This

layer is key towards enabling proper osteoblast adhesion, spreading and phenotypic expression, and is crucial towards ensuring host-tissue osteointegration. i.e. Absence of a bioactive apatite layer is a known cause of fibrous tissue encapsulation.

It has been well established that cellular biomechanics function at the submicron level. Several biochemical pathways involving cellular proliferation, differentiation and regulation are due to the functional changes in the immediate micro/nano environment surrounding the cells. If a group of integrins are engaged in a particular sequence or arrangement, different cellular signalling pathways can be promoted or inhibited. This effect was demonstrated in a study involving an array of nano-scale geometries ranging from nanogroove, nanopost, and nanopit arrays, to study the effects of cellular contact guidance. In the study, it was observed that epithelial cells elongated and aligned along the patterns of grooves and ridges with feature dimensions as small as 70 nm, whereas cells were mostly rounded on smooth surfaces[60]. Certainly, such topological cues would present an opportunity for nano-scale engineering of a bone scaffold where scaffold constructs comprising of nanobioceramic crystals can be made to align to the *c*-axis of the bone, thus allowing for the adhesion of osteoblast cells along this axis, and produce ECM which would further enhance strength and integrity of the implanted scaffold.

Already such a concept has been proposed by Kim *et al.* where they have demonstrated that cellular attachment and proliferation was improved through the use of a nanocomposite of HA nanocrystals embedded in a nanofiber

composed of gelatin[61]. Osteoblast adhesion is dependent on surface topology, and it has been shown that nanophase surfaces promoted better adhesion than microscale materials[62]. The experiments showed that a 30 and 46 % increase in osteoblast adhesion on nanophase titania (grain size 32 nm) and alumina (grain size 23 nm), respectively when compared to the conventional bioceramics[63]. In fact, nanotopology alone may account for 48 – 51 % of the total osteoblast adhesion as shown in an experiment by Palin *et al.* who showed that poly (lactic-co-glycolic acid) PLGA modelled after nanophase titania showed a similar percentage increase in osteoblast adhesion as compared with nanophase titania[64]. Moreover, alkaline phosphatase (ALP) and ECM calcium content were significantly increased when osteoblasts were cultured on nanophase bioceramics, compared with the conventional microscale ceramics (Table 2.4)[65].

Table 2.4. Percent increase in ALP and ECM calcium content for osteoblasts cultured on nanoscale compared to microscale bioceramics after 28 days[65]

Bioceramic	**Grain Size (nm)**		**% Increase in ALP synthesis on nanophase compared to conventional**	**Increase in ECM Calcium content on nanophase compared to conventional**
Alumina	Conventional	167	36	4 times
	Nanophase	24		
Titania	Conventional	4250	22	6 times
	Nanophase	39		
Hydroxyapatite	Conventional	179	37	2 times
	Nanophase	67		

Porosity, pore size and pore interconnectivity of the biomaterial is the last set of considerations that should be taken into account for the development of

bone tissue engineered construct, but it is by no means the least important. In fact, porosity and pore size are important determinants to osteogenicity of the biomaterial, and its long-term performance is directly dependent on this material property. Kuboki *et al.* has demonstrated that presence of pores of hydroxyapatite allowed for migration and proliferation of MSCs and osteoblast, as well as blood vessel formation. Porosity, or percentage void space in a solid, contributed to the availability of the biomaterial's surface for protein adhesion, cellular adhesion and growth. The specific dimensions and interconnectivity of pores relate to the ease of the biomaterial to facilitate host tissue in-growth, facilitating vasculature and enhancing nutrient exchange kinetics. To this extent, several studies have demonstrated the importance of macropores (larger than 100 μm) to enhance tissue penetration and bone formation. Whether or not this is a pre-requisite for bone induction is still unknown, but it has been reported that the optimal pore size should be around 300 μm with interconnectivity to enable adequate vascularisation. Moreover, microporosity (smaller than 10 μm) has also been implicated in enhancement of biomaterial osteogenicity. Habibovic *et al.* highlighted this by demonstrating that elevated microporosity in BCP ceramics resulted in ectopic bone formation in a goat model[66]. Microporosity directly influences the biomaterial's roughness, and hence surface free energy. Ionic compounds, especially bioceramics, are dependent on this characteristic for apatite layer re-precipitation, which in turn affects biomaterial osteoconductivity and osteointegration. Clearly, the use of a biomaterial with high porosity with interconnectivity and a combination of macro and micropores will be

beneficial for bone tissue regeneration and host tissue integration. However, the specification of these parameters is limited by mechanical constraints. Biomaterials begin to lose mechanical strength and hardness with the inclusion of pores, and this represents a compromise between mechanical requirements and bioactivity of the biomaterial.

The design of a biomaterial for bone tissue engineering involves an interdisciplinary approach, which begins with an intimate appreciation of the bone biology and bone healing mechanisms. Through this, a thorough set of considerations can be established with respect to the biocompatibility and bioactivity of the biomaterial. These considerations encompass deliberations to the selection of materials, combining the properties of various types in the synthesis of a composite with complementary properties to enhance its bioactivity, as well as biofunctionality. Engineering techniques of manipulating the surface properties of the biomaterial can be employed to elicit specific biological response that enhances bone regeneration. This can be achieved through nanosurface topology, as well as degradation characteristics so the bone remodelling process can be allowed to occur, which result in proper host-tissue dynamics that responds appropriately to the required stimuli. In addition, attention should be paid towards designing the porosity, interconnectivity and pore size of the biomaterial so as to ensure adequate vascularisation, bone ingrowth and osteogenicity. Nevertheless, biomechanical functions of maintaining structural integrity and sustaining normal mechanical loads during the healing phase should be taken into account as well to prevent structural failure at the healing site. While these considerations can present

conflicting requirements, the effect of these compromises may represent ideal conditions for bone remodelling to occur and the result is a biomaterial with high osteointegration, and responds dynamically to the required load.

2.2.3 Bioceramics

As alluded to in the previous sections, bioceramics play a central role in the development of bone tissue engineered constructs. They have been extensively used in bone grafts and bone graft substitutes due to their excellent biocompatibility, and osteoconductivity[67, 68]. When incorporated with growth factors, these bioceramics can exhibit osteoinductivity[69, 70].

Table 2.5. List of calcium phosphate phases. Abbreviations: calcium-deficient hydroxyapatite (CDHA), precipitated HA (pHA). [71]

Name	Symbol	Formula	Ca/P	Mineral
Monocalcium phosphate monohydrate	MCPM	$Ca(H_2PO_4)_2 \cdot H_2O$	0.50	-
Dicalcium phosphate	DCP	$CaHPO_4$	1.00	Monetite
Dicalcium phosphate dihydrate	DCPD	$CaHPO_4 \cdot 2H_2O$	1.00	Brushite
Octocalcium phosphate	OCP	$Ca_8H_2(PO_4)_6 \cdot 5H_2O$	1.33	-
Precipitated hydroxyapatite	pHA	$Ca_{10-x}(HPO_4)_x(PO_4)_{6-x}(OH)_{2-x}$	1.50 – 1.67	-
x = 1	CDHA	$Ca_9(HPO_4)_1(PO_4)_5(OH)$	1.50	
x = 0	HA	$Ca_{10}(PO_4)_6(OH)_2$	1.67	
Amorphous calcium phosphate	ACP	$Ca_3(PO_4)_2 \cdot nH_2O$ where n = 3–4.5; 15–20% H_2O	1.50	-
Monocalcium phosphate	MCP	$Ca(H_2PO_4)_2$	0.50	-
α-Tricalcium phosphate	α-TCP	$\alpha\text{-}Ca_3(PO_4)_2$	1.50	-
β-Tricalcium phosphate**	β-TCP	$\beta\text{-}Ca_3(PO_4)_2$	1.50	-
Hydroxyapatite	HA	$Ca_{10}(PO_4)_6(OH)_2$	1.67	Hydroxyapatite
Tetracalcium phosphate	TetCP	$Ca_4(PO_4)_2O$	2.00	Hilgenstockite

Among the most commonly researched bioceramics (Table 2.5) are calcium phosphates, with particular attention focused on hydroxyapatite (HA) and β-tricalcium phosphate (β-TCP). Solubility of β-TCP is much higher than HA, and thus β-TCP is termed a bioresorbable ceramic. Development of biphasic calcium phosphate (BCP)-based biomaterials consisting of HA and β-TCP[72, 73] are also of interest to control the degradation properties. Table represents an overview of the different calcium phosphates and their properties. Since this report is concerned with the long-term culture and implantation of bone tissue engineered constructs, stability is of great concern, and thus HA will be the subject of attention. A more detailed review of β-TCP and BCP can be obtained from other references[74-77].

2.2.4 Hydroxyapatite

Hydroxyapatite is a biocompatible ceramic produced through a high-temperature reaction and is highly crystalline form of calcium phosphate. The nominal composition of this mixture is $Ca_{10}(PO_4)_6(OH)_2$ with a calcium-to-phosphate atomic ratio of 1.67. The most unique property of this material is chemical similarity with the mineralised phase of bone; this similarity accounts for their osteoconductive potential and excellent biocompatibility[78, 79]. Calcium hydroxyapatite/tricalcium phosphate (60/40) provide a structure or scaffold which can have a close interface with adjacent bone and have a limited application in the treatment of load-bearing segmental bone defects but did not fail at the early stages of implantation[80].

HA has higher stability in aqueous media than other calcium phosphate ceramics within a pH range of 4.2–8.0. The crystal structure of HA can accommodate substitutions by various other ions for the Ca^{2+}, PO_4^{3-} and OH^- groups. The ionic substitutions can affect the lattice parameters, crystal morphology, crystallinity, solubility and thermal stability of HA. For example, the F^-or Cl^- can substitute for the OH^- group while CO_3^{2-} can substitute for the OH^- (Type A) or the PO_4^{3-} (Type B) group. In the case of carbonate substituted HA (CHA), for both substitutions, the ionic lattice undergoes crystallographic changes to accommodate the imbalance in charge. This results in a reported increased bioactivity of CHA due to increased solubility[81].

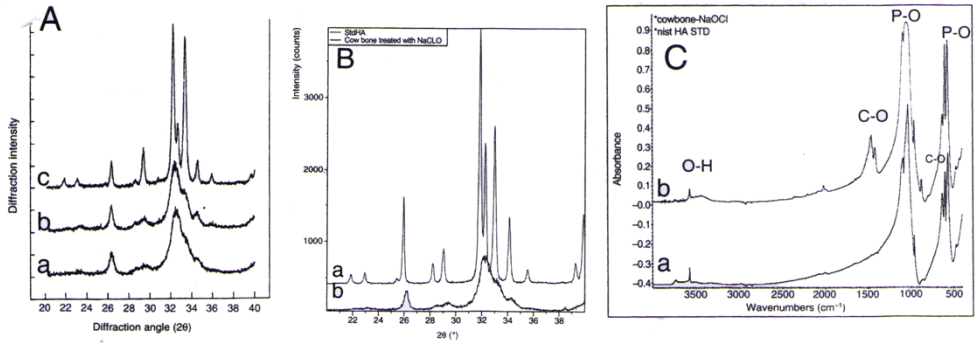

Figure 2.6. X-ray diffraction profiles: **(A)** enamel (a), dentine (b) and bone (c) mineral (carbonate apatites) **(B)** ceramic HA (a), bone (b). **(C)** FTIR spectra of ceramic HA (a) and bone mineral.[82]

The rationale for developing HA biomaterials is its similarity in composition with bone material or bone apatite. XRD profile and FTIR (Fig. 2.6a) spectrum of synthetic HA compared with bone shows similarities and differences in crystallinity (Fig. 2.6b) and composition, e.g. presence of carbonate in bone apatite (Fig. 2.6c)[82]

HA can be derived from both biologic and synthetic origins. Biologic HA can be obtained from coral, bovine bone or marine algae. There are various methods to obtain HA from biologic sources but the review is beyond the scope of this report.

HA can be fabricated synthetically from the following methods: i) Solid state reactions, ii) Hydrothermal reaction, iii) Sol-gel, and iv) Wet Precipitation

i) Solid State Reaction[82]

Calcium compounds are mixed thoroughly, compressed and sintered above 950°C.

$$6CaHPO_4 + 4Ca(OH)_2 \rightarrow Ca_{10}(PO_4)_6(OH)_2 + 6H_2O$$

Reaction of dicalcium phosphate anhydrous (DCPA) and calcium hydroxide to form hydroxyapatite and water

$$3Ca_3(PO_4)_2 + Ca(OH)_2 \rightarrow Ca_{10}(PO_4)_6(OH)_2$$

Reaction of beta-tricalcium phosphate (β-TCP) and calcium hydroxide to form hydroxyapatite

ii) Hydrothermal reactions[83]

In Figure 2.7, the mechanism model of hydrothermal method of HA synthesis is illustrated. HA can be synthesised by hydrothermal treatment of calcite crystals in H_3PO_4 suspensions at 120 °C or 180 °C, according to the equation:

$$10CaCO_3 + 6(NH_4)_2HPO_4 + 2H_2O \text{ --> } Ca_{10}(PO_4)_6(OH)_2 + 6(NH_4)_2CO_3 + 4H_2CO_3$$

Typical treatment time of 24 h under high pressure of approximately 100MPa produced single phase hydroxyapatite powder. Hydrothermal reactions are usually slow.

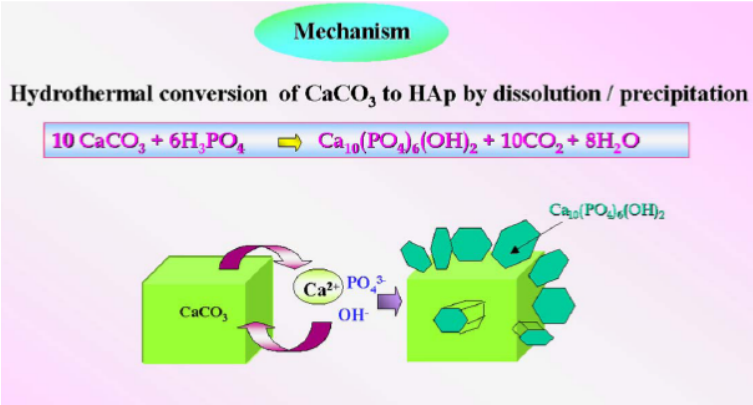

Figure 2.7. Mechanism model of hydrothermal convection of calcite crystals into HAp crystals[83]

iii) Sol-gel preparation[84]

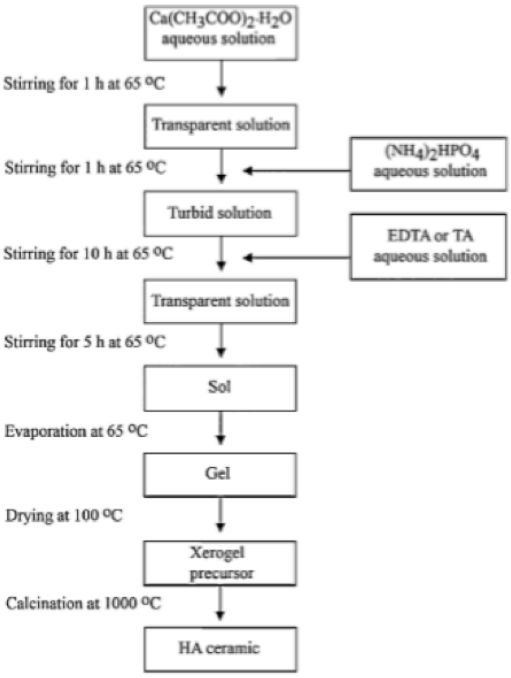

Fig 2.8. Steps involved in the sol-gel preparation of HA [82].

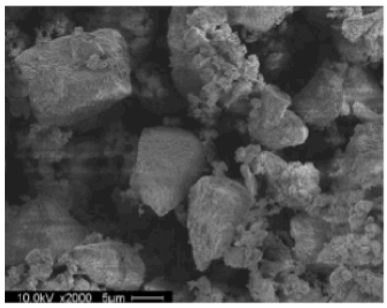

Fig 2.9. HA produced using EDTA route, SEM, 200x [82].

Fig 2.10. HA produced using TA route, SEM, 200x [82].

This method is used to produce hydroxyapatite granules of the highest stoichiometric pureness. Referring to figure 2.8, this method starts from

molecular precursors dissolved in solutions that are organic solvents. These organic molecules include the desired inorganic atoms. This association of inorganic and organic parts is commonly called a metal-organic compound. First step involves polymerization, then subsequently a colloidal condensation of the gel micelle. Polymerization involves condensation coupling. Use of alkoxides is very popular as they can be obtained easily. Use of calcium acetate monohydrate as source of calcium ions and ammonium-hydrogen phosphate as the phosphorus precursor both dissolved in a small amount of distilled water. Aqueous solutions of ethylene diamine tetra-acetic acid (EDTA) or tartaric acid (TA) were used as chelating agents in the sol-gel synthesis of hydroxyapatite. In figure 2.9, HA produced using the EDTA route are composed of grains with no regular shape, and with irregular surface texture. In figure 2.10, HA produced using the TA route results in formation of nicely shaped ultrafine elongated particles (microrods) with average grain size of 5 μm.

HA synthesis using the sol-gel method is usually used to form thin film coatings, which are used in metallic coating biomedical applications.

iv) Wet Precipitation[85]

Wet precipitation is the most preferred method as it is the most established and easiest to synthesise.

$$5Ca(OH)_2 + 3H_3PO_4 \rightarrow Ca_5(PO_4)_3OH + 9H_2O$$

Reaction occurs when H_3PO_4 is added drop wise in a $Ca(OH)_2$ aqueous suspension. Calcium hydroxide is in fact very weakly soluble in water, and

consequently the reaction takes place between the PO_4^{3-} ions diffused from the drop plunged into the suspension and the surface of the colloidal particles. The alkaline pH of the aqueous environment allows the hydroxyapatite to be stable, and is maintained by the complete dissociation of a few dissolved molecules of $Ca(OH)_2$ which is a strong base.

Hydroxyapatite forming reactions is linked to the rate of: i) Diffusion of the ionised phosphatic ionic groups (PO_4^{3-}, HPO_4^{2-}, $H_2PO_4^-$ and H_3PO_4 itself) connected to each other by well known simultaneous equilibra, ii) dissolution of $Ca(OH)_2$ as well as that of Ca^{2+} ions into the aqueous solution, iii) migration of the ionised phosphate groups within the colloidal grains of $Ca(OH)_2$, and iv) success of the transformation depends on the value of the local pH, even if the overall solution may remain alkaline.

Presence of CO_3^{2-} may replace the anionic component of the calcium compounds and give rise to more stable $CaCO_3$. This may then result in the production of other kinds of phosphates, including the carbonate apatites. Presence of CO_2 can be prevented by promoting reaction inside a reactor. All the foreign ions present in the synthesis solution may lead to the formation of molecules different from the hydroxyapatite molecule. These molecules may aggregate and eventually crystallise in foreign phases, or may induce the formation of other phases and hinder the formation of hydroxyapatite, or may associate in the precipitation of hydroxyapatite crystals and, by co-precipitating, replace one or other of the component groups in their regular group. If these replacements occur, defective hydroxyapatite is produced in

which a number of empty sites are present inside the crystal lattice. To favour the escape of foreign ions from the hydroxyapatite lattices and at the same time to increase the thickness and the rate of crystallisation of synthesised hydroxyapatite, it is essential to allow the digestion of the solution once the synthesis has been completed, after addition of the last drop which brings about the correct stoichiometric ration between Ca^{2+} and PO_4^{3-} (in molar ration of 5/3)

Digestion involves maintaining the solution at rest of about 37 °C for at least 48 hours. Highest degree of crystallinity was reached when the solution approached boiling temperature of about 97 °C.

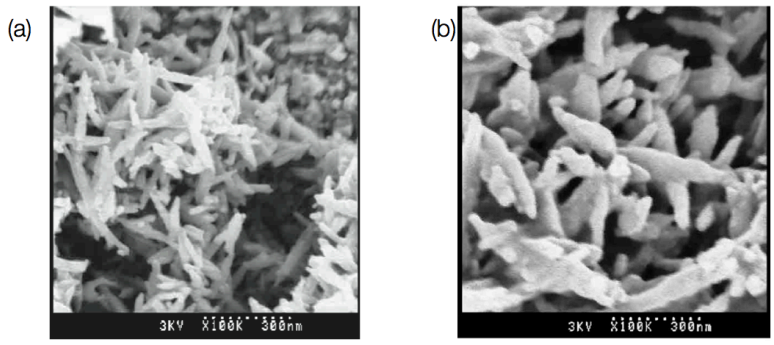

Fig 2.11. SEM micrograph of (a) as-precipitated HA and (b) after the aging process (100,000x)[85]

SEM high magnification micrographs (Fig 2.11a) show that the precipitated HA consists of small rod-like or platy particles. Aging the suspension leads to the growth of the particles and changes the morphology to a more equi-axed status (Fig 2.11b).

Typical HA powders synthesised via wet precipitation typically correspond closely to standard XRD pattern (Fig. 2.12) of pure HA (JCPDS 9-432), with increasing crystallinity as heating temperature is increased.

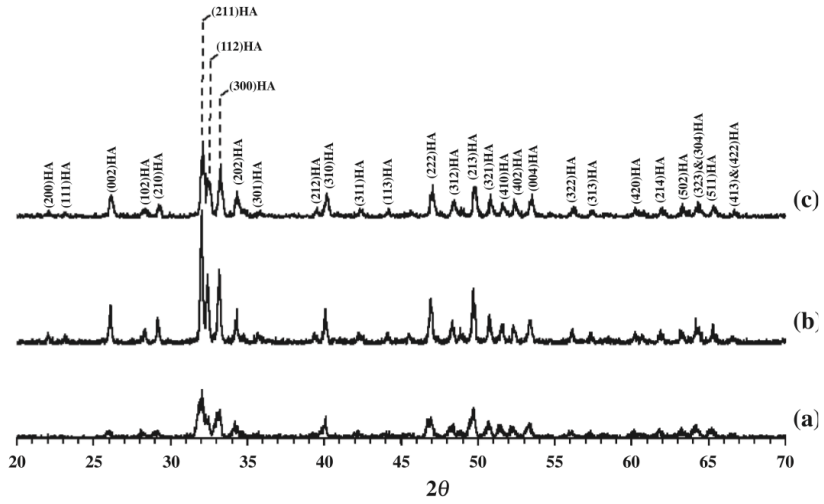

Fig 2.12. XRD pattern of synthesised hydroxyapatite as precipitated (a), heating at 850°C (b) 1200°C (c). Peaks of hydroxyapatite (JCSPDS 9-432)

2.3 Fabrication of spherical bioceramic particles

2.3.1 Alginate as a matrix polymer for microencapsulation

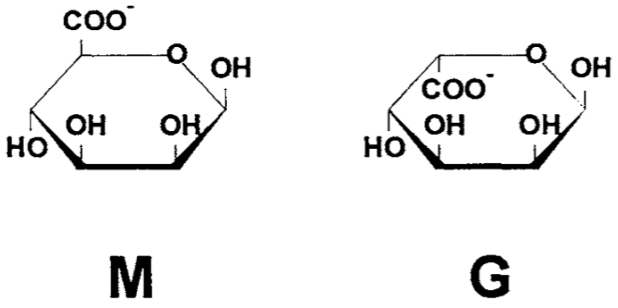

Fig 2.13. The monomers of Alginate[86]

Alginates are naturally occurring polysaccharides that have been finding increasing applications in the biotechnology field. They belong to a family of linear copolymers of β-D- mannuronic acid (M unit) and α-L-guluronic acid (G unit) residues (Fig 8), which can be arranged in different proportions and

sequences along the polymer chain. The G- and M- units are joined together in one of three blocks: GG... , MM... , and MG.... (Fig 9). The proportion, distribution, and length of these blocks determine the chemical and physical properties of the alginate molecules[87].

2.3.1.1 Rheology

The viscosity of an alginate solution depends on the concentration of alginate and the length of the alginate molecules, i.e. the number of monomer units in the chains. The longer the chains the higher the viscosity at similar concentrations (Figure 2.14). Length of chains can be contolled by the degree of polymerisation (DP). DP is directly proportional to the alginate's molecular weight, ranging from 80 to 750, corressponding to a molecular weight from 14000 to 132000. A DP of 80 is considered low viscosity, 400 classified as medium viscosity and 680 as high viscosity[88].

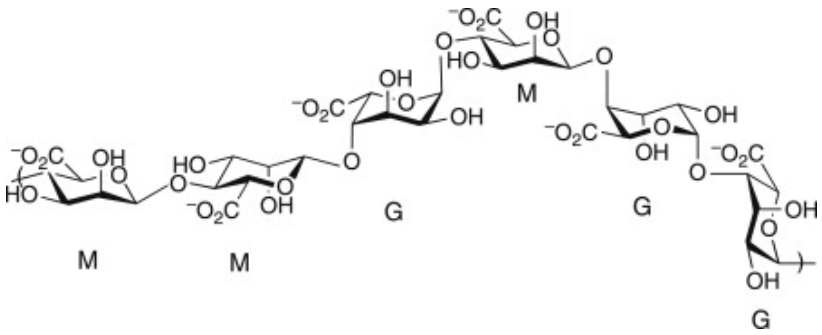

Fig 2.14 Three basic blocks of Alginate polymer chains, the MM-block (left), GM-block (middle), and GG-block (right), which may join together in different proportions, distribution and length.[89]

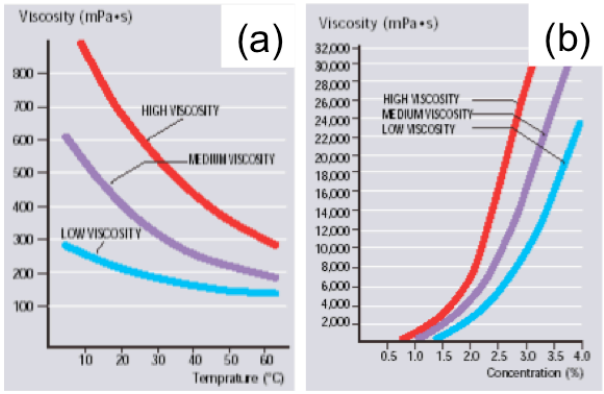

Figure 2.15. (a) Viscosity as a function of Concentration of Alginate in Water. (b) Viscosity as a function of Temperature. Low viscosity: 80 DP alginate, medium viscosity: 400 DP alginate, and high viscosity: 680 DP alginate.[90]

Upon dissolving alginates in water, the molecules hydrate and the solution gain viscosity. The dissolved molecules are not completely flexible; rotation around the glycosidic linkages in the G-block regions is somewhat hindered, resulting in a stiffening of the chain. Solutions of stiff macromolecules are highly viscous. Temperature defines the energetic state of any chemical molecule. Hence, temperature influences the response of alginates to shear forces. As a general rule, temperature increases of 1°C lead to a viscosity drop of approximately 2.5% (Fig 2.15).

2.3.1.2 Gelation of Alginate

Sodium alginate forms relatively stable hydrogels through ionotropic gelation in the presence of many multivalent ions, being Ca^{2+} the most widely used. The crosslinking process can be carried out under very mild conditions, at low temperature and in the absence of organic solvents, and hydrogels of different shapes can be prepared. Divalent cations of Ca^{2+} cooperatively bind between the G-blocks of adjacent alginate chains, creating ionic interchain bridges which cause gelling of aqueous alginate solutions (Fig 2.16).[91]

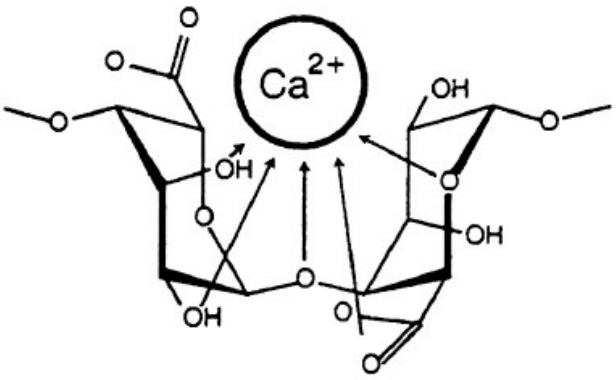

Fig 2.16. Calcium binding site in G-blocks[91]

In the "egg-box model", the divalent calcium cation, Ca^{2+}, fits into the G block structure like eggs in an egg box (Fig 13). This binds the alginate polymers together by forming junction zones, resulting in gelation of the solution[92].

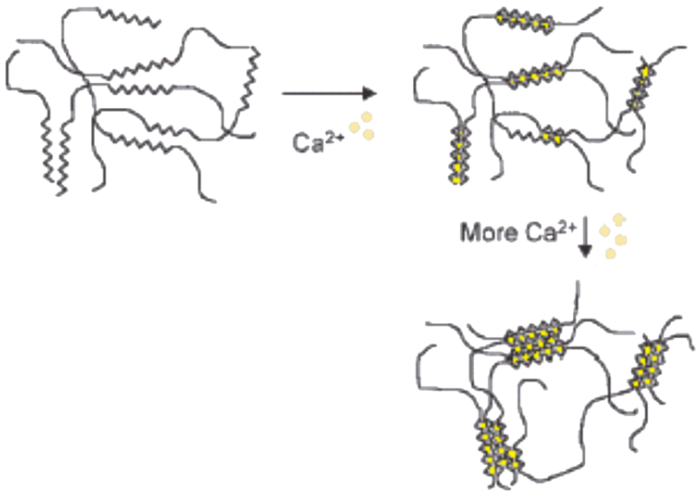

Fig 2.17. Egg-box model of Alginate gel formation[91]

2.3.2 Microsphere Preparation

Several therapeutic agents, including antibiotics, enzymes, growth factors and DNA, have already been successfully incorporated in alginate gels, retaining a high percentage of biological activity. Alginate plays two roles in the microsphere preparation: As a vehicle to form spherical shape particles, and as

pore inducing agent in the sintering process, all of this without any modification on HA.

Ca-Alginate microspheres are generally prepared by two methods: Drop wise extrusion of aqueous alginate into a solution of Calcium salt[93-95], and emulsification method under gentle stirring [96-98]. Particles produced by the first method are generally large (more than 1mm) and the attempts to obtain smaller particles have resulted in various complications such as clogging and high costs associated with special extrusion devices. However, microspheres produced in this route exhibit high spheroidicity and consistent size.

The second method is less commonly used due to the high viscosity associated with the starting alginate solutions. In addition, the resulting microspheres are generally non-spherical with wide variations in size, with high tendency to clump into aggregates.

CHAPTER 3

Fabrication and Characterisation of Apatite Microcarriers

3.1 Introduction

Among the bioceramics being considered for bone implant applications, apatite has been prominently featured due to its similarity to human bone[99] and favourable properties of excellent biocompatibility and osteoconductivity[74]. Applications of apatite based biomaterials range from thin coatings on metallic implants[100, 101] to drug release platforms[102, 103]. One of the most promising area of development for apatites is its use as a bone graft substitute, in which there is a growing demand due to a an increasing gap in the unmet needs in the treatment of dental or bone defects caused by trauma and diseases[104]. Apatite based bone graft substitutes are available in various forms: granules, blocks, cements, non-setting pastes (putties), foams, and films (membranes). Most commercially available bone graft substitutes contain apatite in the form of granules, because of their ease of fabrication, abundance, and proven clinical efficacy[105, 106]. Moreover, non-granular apatites do not have the necessary properties for them to be functional in clinical applications. For example, porous blocks can only be used in situations where the defect is geometrically well-defined such as in an open-wedge tibia osteotomy[107], or use of pastes involving apatite nanoparticles can result in implant migration, due to loss of cohesion and rapid material resorption such that its mechanical function is lost[108]. Through and understanding of the bone biology and design considerations of a biomaterial,

it is apparent that shape, size, porosity and surface morphology of the apatite granules are key towards ensuring its relevance in application, facilitating new bone tissue formation, while allowing for blood vessel in-growth[109]. Spherical particles allow for an optimal surface area to volume ratio for cellular adhesion and proliferation, and allow for ideal hydrodynamic response in dynamic flow conditions, which are particularly relevant in bioreactor culture systems[110]. In addition, spherical particles allow for better flow characteristics, which improve the injectability of these materials during non-invasive procedures[111]. Size of these spherical particles have been suggested to be within 200 – 300 μm[112, 113], with presence of microscale and macroscale pores which are interconnected[66], so as to direct a favourable local and systemic response towards new bone and blood vessel formation.

In view of these considerations, the fabrication, characterisation and optimisation of spherical, porous apatite based microcarriers will be described. It is envisioned that these apatite microcarriers will possess the physicochemical properties that promotes, facilitates and maintains bone regeneration, thus delivering a tissue engineered biomaterial that can adequately meet the needs of the dental and orthopaedic community.

3.2 Materials and Methods

3.2.1 Synthesis of phase-pure HA

HA was synthesized via a wet precipitation route. Calcium hydroxide [$Ca(OH)_2$] and orthophosphoric acid (H_3PO_4) were weighed and dissolved in deionised (DI) water to form solutions. 1 *l* of an aqueous H_3PO_4 (0.6 M) was

added dropwise into 1 *l* of an aqueous Ca $(OH)_2$ (1 M) under continuous stirring at 24 °C. Concentrated ammonia solution was added to maintain a pH value above 10.5. The solution was left to age for 2 weeks before subjecting it to an autoclave process for 2 h. The resulting precipitate was then dried in an oven at 70 °C for 12 h.

3.2.2 Synthesis of apatite microcarriers

A schematic representation of the synthesis process has been provided (Figure 3.1). Varying proportions of Na-Alg and HA powders were used (Table 3.1), and the resulting solution was extruded dropwise into a $CaCl_2$ crosslinking solution of varying concentrations using a droplet extrusion device. Na-Alg was dissolved in DI water for 30 minutes using a magnetic stirrer until total homogenization was achieved. HA, powder was then added to the Na-Alg solution, and stirred at 50 °C for 8 h using a hot plate stirrer, to ensure thorough homogenization. The solution containing HA and Na-Alg was extruded dropwise using a roller pump into $CaCl_2$ crosslinking solution, whereby spherical microcarriers were formed instantaneously.

The solution containing HA-Alg microcarriers and $CaCl_2$ was then allowed to mix for 2 h under gentle magnetic stirring to ensure crosslinking completion. HA-Alg microcarriers were retrieved from the solution and washed twice with distilled water to remove any $CaCl_2$. These microcarriers were left to dry overnight at 24 °C before subjecting to a multi-stage sintering process.

A multi-stage sintering profile (Figure 3.2) was designed so as to produce microcarriers with better characteristics. The stages were designed after the

melting temperature of Alg were obtained so as to allow for a more gradual burnt-off as well as to allow for longer time for the necking process between HA particles to occur.

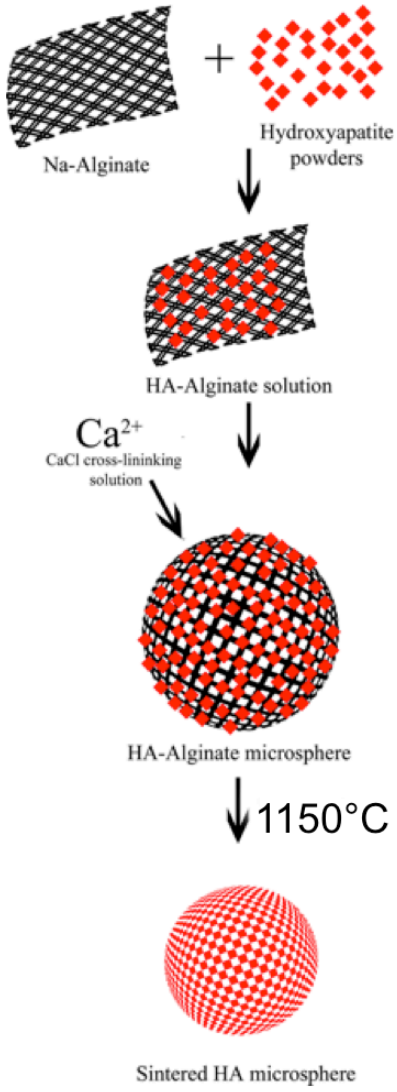

Figure 3.1. Synthesis process of apatite microcarriers. Apatite powder is dispersed in an alginate solution and mixed to ensure thorough homogenisation. The Apatite-Alginate solution is then extruded drop-wise through an electrically controlled valve that ensures consistent size into a calcium chloride cross-linking solution. The resulting microbeads are then washed, dried, and subjected to a multiple-staged sintering process to 1150°C. Alginate serves as the matrix to structure nano-crystalline apatite into a microsphere, and also allows the formation of pores when it is burnt off

Table 3.1. Apatite microcarriers fabricated using different Alg concentrations, HA contents and $CaCl_2$ concentrations

Sample	**Alg concentration (g/ml)**	**HA content (wt.%)**	**$CaCl_2$ concentration (mol/dm^3)**
1	0.0128	20	0.1
2	0.015	20	0.1
3	0.03	20	0.1
4	0.03	40	0.1
5	0.03	40	0.5
6	0.03	50	0.1
7	0.03	50	0.5
8	0.03	40	0.5

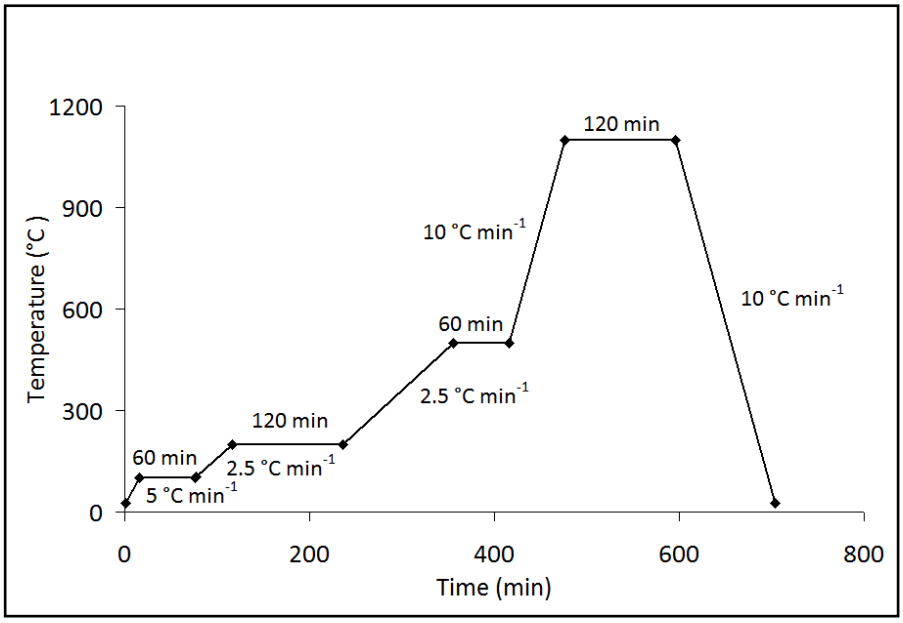

Figure 3.2. 4-stage sintering profile for HA-Alg microcarriers

3.2.3 Characterisation of apatite microcarriers

3.2.3.1 Optical microscopy analysis

The size of the microcarriers was estimated using an optical microscope with a calibrated built-in measurement scale. The mean diameter was determined from a sample of twenty microcarriers.

3.2.3.2 Scanning electron microscopy analysis

The microcarrier's morphology was analysed using a field emission scanning electron microscope (FE-SEM, Hitachi S-4300), operating at an accelerating voltage of 15 kV. The samples were sputtered-coated with a thin layer of gold before examination.

3.2.3.3 Energy dispersive X-ray spectroscopy analysis

Preliminary surface characterization of the apatite microcarriers was analysed using an energy dispersive X-ray spectroscopy (EDS). Samples were loaded into the SEM machine operating at an accelerating voltage of 15 kV, and a working distance of 10 mm. The elemental quantitative analysis used an automatic background subtraction, and a ZAF correction matrix has been used to calculate the elemental composition in weight percentage.

3.2.3.4 Thermogravimetric analysis

Thermogravimetric analysis (TGA) was conducted for the HA-Alg microcarriers to determine its thermal stability and burnt-off characteristics. Sample weight was 14 mg, and a platinum pan was used. TGA was conducted between 25 and 1200 °C at a heating rate of 10 °C/min, in an argon atmosphere.

3.2.3.5 Differential scanning calorimetric analysis

Differential thermal analysis (DTA) analysis was conducted to determine the melting temperature of HA-Alg microcarriers. 22 mg of HA-Alg microcarriers was added onto an aluminium pan, and heated from 25 to 500 °C at a rate of 10 °C/min.

3.2.3.6 X-ray diffraction analysis

The phase composition of apatite microcarriers was investigated using an X-ray diffractometer (XRD, Shimadzu X-ray diffractometer, Model 6000). The microcarriers were crushed and compacted before loading onto the machine. CuK_{α} radiation (λ = 1.5406 nm) at a scanning rate of 0.3 °/min was used over a 2θ range of 20 – 40 °, with a sampling interval of 0.05 °, operating at 30 mA and 40 kV. Phases were identified by comparison of the experimental data with the reference data from the International Centre for Diffraction Data.

3.2.3.7 Fourier transform infrared spectroscopy analysis

Chemical characterisation was performed using a fourier transform infrared spectroscometer (FTIR, Varian 3100 spectrometer). For this purpose, apatite microcarriers were crushed and analysed using potassium bromide pellets. A wavelength ranging from 400 to 4000 cm^{-1} with a spectral resolution of 16cm^{-1} was used.

3.3 Results

3.3.1 Pre-sintered HA-Alg microcarriers

The first step to apatite microcarrier fabrication involved HA-Alg bead formation. The following results report on the physical morphology of HA-Alg beads prepared under various settings.

3.3.1.1 Low HA content, low Alg concentration

The initial batch of HA-Alg beads was fabricated using 20 wt.% HA and 0.015 g/ml Alg. Flow through the tubing during droplet extrusion was rapid as the solution exhibited low viscosity. The fabricated beads in the 0.1 M $CaCl_2$ solution appeared to have good spheroidicity, and they remained intact after removing from the solution and washed. However, upon drying, HA-Alg beads appeared to be more disc-like, with flattened structure. This could be attributed to excessive water loss from the beads during drying, and insufficient Alg content to maintain its integrity of the bead. The appearance of white specks within most HA-Alg beads indicated insufficient homogenisation of HA within the Alg matrix. The size of the pre-sintered particles averaged 1.8 mm, and displayed high tendency to clump together and form agglomerates during drying.

3.3.1.2 High HA content, high Alg concentration

After the initial batch of fabrication, HA-Alg beads were fabricated using 40 and 50 wt.% HA. A higher concentration of Alg solution (0.03 g/ml) was also used. Beads that were formed during the crosslinking process maintained their shape after drying, and were more spherical compared to beads prepared using low Alg concentration. In addition, the beads did not tend to aggregate. The

variation of HA content between 40 and 50 wt.% did not yield any significant change in size. The size of the beads was measured to be 1.4 mm. This value was slightly smaller than beads formed using low Alg concentration, which could be attributed to better crosslinking within the Alg polymer chains.

Some HA-Alg beads were crushed and examined using FE-SEM. The internal morphology of the beads revealed specks of HA embedded within the Alg matrix (Figure 3.3). EDS analysis confirmed that the grey areas consisted mainly of carbon and oxygen whilst the brighter specks contained calcium and phosphorus. The HA distribution within the matrix was homogeneous, with no obvious aggregation of HA particles being observed in any part of the bead.

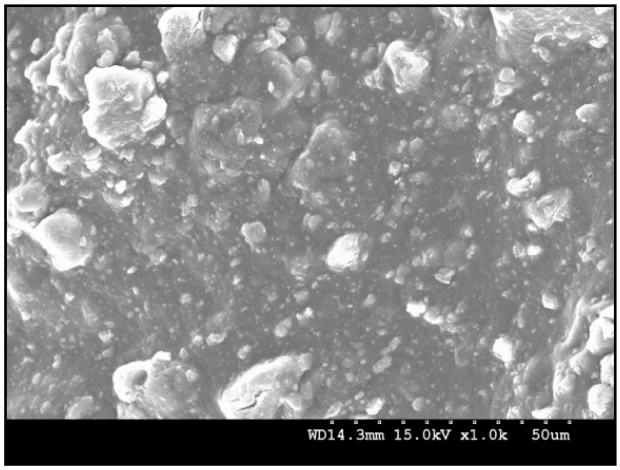

Figure 3.3. SEM micrograph of crushed pre-sintered HA-Alg microcarrier (50 wt.% HA, 0.03 g/ml Alg) to show internal morphology

3.3.1.3 Effect of CaCl2 concentration

To investigate the effect of $CaCl_2$ concentration on bead formation, two batches of HA-Alg suspension (40 wt.% HA, 0.03 g/ml Alg) were extruded into crosslinking solution of 0.1 and 0.5 M $CaCl_2$, respectively.

HA-Alg beads prepared using 0.1 M $CaCl_2$ demonstrated pits and furrows (Figure 3.4a). When a higher concentration of 0.5 M $CaCl_2$ was used, none of the beads exhibited pits (Figure 3.4b). This phenomenon suggested that using a low concentration of $CaCl_2$ could result in incomplete crosslinking of the beads. Beads prepared using 0.1 or 0.5 M $CaCl_2$ had an average size of 1.4 mm.

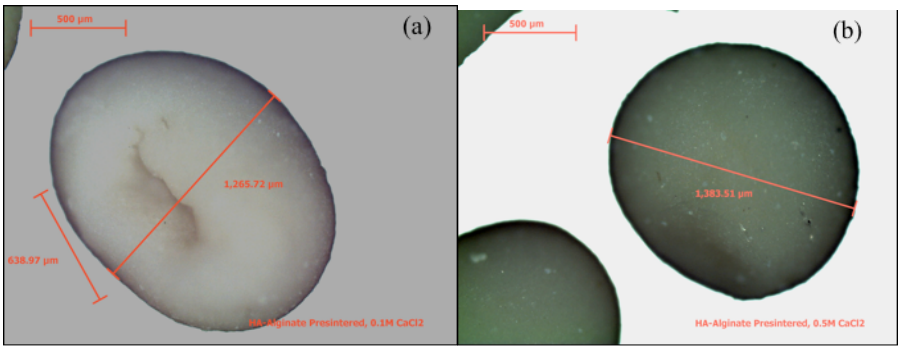

Figure 3.4. Pre-sintered HA-Alg microcarriers fabricated using (a) 0.1 M and (b) 0.5 M $CaCl_2$ crosslinking solution

3.3.2 Thermal analysis

To investigate the thermal stability of HA-Alg beads, TGA (Figure 3.5a) and DTA (Figure 3.5b) were conducted for beads containing 40 wt.% HA and 0.03 g/ml Alg. The HA-Alg beads lost 60 % by weight in total during the sintering process from 23 to 1200 °C. Weight loss occurred almost immediately at 50 °C, and continued all the way to about 1000 °C. The first major weight loss occurred at 200 °C, which registered a weight change of approximately 35 %. This corresponded to the rupture of the Alg monomers as well as the removal of water within the Alg beads. A second weight loss occurred approximately 400 °C, which accounted for 20 % weight loss. A third weight transition occurred at 640 °C, which accounted for a 5 % weight loss. The second and

third weight losses could be due to the thermal decomposition of sodium and calcium Alg complexes to intermediate compounds and subsequently, breakdown of these intermediates to metal oxides. The suggested mechanisms were as follows[18]:

At temperature ≤ 200 °C,

$$C_{12}H_{14}O_{11}M.xH_2O \rightarrow C_{12}H_{14}O_{11}M + xH2O$$

At temperature > 200 °C,

$$C_{12}H_{14}O_{11}M + 10CO_2 \rightarrow M(COO)_2 + 10CO_2 + 7H_2O$$

At temperature > 350 °C,

$$M(COO)_2 \rightarrow MO \text{ (metal oxide)} + 2CO_2$$

The stages of decomposition were supported using the DTA graph. The initial drop in energy value up to 82 °C was an endothermic process, which could be explained by the absorption of energy by the beads to break the bonds needed for the liberation of water molecules. A small peak observed at around 200 °C corresponded to the stage where the HA-Alg broke down into an intermediate metal-oxalate. Subsequently, the strong exothermic peak at 420 °C corresponded to the third stage where the metal-oxalate began to form the more stable metal oxide. Beyond 1000 °C, no further weight change occurred, and the sample remained stable up to 1200 °C.

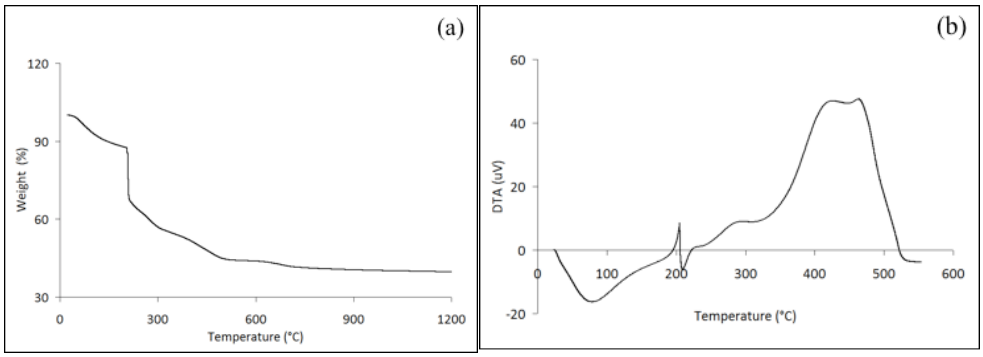

Figure 3.5. Thermal analyses of HA-Alg microcarriers (40 wt.% HA, 0.03 g/ml Alg). (a) TGA graph, and (b) DTA graph

3.3.3 Sintered apatite microcarriers

HA-Alg microcarriers containing 40 wt.% HA and 0.03 g/ml Alg were sintered using a 4-stage sintering profile (Figure 3.2). SEM image (Figure 3.6a) revealed that the sintered microcarriers displayed good spherical morphology, with a mean diameter of about 1 mm. Some microcarriers displayed occasional surface cracks. The cross-sectional view demonstrated that these microcarriers displayed high interconnectivity, and HA necking regions were clearly visible (Figure 3.6b). Distinct micropores could also be observed. Similar to the surface, the inner core displayed highly packed, interconnected HA structure that was rough and porous.

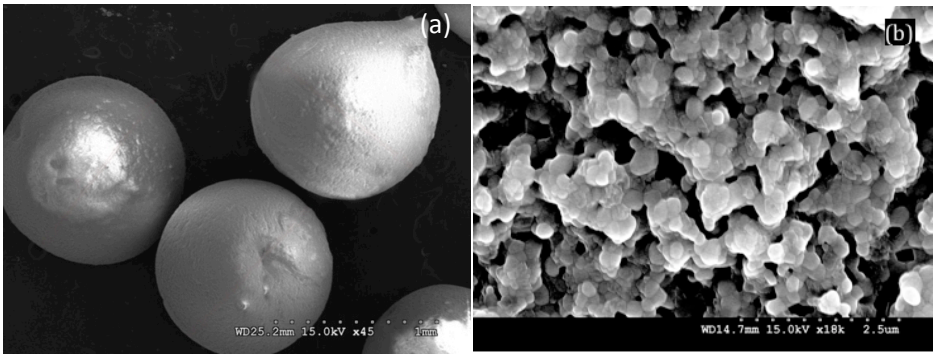

Figure 3.6. Sintered apatite microcarrier (40 wt.% HA, 0.03 g/ml Alg). (a) Normal view, and (b) Cross-sectional view

3.3.4 XRD analysis

XRD was done for the autoclaved HA powder, and sintered apatite microcarriers containing 40 wt.% HA (Figure 3.7). The results were then compared with the standard XRD patterns of HA (JCPDS 9-432). All the peaks corresponded to that of apatite. The peaks obtained for the sintered microcarriers were well-defined and distinct, indicating that apatite had a good crystalline phase. By comparing the XRD patterns of the sintered microcarriers with the HA powder that was used to synthesise the microcarriers, it could be seen that after sintering, the peaks obtained from the microcarriers represented a more crystalline phase, suggesting that an increase in temperature increased the amount of crystallinity. Phases corresponding to tricalcium phosphate and tetracalcium phosphate were not observed, confirming that HA in the microcarriers remained chemically stable during the sintering process.

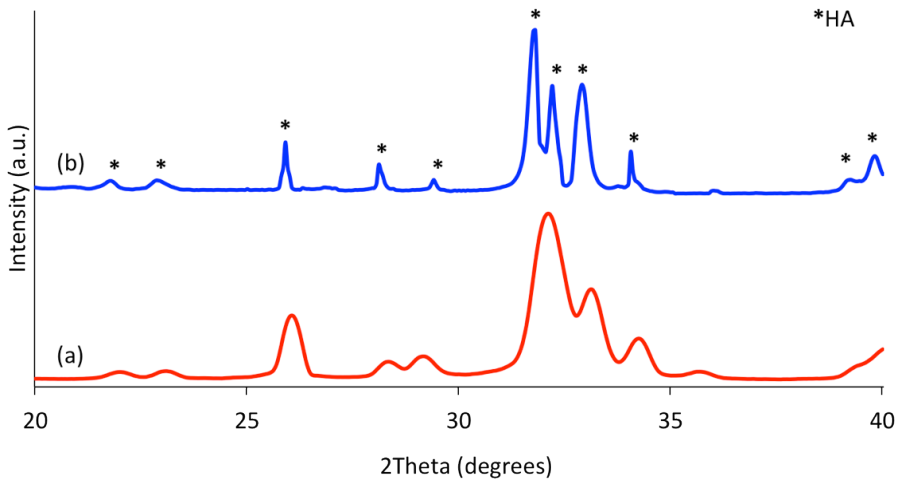

Figure 3.7. XRD patterns of (a) as-synthesised apatite powder and (b) sintered apatite microcarriers. Asterisks indicate phases of apatite

3.3.5 FTIR analysis

FTIR was conducted for the as-synthesised apatite powder, and sintered microcarriers containing 40 wt.% HA (Figure 3.8). Table 3.2 lists the band assignments of the spectra. For the apatite microcarriers, sharp bands at 567, 603 and 632 cm^{-1} were detected and corresponded to the v_4 phosphate bands. These peaks were also present in the autoclaved HA powder, but were less distinct, implying that crystallinity increased with sintering temperature. Furthermore, sharp bands at 960, 1047 and 1093 cm^{-1} were seen for both HA powder and microcarriers, which were definitive of the v_3 phosphate band, present in HA. The characteristic bands of the COO- groups at 1318, 1420 and 1619 cm^{-1} as well as the –CCH group at 809, 903 and 945 cm^{-1} were absent, indicating that there was no significant contamination of Alg residues being present[19]. Referring to HA powder, the broad band at 3500 cm^{-1} suggested that there were inclusions of water as well as structural hydroxyl group. Upon sintering, this band resolved into a sharp peak at 3571 cm^{-1}, which could be seen for the sintered microcarriers. This peak was the characteristic band for hydroxyl stretching.

Bands present at 875, 1423, 1454 and 1641 cm^{-1} corresponded to the presence of a carbonate phase, implying that carbonate had been incorporated into the HA structure. This effect could be due to the decomposition of Alg whereby carbonate ions substitute for either phosphate groups or hydroxyl group.

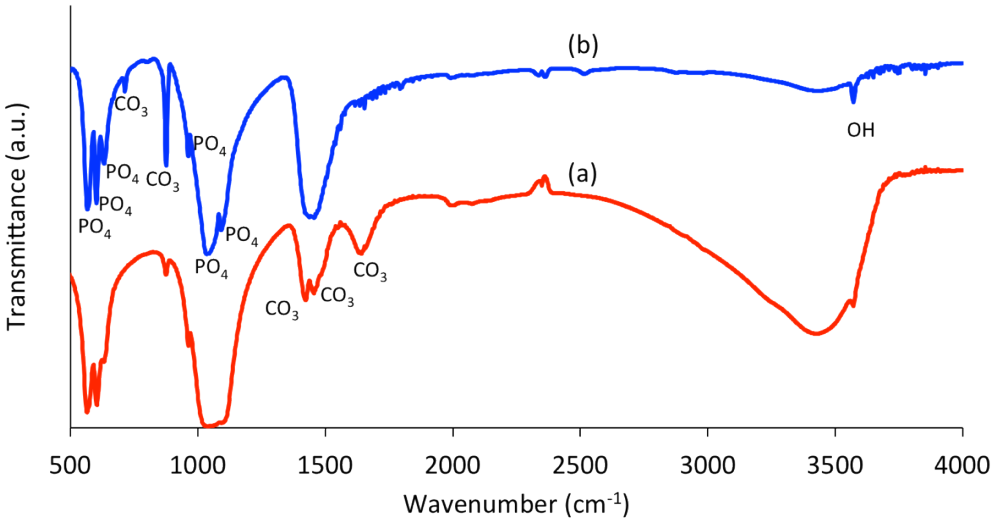

Figure 3.8. FTIR spectra of (a) as-synthesised apatite powder and (b) sintered apatite microcarriers. Bands of phosphate and carbonate are labelled.

Table 3.2. FTIR band assignments

Peak assignment	**HA (Reference)**	**As-synthesised powder**	**Sintered microcarriers**
Hydroxyl Stretch	3571	3000 – 3800	3572
Carbonate ν_3	1650	1454	1454
	1417	1423	-
Phosphate ν_3	1091	-	1093
	1041	1047	1047
Phosphate ν_1	961	960	960
Carbonate ν_2	873	876	876
Phosphate ν_4	629	629	633
	603	604	604
	567	567	567

3.4 Discussion

During the fabrication of apatite microcarriers, Alg concentration, HA content and $CaCl_2$ were factors that affected the overall morphology of the microcarriers. A low Alg concentration (0.01 g/ml) resulted in insufficient HA encapsulation and excessive water loss during the drying process would cause the microcarriers to agglomerate and flatten. Increasing Alg concentration increased microcarrier integrity during drying. Apatite microcarriers formed using 0.03 g/ml Alg was found to be the optimal concentration as the microcarriers that resulted after drying were well rounded. Next, low HA content (20 wt. %) resulted in microcarriers that were inhomogeneous as HA were not evenly distributed throughout the microcarrier. This caused the sintered apatite microcarriers to have an irregular shape with large variation in size. By increasing HA content to 40 wt.%, apatite particles seemed well distributed, and the resultant sintered microcarriers have a generally spherical shape. An important point to note would be that as Alg concentration and HA content increased, viscosity of the HA-Alg increased, and this would lead to an increase in the incidence of tube occlusions. The authors have found that 0.03 g/ml Alg and 40 wt. % HA represented the optimal parameters for obtaining spherical sintered apatite microcarriers with minimal risks of tube occlusions.

$CaCl_2$ concentration determined the extent to which crosslinking occurred during the gelation process. A low $CaCl_2$ concentration (0.1 M) resulted in insufficient Ca^{2+} ions available for crosslinking, causing apatite microcarriers to have deep furrows and pits, which would result in high susceptibility to

brittle fracture during the sintering process. Using a 0.5 M $CaCl_2$ eliminated this effect, and the stronger crosslink produced during ionotropic gelation promoted denser HA particle-particle packing, thus creating greater necking during the sintering process. This would be beneficial towards maintaining structural integrity of the sintered apatite microcarriers.

TGA analysis identified the different stages in which decomposition of the Alg occurred. By designing a multi-stage sintering profile, sufficient time would be allowed for the different reactions to take place. This would be crucial in obtaining pure apatite microcarriers with minimal impurities. Furthermore, by allowing sufficient time at the hold temperatures, defects and cracks in the sintered apatite microcarriers could be minimised.

While $CaCl_2$ concentration and sintering profile could be controlled to minimise crack formation, occasional surface cracks can be observed after sintering. This could be attributed to non-homogenous cooling experienced by the microcarriers during sintering. The outer surface of the microcarrier may be undergoing greater contraction due to more rapid cooling compared to the inner core of the microcarrier. The uneven contraction causes tensile forces to be experienced at the outer surface and this causes a crack to be formed at the surface. As the microcarrier cools further, stress concentration at the crack tip causes it to propagate inwards, but this does not extend all the way to cleave the sphere in half. This is because past the halfway point of the sphere, the area of the sphere away from the crack is in compression, thus arresting the crack as it progresses. Furthermore, with the presence of pores in the

microcarrier, random cracks are inevitable because voids within the microcarrier act as stress amplifiers, placing some areas in greater stress than others when a force is applied. As the size and shape of each individual void cannot be completely controlled, the presence of any adnormally large pore could cause the microcarrier to fail by brittle fracture. One way to reduce the occurrence of this is by increasing the content of apatite used during fabrication, thus reducing pore size and density. However, since presence of pores is actually desired in a tissue engineered biomaterial, a balance has to be achieved between level of porosity required and maintaining structural integrity.

From the SEM images, the fabricated apatite microcarriers were substantially spherical, with a rough surface morphology. These, combined with the presence of an interconnected pore structure, would be beneficial towards increasing apparent surface area as well as surface energy for protein adsorption, which would enhance cellular adhesion. XRD result demonstrated that apatite microcarriers consisted of a pure apatite material, with a crystalline phase. Undesirable phases such as tricalcium phosphate or tetracalcium phosphate, which would otherwise compromise *in-vivo* stability, were not detected. FTIR analysis confirmed that all bands of the apatite microcarriers corresponded to functional groups of apatite, without any residual alginate functional groups. A phase-pure apatite material would be advantageous towards promoting osteoconductivity and its chemical similarity to the mineral phase of natural bone would address issues of biocompatibility[67]. Furthermore, apatite has low degradation rate, making it an ideal choice for a

long-term tissue engineered solution that would not only encourage bone regeneration, but also undertake part of the defect site's structural functions as the wound site heals. Its high thermal stability also makes it easily autoclavable and eliminates theneed for complex sterilization techniques.

3.5 Summary

The fabrication technique for apatite microcarriers was reported. This involved mixing HA with a solution of Alg. The suspension was then extruded via a droplet-extrusion method into a $CaCl_2$ crosslinking solution. Subsequently, the HA-Alg microcarriers were subjected to a sintering profile, to produce the sintered apatite microcarriers. Various processing parameters such as HA content, Alg concentration and $CaCl_2$ crosslinking concentration would influence the overall morphology and physicochemical characteristics of the microcarriers, and these parameters could be controlled to produce the desired apatite microcarriers. The authors proposed that a 40 wt.% HA, 0.03 g/ml Alg concentration, 0.5 M $CaCl_2$ crosslinking solution, and a 4-stage sintering profile represented the optimal parameters. SEM images revealed that the sintered microcarriers displayed a rough surface morphology with presence of interconnected pores. In addition, sintered microcarriers displayed high phase-purity as determined by XRD and FTIR analyses. These properties could be ideal for cell adhesion and proliferation.

Chapter 4

In-vitro Evaluation of Apatite Microcarriers

4.1 Introduction

Bone-related injuries and diseases are often debilitating in nature, and while it may not be as apparent as acute diseases, the development of these conditions can cause a considerable strain on healthcare resources due to the long-term care required for treatment and rehabilitation. Traditionally, bone grafts (allografts or autografts) are used for the treatment of bone defects. However, the lack of availability of suitable donors and sufficient grafts have prompted search into tissue engineering solutions to address this growing need. Most bone tissue-engineered solutions involve the use of stem cells or scaffolds, or a combination of both. In this regard, mesenchymal stem cells (MSCs) have been identified as promising stem cell candidates for bone tissue-engineered applications. MSCs are rare multipotent cells, which are readily isolated and expanded from bone marrow, with a well-defined osteogenic differentiation pathway [114], and demonstrated great potential for tissue engineering applications [115]. Existing expansion technique based on culture flasks requires trypsin-mediate multiple passages of monolayer cells to achieve cell numbers. This method is certainly costly, time-consuming, and susceptible to contamination due to numerous passages needed to generate sufficient cells for transplantation. Furthermore, the removal of extracellular matrix laid down during stem cell expansion by repeated trypsinisation is likely to lead to reduced intra-cellular signalling responsible for cell viability, proliferation and differentiation [8]. Thus, microcarriers that provide a high surface area for cell

attachment has generated great interest nowadays[116-118]. The currently available microcarriers are made of polymers or glass-based matrices[9, 119], mainly designed and developed for *in-vitro* applications in pharmaceutical industries, and may not be suitable for therapeutic implantation. Certainly, the need for such technology is potentially huge.

Here, the use of apatite microcarriers as an alternative to conventional cell culture methods is featured. These novel biomaterials offer the advantage of a high surface area to volume ratio, which can be utilised in dynamic culture conditions for higher cell yield. In addition, the physiochemistry of the microcarriers make it particularly relevant for bone tissue engineering applications, where MSCs can be expanded, differentiated and implanted in a one-step solution to heal bone defects. The purpose of this work is to assess the cytocompatibility of the synthesised apatite microcarriers, but culturing human foetal mesenchymal stem cells (hfMSCs) on the microcarriers *in-vitro*. In addition, the osteogenic potency of the cell loaded apatite microcarriers will also be compared with conventional monolayer culture.

4.2 Materials and methods

4.2.1 hfMSC isolation

Single-cell suspension of foetal bone marrow are prepared by flushing the marrow cells out of humeri and femurs using a 22-gauge needle into Dulbecco's modified Eagle's medium (DMEM, Sigma, USA)-GlutaMAX (GIBCO, USA) supplemented with 10 % foetal bovine serum (FBS), 50 U/ml penicillin, and 50 mg/ml streptomycin (GIBCO, USA) (referred as D10 medium), and then plated onto 100 mm diameter dishes at 10^6 mononuclear

cells/ml in D10 medium. Media is changed every 2 - 3 days, and non-adherent cells are removed, and sub-cultured at $10^4/cm^2$ to sub-confluence. hfMSCs at passage 3 are used in this study.

4.2.2 Cytocompatibility study

Eighteen milligrams of apatite microcarriers and 3.7 mg of Cytodex 3 microcarriers (GE Healthcare, USA) is added to each well. The calculation of weights to be used is based on the total surface area added per well. For the apatite microcarriers, this was 0.55 cm^2/mg, and 2.7 cm^2/mg for Cytodex 3. This allows for the total surface area per well of each microcarrier type to be 10 cm^2. 1.0 x 10^5 cells are then added to each well, such that the seeding density for both microcarrier type is 1.0 x 10^4 cells/cm^2. For the adherent monolayer culture, 1.0 x 10^4 cells are added to each 24-well plate such that seeding density is 5.0 x 10^3 cells/cm^2. The difference in seeding density between microcarrier culture and the adherent monolayer culture is to account for the low seeding efficiency of the microcarriers under static conditions, such that after 24 h, cells attached on all three surfaces are of similar density. Cell viability was assessed quantitatively using PrestoBlue assay (Invitrogen, USA), which measures cell viability through the reduction of resazurin to resorufin. On the designated time points, 10 % PrestoBlue reagent is added to each well and incubated for 25 min at 37 °C. Each time point is measured in triplicates. Absorbance at 570 nm, referenced at 600 nm is read using a microplate reader (Tecan, USA). The intensity cross-referenced to a standard calibration curve of MSC count against absorbance done at the beginning of the study to obtain the live cell count at each time point.

The qualitative analysis of cell viability on apatite microcarriers is performed by fluorescein di-acetate/propidium iodide (FDA/PI) staining, where FDA stains viable cells green, and PI stains necrotic and apoptotic cell nuclei red. In this assay, hfMSCs cultured on apatite microcarriers for 1, 3, 7 and 14 days are retrieved from the well, rinsed with phosphate buffer saline (PBS) solution and incubated with 8 μg/ml FDA for 10 min. The microcarriers are then washed, and incubated with 4 μg/ml PI for 5 min followed by PBS washing for two times. Cellular behaviour is also assessed qualitatively by examining the cytoskeletal network for any abnormalities. In this assay, hfMSCs cultured on apatite microcarriers at day 9 are washed with PBS solution, and fixed in 4% paraformaldehyde for 10 min. The microcarriers are then washed and permeabilised for 15 min with 0.1 % Triton X-100. The samples are again washed and blocked with 2 % bovine serum albumin for 1 h. The washed samples are then washed, and stained with 1:500 TRITC-conjugated phalloidin. After washing, the samples counterstained with 1:1000 4'-6-diamidino-2-phenylindole (DAPI) for 5 min to visualize the nucleus. Samples are finally viewed under a confocal laser-scanning microscope (CLSM, Olympus FV1000).

4.2.3 Osteogenic differentiation study

On day 7 of cell culturing, hfMSCs cultured on both apatite microcarriers and the adherent monolayer are induced to differentiate down the osteogenic lineage by replacing the D10 medium with bone induction media (D10 medium supplemented with 10 mM β-glycerophosphate, 10^{-8} M dexamethasone and 0.2 mM ascorbic acid). Media is changed every 2 - 3 days.

Alkaline phosphatase (ALP) plays a key role in signal transduction and cellular modulations. ALP is measured using SensoLyte pNPP Alkaline Phosphatase Assay Kit (AnaSpec USA). hfMSCs cultured on both apatite microcarriers and the adherent monolayer are lysed using the provided lysis buffer and Triton X-100. The cell suspension is incubated at 4 °C for 10 min under agitation and centrifuged at 2500 rpm for 10 min. The supernatant collected is then used for ALP assay. The level of ALP activity is determined by absorbance measurements at 405 nm using p-nitrophenyl phosphate (pNPP). ALP level is normalized to the total cell count.

As the primary organic constituent of bone, type I collagen level has been linked to bone growth and formation. A MicroVue CICP EIA Kit (Quidel, USA) is used to quantitatively determine the levels of C-Terminal of type I collagen (CICP) released into the media by the cells. Seventy two hours after each media change, the media of each sample is drawn and diluted 1:12 with the assay buffer. They are then added to coated strips of purified murine monoclonal anti-CICP antibody and incubated for 120 min at 25 °C. Wells are washed twice with the wash buffer and rabbit anti-CICP is then added to each well, and incubated for another 45 min at 25 °C. Wells are washed 3 times, before adding the lyophilized goat anti-rabbit IgG antibody conjugated to alkaline phosphatase and incubated for another 45 min at 25 °C. After washing for 3 times, a working substrate of pNPP dissolved in a diethanolamine and magnesium chloride solution is added to each well and incubated for 30 min at 25 °C. Finally, a solution of 0.5 N NaOH is added to stop the reaction and the optical density at 405 nm is read using the microplate reader. The intensity

obtained from the samples is compared to a calibration curve obtained using known CICP standards to determine the concentration of CICP in the samples. CICP values are normalised to total cell count.

During mineralisation, cells convert calcium ions from the surrounding media into insoluble apatite, which is deposited as extra cellular matrix (ECM). The amount of calcium ions that the cells take up from the surrounding media can thus be measured to determine the level of mineralisation. Calcium ions in the samples are quantified using a QuantiChrom calcium assay kit (BioAssay Systems, USA). Samples are diluted and incubated with a phenolsulphonephthalein dye which forms stable blue coloured complex specifically with free calcium in the sample. After the incubation, the intensity of the colour is then measured at 575 nm and calcium concentration is calculated with a standard curve. Control cell-free apatite microcarriers are used as negative controls. Calcium uptake is then calculated by recording the initial amount of calcium concentration from the bone induction medium, and subtracting it by the calcium concentration of the sample. Calcium uptake is normalised to total cell count.

4.2.4 Statistical analysis

Data from each time point is obtained in triplicates. All the data have been represented as mean ± standard deviation, and compared using either two-way ANOVA or student *t*-test. A value of $p < 0.05$ or $p < 0.01$ or $p < 0.001$ is taken as significant.

4.3 Results

4.3.1 Proliferation and viability of hfMSCs

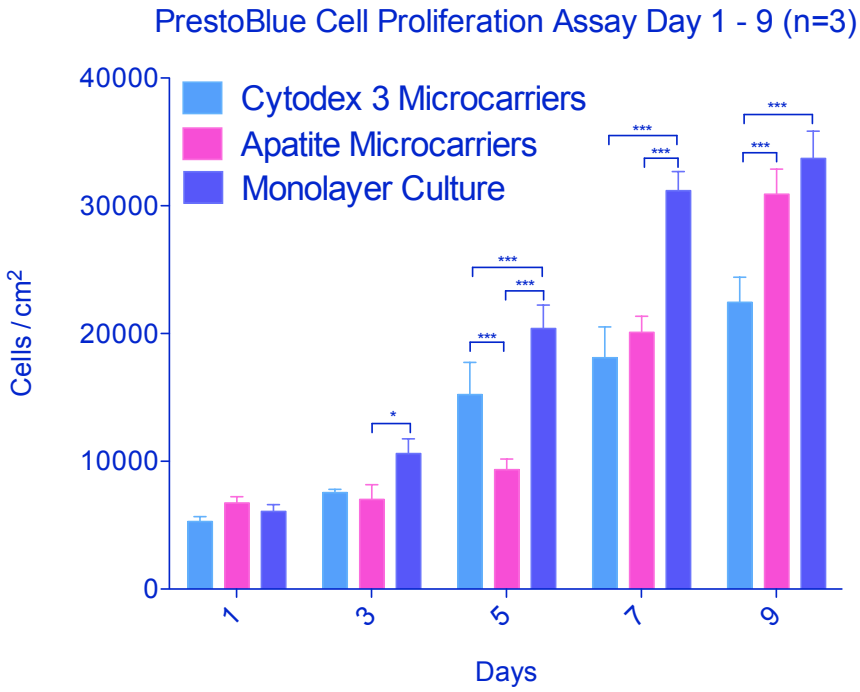

Figure 4.1. PrestoBlue proliferation assay of hfMSCs cultured on Cytodex 3, apatite microcarriers and on conventional monolayer culture (*p < 0.05, ***p < 0.001)

PrestoBlue cell viability (Figure 4.1) showed that after 24 h, attachment of hfMSCs on apatite microcarriers was 67 %, compared with 50 % for Cytodex 3 microcarriers. Log expansion phase was achieved between day 3 and 5 for adherent monolayer culture and Cytodex 3 microcarriers, and between day 5 and 7 for apatite microcarriers. Proliferation of hfMSCs on apatite microcarriers was slower between day 3 and 5 when compared to Cytodex 3 microcarriers although apatite microcarriers achieved a 1.4-fold higher cell count at day 9.

FDA/PI staining observed through CLSM (Figure 4) demonstrated that as the hfMSCs proliferate, they remained largely viable throughout the days in culture. Actin staining of hfMSCs cultured on apatite microcarriers was conducted on day 7 (Figure 5a) and day 9 (Figure 5b). Through CLSM, cells resembled a spindle-like morphology; with actin filaments aligned along the curvature of the apatite microcarriers. By day 9, extensive cell bridging across microcarriers could be observed.

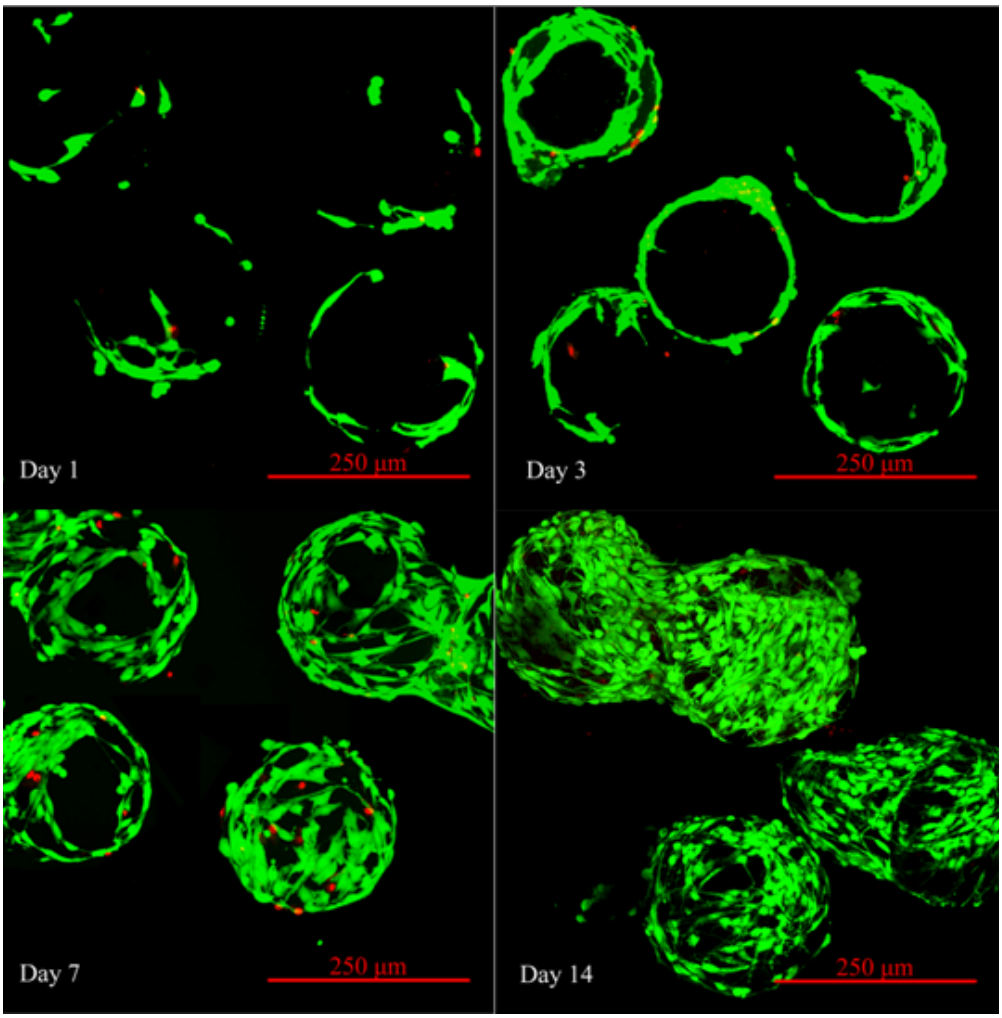

Figure 4.2. CLSM images of hfMSCs cultured on the apatite microcarriers at day 1, 3, 7 and 14. FDA/PI staining was used. Live and dead cells were stained green and red, respectively.

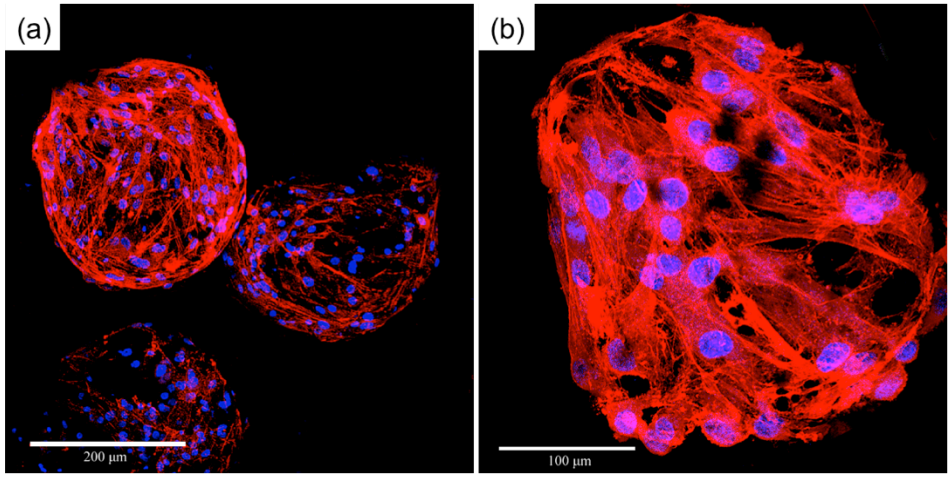

Figure 4.3. Phalloidin-DAPI staining of hfMSC loaded apatite microcarriers. Actin filaments were stained red, and nuclei stained blue. (a) Image showing extensive cell coverage over the entire carrier. Actin filaments were aligned along the curvature of the microcarrier, demonstrating good cell adhesion characteristics. (b) Image of a 3-microcarrier aggregate. Cells tended to form bridges across each other, creating an interconnected network between microcarriers

4.3.2 Osteogenic potency of hfMSCs

The osteogenic potential of hfMSCs seeded on apatite microcarriers was investigated. Alkaline phosphatase (ALP) activity, type I collagen production and calcium uptake were measured at various time points, and compared to the adherent monolayer culture. Results (Figures 4.4a-c) demonstrated that the osteogenic potential of hfMSCs seeded on apatite microcarriers was enhanced as compared to that of the adherent monolayer culture. On day 12, ALP expressed by hfMSCs seeded on the apatite microcarriers continued to increase, while those seeded on the adherent monolayer culture declined sharply after day 9 (Figure 4.4a). Type I collagen production on apatite microcarriers was higher at all time points, and production level continued to rise after day 9 (Figure 4.4b). Osteocalcin expression by hfMSCs seeded on apatite microcarriers exhibited a similar trend, while the adherent monolayer

culture remained low after an initial increase at day 3 (Figure 6c). On day 12, hfMSCs seeded on apatite microcarriers exhibited 1.8 - and 1.5-fold increase in type I collagen production and osteocalcin, respectively, relative to the adherent to the adherent monolayer culture. Apatite microcarriers without hfMSCs (acting as a control) immersed in BM was maintained throughout the days in culture, and no significant change in ALP, type I collagen and osteocalcin levels ($p > 0.05$) were detected.

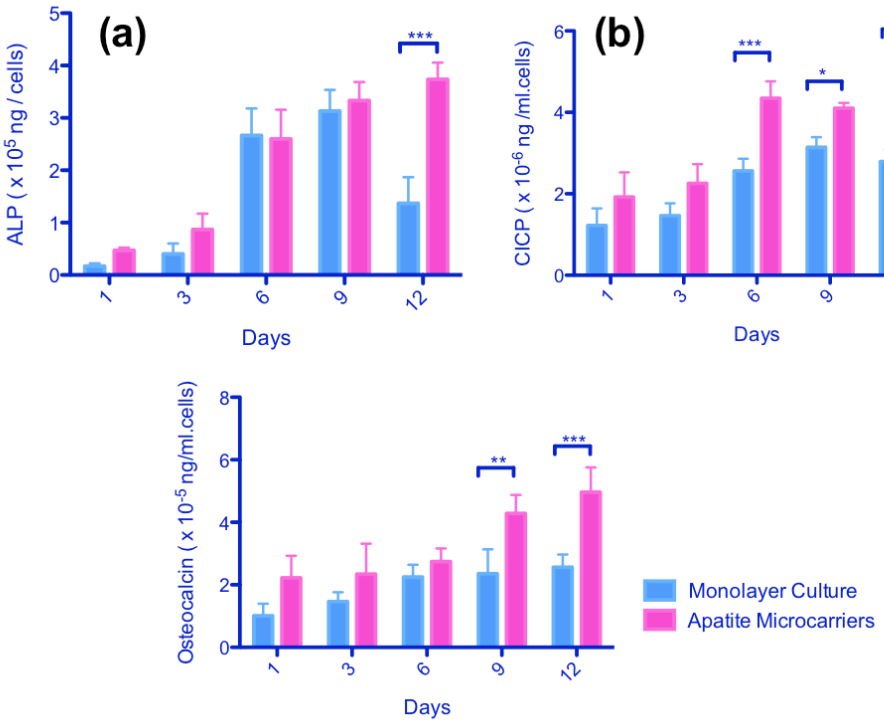

Figure 4.4. (a) ALP assay was performed on adherent monolayer culture and apatite microcarriers. On day 12, ALP expression for hfMSCs cultured on the apatite microcarriers was 2.7-fold higher than that of the adherent monolayer culture. (b) Collagen type I synthesis was measured. hfMSCs cultured on the apatite microcarrier produced greater amount of collagen type I throughout the culture days. (c) Osteocalcin in BM was measured. Osteocalcin expression was the highest for hfMSCs cultured on apatite microcarriers. (*$p < 0.05$, **$p < 0.01$, ***$p < 0.001$). Osteocalcin for control (not shown) was statistically insignificant ($p > 0.05$).

4.4 Discussion

One major obstacle in translating tissue-engineered solutions involving stem cell therapy from bench to bedside is the sheer number of cells required for successful transplantation. A dose of 3 - 5 x 10^7 cells/patient is needed to treat patients with advanced multiple sclerosis [6] whilst 5.7 - 7.5 x 10^8 cells/kg is required for the treatment of osteogenesis imperfecta [7]. The conventional technique to achieve such cell numbers involves the expansion of cells on monolayer tissue culture flasks. Given that a standard T-175 flask is able to yield only 3.5 - 5 x 10^6 hfMSCs at confluency, considerable resources have to be spent on cell medium, flasks and incubators, making such a method neither efficient nor economically feasible. Moreover, at the cellular level, 2D culture is insufficient to ensure proper cellular behaviour. Thus, it is necessary to develop suitable biomaterials with the appropriate biomolecular cues that can mediate and facilitate the response and efficacy of stem cells to their intended function.

On the first issue, microcarriers offer an attractive alternative to conventional adherent monolayer culture due to their superior surface area to volume ratio. This, combined with the use of bioreactors, allows for a rapid and efficient mass production of cells required for stem cell therapy. To address the second issue, it is necessary to consider the specific application that the biomaterial is intended for. In the case of bone tissue engineering, apatite-based biomaterials are ideal candidates because of their close chemical similarity to the mineral phase of bone, and beneficial properties of excellent bioactivity and osteoconductivity.

By developing apatite microcarriers, an implantable stem cell-seeded microcarrier system for treating bone defects is possible. These microcarriers provide a 3D microenvironment with high surface area to volume ratio for cell adhesion and proliferation. When used in combination with dynamic culture techniques, this cell culture technique simulates the natural *in vivo* conditions of cells[120, 121]. Furthermore, by being apatite-based material, stem cells seeded on these microcarriers can be induced to differentiate down the osteogenic lineage *in situ*, and injected directly into the defect site without the need for further treatment. This method not only represents a significant reduction in steps needed for stem cell therapy, but also presents a non-invasive solution for treating bone defects, thus reducing risks of infections and inflammations.

In-vitro studies have thus far shown that hfMSC attachment for the apatite microcarriers is 1.3-fold higher as compared to Cytodex 3 (a collagen I-dextran based) microcarriers. The disparity in hfMSC attachment may be attributed to several reasons. For apatite, the mechanism underlying cellular attachment is governed by the material. When immersed in biological fluids, calcium and phosphate ions are released, thereby increasing the degree of saturation in the culture medium. This effect will facilitate the reprecipitation of CaP layer, which will then incorporate other organic macromolecules from the biological fluids. The formation of such a layer will be the initial step towards cell attachment.

On the other hand, cellular attachment on collagen I differs somewhat. For collagen, a direct integrin binding to the collagen ligand is involved. hfMSCs may express the kind of integrins, which will result in collagen-specific binding. This is because fibronectin-ligand receptor integrin types on hfMSCs are present in greater in amounts as compared to type I collagen specific ones[122, 123]. Already, fibronectin has been identified to promote greater hfMSC adhesion than type I collagen[124]. Apatite materials will thus be advantageous in this case due to its ability to absorb proteins from the serum, which includes fibronectin[125, 126].

An apatite material with rough surface will further enhance the cellular adhesion. In a study conducted by Santos *et al.,* results indicated that nano-topography of CaP samples strongly affected the protein adsorption process [127]. As such, a rough will increase the adsorption of fibronectin, which then leads to greater hfMSC attachment over the smooth, polymeric microcarriers. This has been confirmed in this study. From the FDA/PI and PrestoBlue results, proliferation and viability of hfMSCs seeded on apatite microcarriers were assessed. Through CLSM, hfMSCs appeared to be largely viable throughout the culture days, suggesting that the material composition of the apatite microcarriers had little or no cytotoxic effects. This was further confirmed through PrestoBlue results, showing that cell proliferation on apatite microcarriers was 1.4-fold higher than that of Cytodex 3 microcarriers, by day 9.

Although adherent monolayer culture resulted in the highest proliferation of hfMSCs, apatite microcarriers could have yielded higher cell numbers per unit volume of media used. Apatite microcarriers were able to yield 3.3 x 10^5 cells/ml, while conventional adherent monolayer culture flasks were only able to yield approximately 1.5 x 10^5 cells/ml. This translates to a 2.2-fold increase in cell yield for apatite microcarriers, compared to monolayer culture flask. In this regard, apatite microcarriers offers higher cell yield while requiring less space and cell medium.

To evaluate if the apatite microcarriers could be used for bone regenerative applications, the *in-vitro* osteogenic potential of hfMSCs cultured on apatite microcarriers was investigated. ALP expression of hfMSCs culture on apatite microcarriers remained high after day 12, suggesting that osteogenic differentiation and expression were maintained, thus promoting greater mineralisation of ECM. Indeed, the trend in ALP expression was closely related to collagen I synthesis and calcium uptake. In contrast, ALP expression for hfMSCs cultured on the adherent monolayer culture saw a dip after day 9, accompanied by a levelling off for collagen I synthesis and calcium uptake. Apatite microcarriers without cells cultured onto them did not result in any significant change in the ALP, collagen I or calcium uptake, thus confirming that hfMSCs were the main contributors to the indicators of osteogenic potency.

The information obtained from the *in-vitro* evaluation of apatite microcarriers are in agreement with studies, which have shown that hfMSCs exhibit higher

osteogenic potency when cultured on 3D substrates that mimics the chemical and morphological structure of physiological bone mineral [128]. While the exact reason for the disparity between monolayer and microcarrier culture for osteogenic differentiation is unclear, it can be speculated that hfMSCs respond favourably to the chemical and morphological cues that the apatite microcarriers provide *in-vitro* [129]. Moreover, the adsorption of Matrix-Gla-Protein (MGP) from the serum onto apatite acts as a precursor for osteogenesis, by binding and regulating the function of bone morphogenic proteins (BMPs) [130].

It has been established that cell-matrix and cell-cell interactions are vital factors influencing cell behaviour and osteogenic potency [131]. The underpinning relationship between microporous structure and cell behaviour is not fully understood, but it is possible that the microporous architecture facilitates the building of cytoskeletal cell bridging networks. This was observed during immunoflourescent staining, where the presence of dense cell-cell connections within each microcarrier, and organisation of F-actin from the attached cell surface, would indicate that an apatite microporous structure was an appropriate substrate for hfMSC proliferation. Additionally, the size of the microcarriers played an important role in osteogenic potency of hfMSCs. Fischer *et al*. reported that small micrometre-sized apatites of diameter ~260 μm exhibit greater osteogenic potency as compared to large micrometre-sized apatites of diameter ~600 μm [112], thus supporting results presented in this study. It is plausible that the packing of the particles has created a three-dimensional microenvironment suitable for bone formation to

occur. This 3D environment created by the packing of the particles provides the macroporosity and free space required for invasion by body fluids, nutrients, host cells, and blood vessels. On day 9 of *in-vitro* culture, hfMSC-loaded apatite microcarriers tended to form aggregates of 3 carriers or more, and this was accompanied by high expression of ALP, collagen I and osteocalcin. Whether or not aggregation was a prerequisite for or consequence of osteogenic potency requires further study, but the presence of aggregation among microcarriers would indicate good osteogenic expression in hfMSCs.

4.5 Summary

Current bone tissue engineering solutions require a large dosage of stem cells, and the incorporation of a scaffold that is chemically similar to natural bone, in providing a microenvironment that mimics the *in vivo* physiological conditions. The authors have developed apatite microcarriers to address these needs. *In-vitro* cytocompatibility study of hfMSCs cultured on the microcarriers shows higher cell attachment and proliferation as compared to Cytodex 3 microcarriers. This observation indicates that apatite microcarriers have the potential for greater cell yield per unit volume. In addition, *in-situ* osteogenic differentiation of hfMSCs is supported, with cells showing greater ALP, collagen I and osteocalcin expression than that of the adherent monolayer culture. Certainly, apatite microcarriers present an effective and scalable approach for stem cell culturing.

Chapter 5

In-vivo Evaluation of Subcutaneously Implanted Apatite Microcarriers

5.1 Introduction

While the *in-vitro* assessments of apatite microcarriers have thus far been favourable in proving its feasibility as a platform for MSC culture and osteogenic differentiation, there were still significant gaps before the efficacy and biocompatibility of the biomaterial could be ascertained for its application as an injectable, MSC-loaded microcarrier for bone tissue engineering applications.

Firstly, *in-vitro* osteogenic potency assays were limited to studies of expression of specific protein markers for osteogenesis, which does not necessarily prove its *in-vivo* bone formation capacity. Furthermore, *in-vitro* studies involving just MSCs did not take into account the various cell types that are involved with *in-vivo* osteogenesis, and their associated biomolecular processes. As mentioned in Section 2.1, bone healing and formation is a complex biological process involving both extrinsic and intrinsic biological factors orchestrated in a specific sequence. The *in-vitro* study could not truly replicate the *in-vivo* diversity of cell types and provide the physical, mechanical and biological microenvironment that simulates the conditions at the defect site. Finally, *in-vitro* studies of the apatite microcarriers were limited to studies of cytocompatibility, which were not a true reflection of the biocompatibility of the biomaterial. The host-tissue interaction following

implantation has to be conducted in an *in-vivo* environment so as to assess the host's immune response to the biomaterial. While certain indicators of undesirable cell response or release of harmful products can be obtained from studies of *in-vitro* cytotoxicity, several other responses such as macrophage activity, cytokine release and formation of granulation tissue cannot be replicated in an *in-vitro* setting. Moreover, long-term biocompatibility issues such as tissue necrosis and fibrous tissue encapsulation cannot be anticipated by *in-vitro* studies.

For these reasons, it is necessary to conduct *in-vivo* studies to assess the apatite microcarrier's capacity for bone regeneration, the host tissue response to MSCs, as well as overall biocompatibility. Several *in-vivo* models have been established in assessing osteogenic potency and biocompatibility. Small animal studies such as mice, rats, and guinea pigs represent the very first step towards predicting clinical performance of biomaterials. The advantages of using these animals are their ease of availability, low husbandry requirements and low costs associated with holding the animals. In bone tissue engineering applications, their high bone turnover rates also make it particularly attractive by allowing for faster product development cycles. Medium (e.g. rabbits) and large animal (e.g. cows, sheep) represent an incremental approach towards obtaining relevant pre-clinical information, which would accurately predict its performance in the patient. These animals provide better representation of the human physiological processes, and would allow for more surgically appropriate techniques to be implemented so as to assess the biomaterial's ease of application.

In summary, *in-vivo* studies are indispensible in biomaterial development. Individually, no one animal model can simulate an exact representation of the human system, but together, they bridge the gap in determining clinical performance of the product. For the purposes of this report, focus will be on the small animal *in-vivo* assessment of the apatite microcarriers, although medium animal and large animal studies should be considered in its subsequent development.

5.2 Materials and methods

5.2.1 Samples, animals and ethics

Foetal tissue collection was approved by the Domain Specific Review Board of National University Hospital (DSRB-D-06-154), Singapore in compliance with international guidelines regarding the use of foetal tissue for research[132]. Pregnant women gave separate written consent for the clinical procedure and for the use of foetal tissue for research purposes. And foetal tissues were collected from foetuses after clinically indicated termination of pregnancy. Foetal gestational age was determined by crown-rump length measurement. Two foetal samples at 10^{+6} and 14^{+2} (weeks + days) gestations were utilized for this study.

Six to eight weeks old immunodeficient female NOD/SCID mice were acquired through Jackson Labs, and all procedures were approved by the Institutional Animal Care and Use Committee (IACUC) at National University of Singapore. All materials used were purchased from Sigma–Aldrich (Singapore) unless otherwise stated.

5.2.2 Isolation and characterisation of hfMSCs

hfMSC was isolated through plastic adherence, and culture expansion, and characterized through immunophenotyping, colony-forming capacity and tri-lineage differentiation into osteoblasts, adipocytes and chondrocytes as previously described. Briefly, single-cell suspensions of foetal bone marrow were prepared by flushing the marrow cells out of humeri and femurs using a 22-gauge needle into Dulbecco's modified Eagle's medium (DMEM, Sigma, USA) eGlutaMAX (GIBCO, USA) supplemented with 10% foetal bovine serum (FBS), 50 U/ml penicillin, and 50 mg/ml streptomycin (GIBCO, USA) (referred as D10 medium), and then plated onto T-175 flasks at 10^6 mononuclear cells/ml in D10 medium. Media was changed every 2-3 days and non-adherent cells were removed, and sub-cultured at $10^3/cm^2$ to sub-confluence (Day 1 to day 7). hfMSCs at passage 3 were used in this study.

5.2.3 Microcarrier Culture

20 mg of apatite microcarriers were weighed and washed with PBS (Mg^{2+}, Ca^{2+} free) two times. They were then sterilised by autoclaving at 121°C for 20 minutes. Before use, the microcarriers were soaked in 12 ml D10 medium 2 hours at 37°C. For microcarrier culture, non-adherent 6-well plates were used. The carriers were then separated to 6 wells containing 2 ml of apatite microcarriers each. Cells were seeded with a density of 5 $x10^5$ cells per well. The initial seeding regime consists of an agitation phase using a rocker device for 5 minutes, followed by a rest phase of 25 minutes. This process was conducted for another 3 hours, after which the well plate was placed in an incubator at 37°C, 5% CO2 and 95% humidity.

In-vitro culture of the cell-loaded microcarriers is conducted in two phases: expansion and pre-differentiation. In the expansion phase (Day 7 to 14), cells were cultured in D10 medium, and medium changed every 2 – 3 days. Cell medium was then changed to bone induction medium (D10 supplemented with 10mM β-glycerophosphate, 10 nM dexamethasone and 0.2 mM ascorbic acid) and cultured for another 14 days (Day 14 to 28) with medium changed every 2 – 3 days (Figure 5.1).

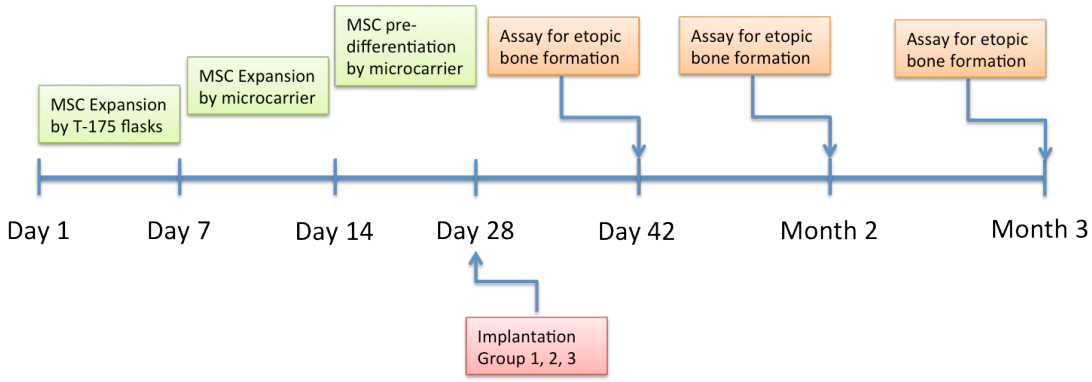

Figure 5.1. Experimental time line for the *in-vivo* study of hfMSC-loaded apatite microcarriers.

Days 1 through 28 represented the pre-implantation stage, involving expansion and pre- differentiation phases. Day 42, month 2 and month 3 corresponded to the time points of 2 weeks, 1 month and 2 months post-implantation respectively.

5.2.4 *In-vivo* implantation and ectopic bone formation

Three groups of implants were prepared such that the study consisted of the following groups of implants:

Group 1: Control groups in which dorsal pockets implanted with fibrin gel only

Group 2: Fibrin gel + apatite microcarriers

Group 3: Fibrin gel + hfMSC-loaded apatite microcarriers

Ectopic bone formation was examined at on day 42, month 2 and month 3 (2 weeks, 1 month and 2 month after implantation), with a sample size of n = 5 at each time point, resulting in a total of 15 NOD/SCID mice used.

Prior to the procedure implants group 2 and group 3 was created by mixing 20 mg of apatite microcarriers (hfMSC-loaded for group 3) with 20 ul of fibrin solution. After thorough mixing, another 20 ul of thrombin solution is then added to convert the soluble fibrinogen into an insoluble mass, in accordance with the manufacturer's directions (Tisseel Kit, Baxter). Group 1 was created in a similar manner, without the addition of the apatite microcarriers. The implants were kept bathed in 37 °C D10 solution until its use is required.

Two 20 mm midline dorsal skin incisions were made (one upper and one lower dorsal midline) on anesthetized NOD/SCID mice. 4% isoflurane at 2L/min was used to induce anaesthesia, while 1 – 2% isoflurane at 2L/min was use to maintain anaesthesia. Subcutaneous pouches were produced using a sterile blunt forceps through bunt dissections. Each mouse received three implants (Groups 1 – 3), one on the upper dorsa area and two on opposite sides of the lower dorsa area. Wounds were closed with interrupted 6-O vicryl sutures. Mice were weighed pre and postoperatively to monitor weight changes, and given Caprofen as a painkiller postoperatively for three days at 5mg/kg and Enrofloxacin as an antibiotic administered twice daily for five days postoperatively at 10mg/kg. At the designated time points (Figure 5.1),

mice were euthanized using CO_2, and samples were retrieved and stored for examination.

5.2.5 Sample preparation

For histological analysis, samples were fixed in 10% neutral buffered formalin (Sigma) for 3 – 4 hours and immersed in 10% formic acid (Sigma) for decalcification overnight. After dehydration in ascending concentrations of ethanol and xylene, they were then embedded in paraffin, cut into 5 μm sections and mounted on silane-coated slides. For von Kossa analysis, the decalcification step was excluded.

For immunohistological analysis, samples were immersed in a 30% sucrose solution overnight at 4 °C for gradual dehydration, snap frozen in dry ice and stored at -70 °C prior to cryosectioning. Samples were then embedded in OCT medium (Tissue-Tek, USA), allowed to solidify at -80 °C and sectioned to 8 μm using a cryostat (Leica CM1950, Germany). Sections were then mounted on poly-L-lysine slides, and fixed with 4% paraformaldehyde for 10 min.

5.2.6 Histological analysis

Sections were deparaffinised and rehydrated using xylene and graded concentrations of ethanol. They were then washed twice and immersed in Harris haematoxylin (Sigma) for 10 minutes before blueing by rinsing in Scott's tap water (Sigma). The section was then counterstained with eosin (Sigma) and passed through graded series to ethanol to dehydrate the sample. Finally, it was cleared with xylene and mounted with DPX and closed with a coverslip.

In Masson's trichrome staining, sections were deparaffinised and rehydrated similar to the H&E staining step and mordant in Bouin's solution (Sigma) at 56 °C for 15 minutes. The slide was then rinsed in running tap water until the yellow colour was removed. Weigert's iron haematoxylin (Sigma) was then added to the slide for 5 minutes followed by a washing in deionised water. The slide was then stained with Biebrich scarlet acid fuchin solution for 5 minutes and washed with deionised water. The slide was placed in phosphotungstic-phosphomolybdic acid solution (Sigma) for 5 minutes before it is stained with aniline blue solution for 5 minutes. Finally, the slides were immersed in 1% acetic acid solution for 2 minutes, rinsed, dehydrated, cleared and mounted with a coverslip.

All slides used for H&E and Masson's trichrome were visualised using an inverted light microscope (Olympus IX83, USA) at various magnifications.

5.2.7 Immunohistological analysis

Slides were permeabilised with 2% Triton-X (Sigma) for 15 minutes, followed by a washing step with deionised water. The slides are then blocked with 5% bovine serum albumin for 4 hours and incubated at 4 °C overnight with either i) Rabbit anti- osteopontin (1:200 Abcam, USA) or ii) Rabbit anti-human osteonectin (1:200 Abcam, USA). Samples were then washed twice with deionised water and incubated with AlexFlour 594 goat anti-rabbit IgG (1:200 Life Technologies, UK). Samples are then counterstained with 4',6-diamidino-2-phenylindole (DAPI) (Life Technologies, USA) and mounted with coverslip. Stained samples were viewed under a confocal laser microscope (Olympus, FV300 Fluoview, Japan) at various magnifications.

5.2.8 Statistics

Parametric data are shown as mean ± standard deviation. Student's t-tests were carried out to determine the significance between different experimental conditions (a $p<0.05$ is considered as significant).

5.3 Results

5.3.1 Haematoxylin and eosin study

A haematoxylin and eosin (H&E) staining was conducted to examine general tissue morphology of the implanted groups (Figure 5.2).

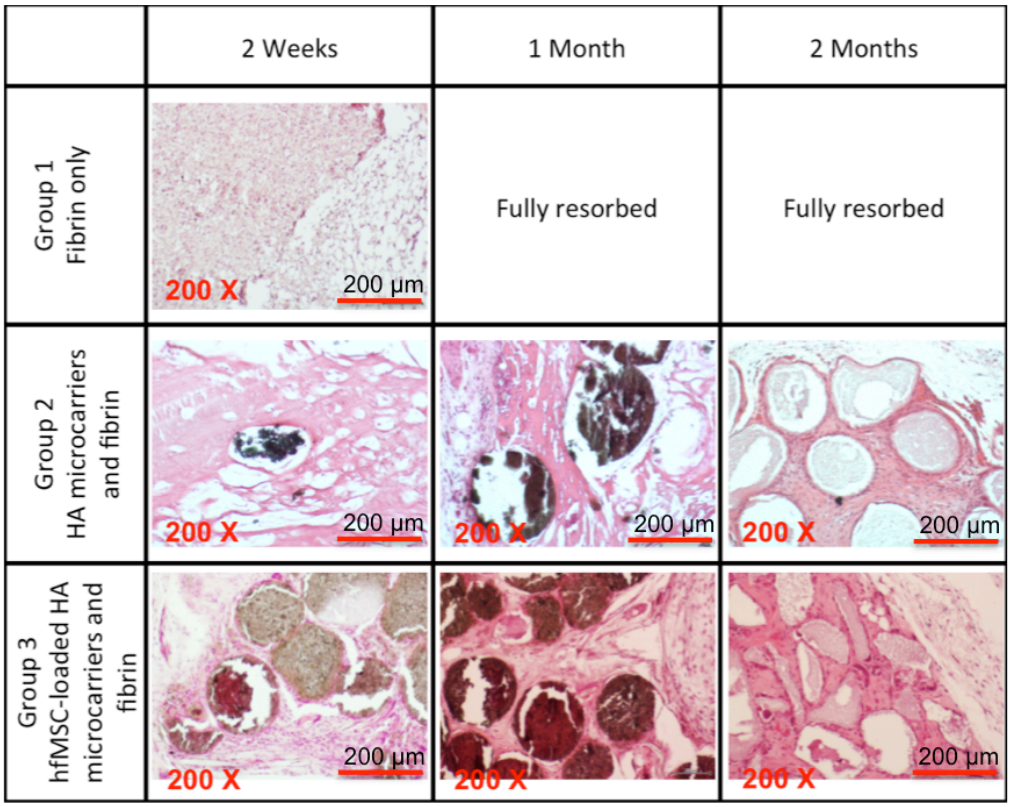

Figure 5.2. Haematoxylin and eosin staining of subcutaneously implanted apatite microcarriers. Group 1 (Fibrin only), Group 2 (Apatite microcarriers + fibrin) and Group 3 (hfMSC loaded apatite microcarriers + fibrin)

By comparing tissue morphology of the H&E stained sample groups across the period of the study, it could be observed that both apatite microcarriers only and hfMSC loaded apatite microcarriers exhibited continuous tissue formation across the period. During the first 2 weeks of implantation, fibrin was resorbed into the body of the mouse as evidenced by the general sparsing out of tissue seen at 2 weeks. From day 30 to month 2, tissue formation increased as seen from the figures showing denser tissue organisation. By the second month, the surrounding tissue was tightly associated with the apatite microcarriers indicating good bioactivity between the apatite microcarrier and the surrounding cells, and absence of fibrous tissue encapsulation. In group 1, implants with fibrin gel only resulted in loosely dispersed tissue morphology on week 2. By day 30, all the fibrin had been resorbed by the body and can no longer be retrieved for examination.

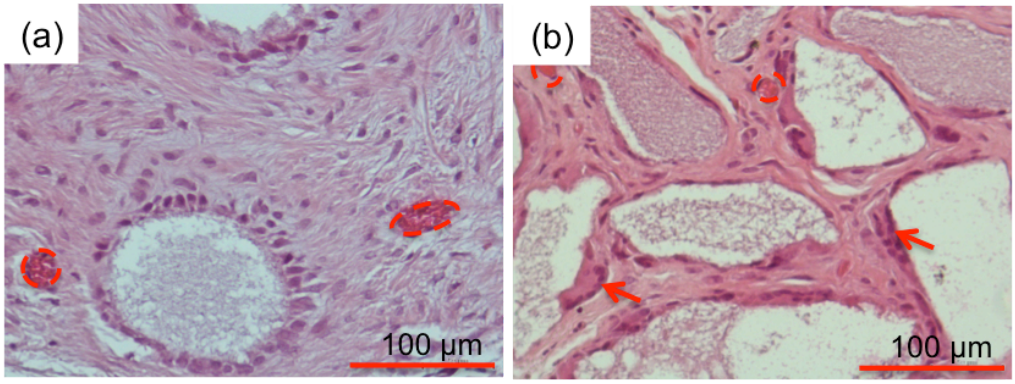

Figure 5.3. High magnification H&E of (a) apatite microcarriers + fibrin and (b) hfMSC loaded apatite microcarriers + fibrin at 2 months of implantation. Circle (dotted) indicates capillary formation while arrow indicates osteoclast bone remodelling.

Comparing between groups 2 and 3, tissue formation around hfMSC loaded apatite microcarriers appeared to be denser and better organised as compared to those of apatite microcarriers only. At higher magnification (Fig. 5.3), cells attached to the microcarriers in (Figure 5.3b) seem more flattened and elongated, suggesting that these cells were osteoblasts. There was also presence of multi-nuclei units (arrows), which indicated possible osteoclasts, thus suggesting that bone remodelling was occurring within groups containing hfMSC loaded apatite microcarriers. In both groups, microcapillaries could be seen interspaced between the microcarriers. Neo-vascularisation within the implants would be beneficial towards the supply of nutrients and removal of waste to and from the cells growing on and around the apatite microcarriers.

5.3.2 Masson's trichrome study

To differentiate between the types of tissue formed, a Masson's trichrome histology staining was also done (Fig. 5.4).

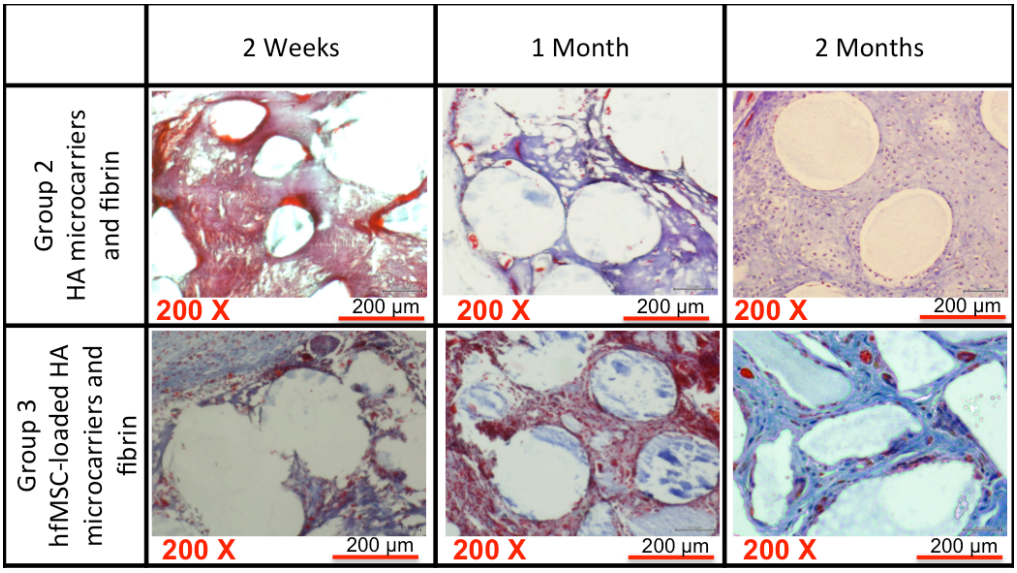

Figure 5.4. Masson's trichrome staining of group 2 (apatite microcarriers + fibrin) and group 3 (hfMSC-loaded apatite microcarriers+ fibrin)

Comparing tissue formation across the days, it was evident that the tissue type formed by group 3 was different from group 2; in addition to the denser tissue formation, hfMSC loaded apatite microcarriers exhibited greater production of connective tissue (blue colouration). The blue colouration observed was mainly due to staining of collagen I fibres, regarded as the main organic constituent of bone. Connective tissue organisation of group 3 at 2 months also resembled that of native woven bone formation.

5.3.3 Von Kossa study

Von Kossa staining of the implanted apatite microcarriers to observe for presence of tissue mineralisation (Figure 5.5). This stain results in dark, opaque spots when calcium deposits are encountered, and required samples to be prepared without a decalcification step.

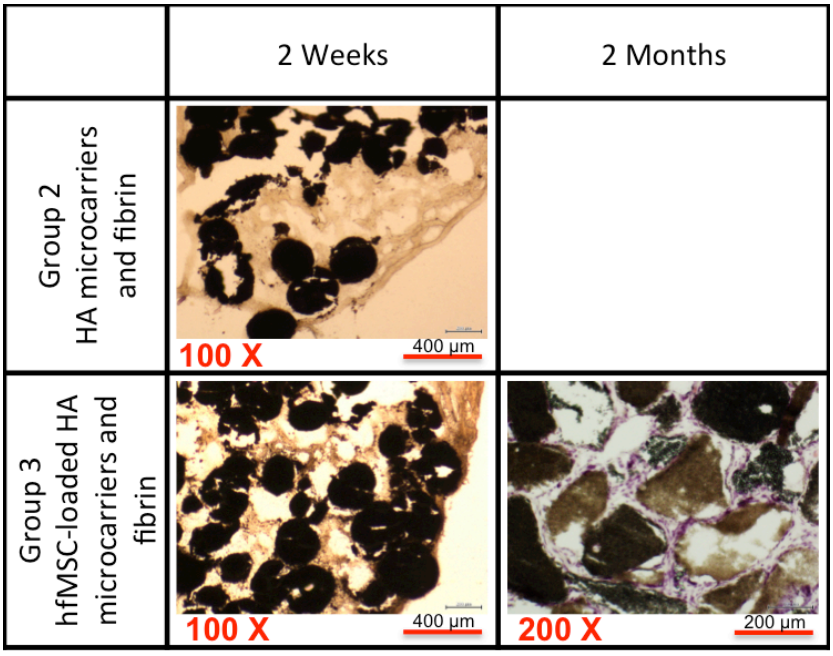

Figure 5.5. Von Kossa staining of implanted apatite microcarriers alone (group 2) and hfMSC-loaded (group 3). Black spots indicate heavy mineralisation.

For group 2, insufficient dense tissue around the microcarriers at month 2 resulted in disintegration of the sampled sections, and as a result, von Kossa staining cannot be obtained. While it was expected for apatite microcarriers to be stained heavily, calcium deposits could be observed in the intergranular space of both groups as early as week 2. By 2 months after implantation, apatite microcarriers appeared more porous, with higher mineralisation observed between the granules.

5.3.4 Osteopontin and osteonectin expression

To identify the contribution of osseous tissue by hfMSCs, samples were cryosectioned and stained for human specific osteopontin. Osteopontin (OP), also known as bone sialoprotein I (BSP-1) is synthesised predominantly by osteoblasts and osteoclast, and is involved with tissue mineralisation as well as bone remodelling. The tissue samples were also counterstained with DAPI and viewed under a confocal laser-scanning microscope.

From figure 5.6, it could be observed that the hfMSC loaded apatite microcarriers expressed osteopontin, while low levels of expression was observed with the apatite microcarriers alone. This indicated that the hfMSCs remained viable throughout the study, and they were actively contributing to osteogenesis.

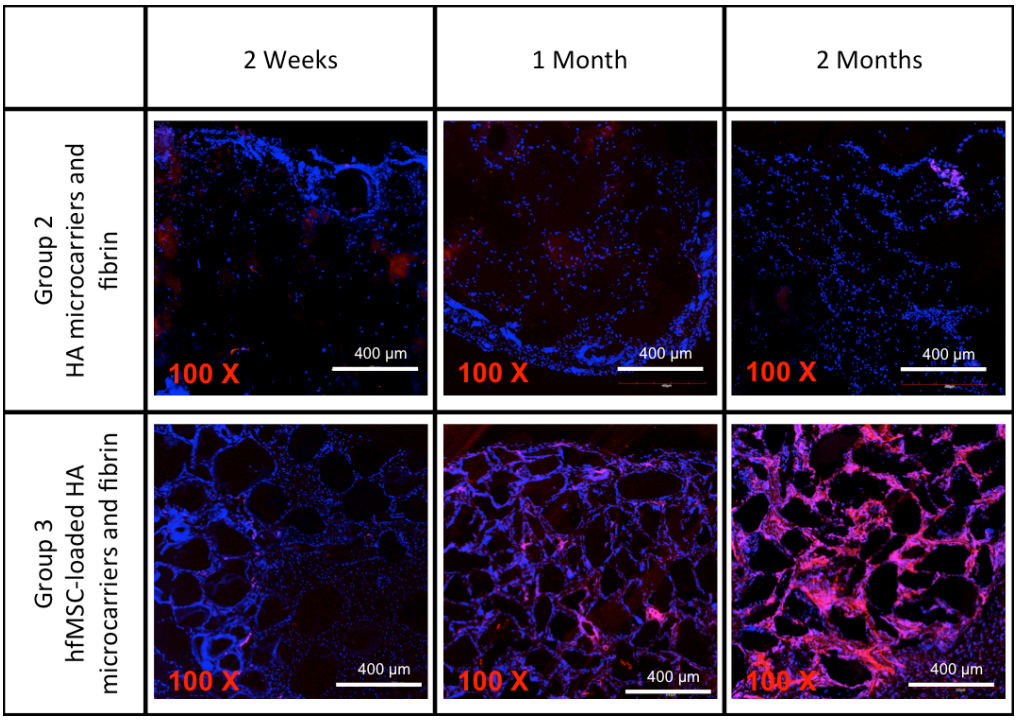

Figure 5.6. Immunohistology of group 2 (apatite microcarriers + fibrin) and group 3 (hfMSC loaded apatite microcarriers + fibrin) tissue samples. Slides were stained for human specific osteopontin (red) and counterstained with DAPI (blue).

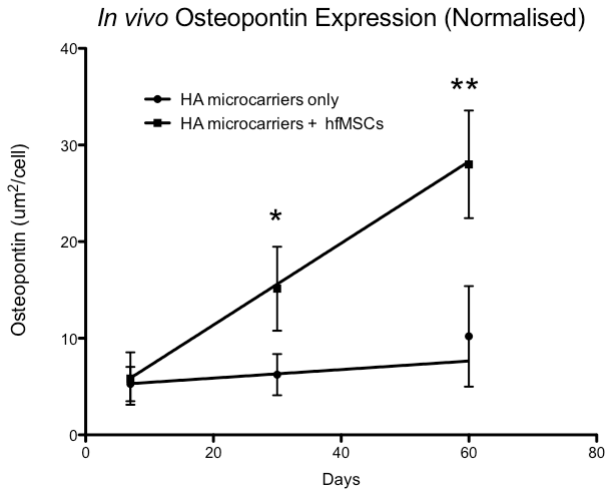

Figure 5.7. Osteopontin coverage normalised to cell nuclei count (n = 5) at various time points. hfMSC-loaded apatite microcarriers express 2.7-fold greater osteopontin compared to the group containing apatite microcarriers only(*$p < 0.05$, **$p < 0.001$).

The expression of osteopontin relative to the number of cells present was then quantified to further demonstrate the contribution of hfMSCs to osteogenesis. As can be seen from figure 5.7, groups containing just apatite microcarriers alone resulted in approximately 1.9 fold increase in osteopontin expression after 2 months of study. In contrast, hfMSC-loaded microcarriers exhibited an increasing trend in osteopontin expression, with a 4.8 fold increase after 2 months. Comparing between apatite microcarriers only and hfMSC-loaded apatite microcarriers, there was a 2.7 fold greater osteopontin expression after 2 months post implantation.

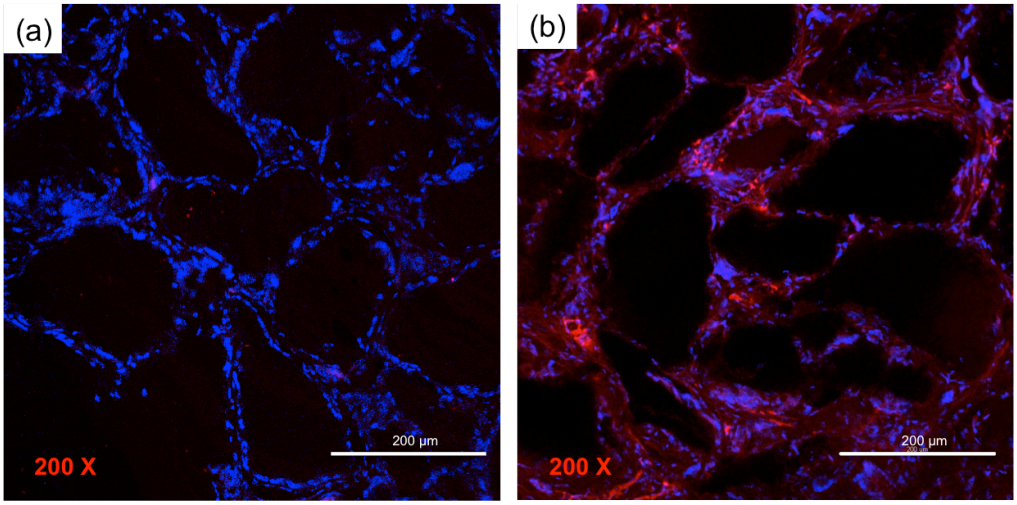

Figure 5.8. Immunohistology of human specific osteonectin (red) on (a) apatite microcarriers only (Group 2) and (b) hfMSC-loaded apatite microcarriers (Group 3), 1 month post-implantation. Samples were counterstained with DAPI (blue).

Osteonectin (ON), also known as secreted protein acidic and rich in cysteine (SPARC) is an acidic ECM secreted predominantly by mature osteoblasts. ON displays affinity for type I collagen and calcium, and has been implicated in playing a major role in bone formation, initiating mineralisation and

promoting mineral crystal formation. Immunohistological staining of human specific ON in group 2 and 3 at day 30 demonstrated high expressions of ON with the hfMSC-loaded group, but negative with the apatite microcarriers only group (Figure 5.8). This suggested that hfMSCs that are proliferating and differentiating on the apatite microcarriers remain viable after implantation, and that the osteogenic phenotype was maintained.

5.4 Discussion

In this study, the *in-vivo* osteogenic potency of hfMSCs when cultured on apatite microcarriers was demonstrated. Osteogenic differentiation of the hfMSC loaded apatite microcarriers during the *in-vitro* cell culture phase prior to implantation resulted in proliferation of hfMSC, and expression of key osteogenic markers (ALP, COL I and osteocalcin) with evidence of ECM production (Section 4.3). These factors would contribute to the *in-vivo* formation of new bone tissue. With respect to the *in-vivo* results, by comparing between empty apatite microcarriers (group 2) and hfMSC-loaded apatite microcarriers (group 3), an increase in tissue density, organisation, and mineralisation can be observed. Various cell morphologies resembling that of osteoblasts and osteoclasts could be observed on the surface of the hfMSC-loaded apatite microcarriers, with presence of woven bone tissue formation observed at the intergranular space. These observations were consistent with evidence of ectopic bone formation, which were absent in groups containing apatite microcarriers only. Formation of ectopic bone *in-vivo* was the result of a complex process that involved several factors including i) presence of donor

cells responsible for osteogenesis, ii) intrinsic host condition, and iii) the physiochemistry of the biomaterial.

The incorporation of donor cells in the stimulation of osteogenesis is a known factor in the paradigm of bone tissue engineering, with MSCs being the most commonly used cell type in such an application. MSCs are found in all stages of life, and can be obtained from perinatal and postnatal sources including adipose tissue, bone marrow and umbilical cord blood [133-135]. These cells have been reported to result *in-vivo* osteogenicity, both in ectopic bone formation models and orthopaedic bone defect models. Human foetal MSCs were chosen because they have been reported to possess superior osteogenicity and reduced immunogenicity[136-138]. When cultured with the apatite microcarriers, they demonstrated enhanced osteogenic potency over those cultured on conventional monolayer tissue culture flasks. This presented advantages of reducing time and resources required for high throughput applications and treatments requiring large doses of MSCs, while ensuring high phenotypic fidelity. The culture of MSCs on the apatite microcarriers also presented a highly attractive platform as an injectable bone graft substitute with osteoconductive and osteogenic properties that have the potential for enhanced bone healing rates and reduced recovery time. The role of donor MSCs in induced osteogenesis had not yet been fully established, although several mechanisms have been proposed. These included i) direct provision of an osteogenic cell source capable of self-renewal and bone formation[139-141], ii) expression and regulation of osteogenic factors which influence and modulate the migration and differentiation of the host's osteoprogenitors[142,

143] and iii) creation of a hyperbaric microenvironment conducive for *de novo* bone formation through the enhancement of implant neovascularisation[144-147].

The information obtained this *in-vivo* study of hfMSC-loaded apatite microcarriers suggested a strong relationship between presence of hfMSC and new bone formation in an ectopic mouse model. It was possible that a combination of the aforementioned mechanisms were responsible for the presence of woven bone tissue formation. In addition to the enhanced expressions of type I collagen, osteocalcin and ALP as reported in the *in-vitro* study, high levels of osteopontin and osteonectin were observed in groups containing hfMSC-loaded apatite microcarriers. These proteins played a crucial role in bone formation and mineralisation, in which OP was responsible for the attraction and distribution of osteoblasts and its progenitors as well as regulating osteoclast activity[148, 149] while ON was involved with the mineralisation of bone[150]. Together, both OP and ON expressions observed were in agreement with histological studies, which revealed the presence of osteoblasts and osteoclasts and indications of bone mineralisation. This contrasted strongly against groups containing apatite microcarriers only, in which OP and ON expression remained low throughout the days of study, and new bone formation could not be clearly established.

Accounting for the variability of the intrinsic host condition, NOD/SCID mice (n = 15) were used in this study. Krebsbach *et al.* found no obvious difference

in host dependent parameters with respect to the strain of immunodeficient mouse recipients (SCID, beige or beige/SCID)[151].

Concerning the physicochemistry of the biomaterial, apatite microcarriers were similar to the mineral phase of bone in terms of chemical composition. Apatite possesses osteoconductive properties, which allowed for the migration of osteoblasts and in-growth of tissue for proper osteointegration between host tissue and biomaterial. Osteoconductivity and bioactivity were also dependent on the bulk properties of the biomaterial, its pore size (micro and marco-scale), porosity, interconnectivity and resorption characteristics[152, 153]. For example, Krebsbach *et al.* found more extensive bone formation with HA/TCP powder than in HA/TCP blocks[139]. The apatite microcarriers featured in this study were porous spherical particles measuring approximately 0.23 mm, which fell within the range reported by Makani *et al.*, reporting that peak bone formation was observed with spherical particles between 0.1 – 0.25 mm[152]. It was possible that the apatite microcarriers had a size range necessary for optimal intergranular spacing, enabling the creation of macropores necessary for tissue in-growth and blood vessel formation[109]. A microporosity of 2 – 3 μm was also observed with the apatite microcarriers, and this was suggested to be beneficial towards *in-vivo* bone formation, consistent with other reports featuring apatite scaffolds with micro scale (< 10 μm) pore size[112, 154, 155]. This was so because micropores of the apatite microcarriers confer a high surface area for protein adsorption. Furthermore, the roughness and surface topology resulting from micropores allowed for appropriate physical cues for osteoblast adhesion, proliferation and differentiation.

It should be noted however, that intrinsically, apatite did not possess osteoinductive properties, which was the reason why implant groups containing apatite microcarriers only did not result in substantiated ectopic bone formation. In ectopic implant conditions, bone formation required the active recruitment and stimulation of MSCs, which were usually found in the periosteum of the bone. Subcutaneous implantation of the apatite microcarriers meant that the biomaterial was separated from this source by a thick layer of muscle and connective tissue, thus preventing any direct contact with the host's MSCs. In addition, as there was little or no rupture of blood vessels during the implant procedure, no hematoma was created, thus disrupting the initial inflammation cascade; an important step towards initiating bone healing and regeneration. Hence, without the incorporation of hfMSCs, the ability of the host to initiate bone regeneration at the implant site was hindered, thus resulting in a less defined tissue morphology with little mineralisation. This was consistent with studies confirming that osteoinductive factors or osteogenic cells had to be incorporated in the biomaterial for any osteoinductive effect to be realised in a bone defect model[112, 156-159].

Neovascularisation is integral towards long-term success of the biomaterial, and plays a major role in facilitating endochondral and intramembranous ossification, thus determining the rate of new bone formation[160]. Microcapillaries could be observed with implant groups containing hfMSC loaded apatite microcarriers. This was in agreement with reports proposing the use of MSCs for the treatment of tissue ischemia and myocardial deficiencies, due to their angiogenic effects[161, 162]. It had been reported that MSCs

express a range of blood vessel inductive factors such as angio-associated migratory cell protein (ANG) 1 and 2, endothelial growth factor (EGF) 1, and vascular endothelial growth factor (VEGF)[163]. This had been confirmed by Kinnaird *et al.*, in which proliferation and migration of endothelial cells were promoted with the addition of MSCs in a dose-dependent manner, reducing muscle atrophy in a murine hind limb ischemia model [164]. In addition, the macrostructural properties of the apatite microcarriers had an important function of creating macropores, which was crucial towards facilitating vascularisation and angiogenesis. For granular particles, macropores were created as a result of intergranular spacing, governed by particle packing principles. In general, spherical particles resulted in the greatest void spaces being created between the particles. In bone tissue engineering, macropores of around 300 μm have been recommended for the formation of capillaries[112]. The apatite microcarrier's size and shape made it possible to fulfil this requirement. Indeed, intergranular space (macropores) of approximately 200 μm had been observed with implanted apatite microcarriers, and this was accompanied by presence of microcapillaries (Figure 5.3a).

5.5 Summary

The subcutaneous implantation of hfMSC-loaded apatite microcarriers in a mouse model was described. Over a 2-month long implantation period, implant groups containing hfMSC-loaded apatite microcarriers exhibited a dense of tissue organisation, with evidence of tissue mineralisation. Histological staining of decalcified sections also reveal presence of osteoblast and osteoclast-like cell morphologies, indicating that the processes of

osteogenesis and bone remodelling are occurring. These indications suggested the formation of ectopic new bone. In contrast, samples obtained from implant groups containing apatite microcarriers alone resulted in loosely organised fibrous tissue, with little evidence of mineralisation. Cells also resembled a more fibroblastic morphology, which do not indicate presence of new bone formation. These findings suggested that ectopic bone formation could be predominantly attributed to the presence of hfMSCs cultured on the apatite microcarriers. These was further confirmed through immunohistological staining, in which OC and ON were highly expressed in implant groups containing hfMSC-loaded apatite microcarriers.

Overall, it had been demonstrated that hfMSCs that were cultured on the apatite microcarriers remained highly viable during the expansion and differentiation phase, which occurred *in-vitro*. When implanted subcutaneously, these cells secreted factors responsible for osteogenesis and mineralisation of the implant, thus supporting ectopic new bone formation. Moreover, the apatite microcarriers exhibited little to no cytotoxic effects when implanted subcutaneously in the mice, thus suggesting that the microcarriers would not elicit an adverse host immunologic response. Lastly, neo-vascularisation was permitted, as evidenced by the presence of microcapillaries in both implant groups. This was possible because the apatite microcarriers fell between the recommended size range necessary for bone tissue formation and vascular invasion, whilst possessing favourable roughness, microporosity and physicochemical properties that would promote the conduction of osseous tissue over its surface.

Chapter 6

Conclusions

The fabrication, characterisation, *in-vitro* and *in-vivo* evaluations of porous, apatite microcarriers for bone tissue engineering applications has been presented. The development and optimisation of such microcarriers have been performed, and this process allows for various parameters to be experimented with, and with careful manipulation of these factors, it is possible to fabricate phase-pure apatite microcarriers of appropriate size and spherical macromorphology. Moreover, micro-scale features can be engineered on the microbeads such that it adequately recreates the *in-vivo* micro-architecture of the native bone. This includes the control of the microcarriers' chemical composition and crystallinity, surface roughness, pore size and overall porosity, which are all crucial factors that influence stem cell behaviour and long-term viability. In addition, the chemical properties of apatite, as confirmed through chemical characterisations, will enable the microcarriers to have a chemistry similar to the mineral phase of native bone, and adsorb proteins, which will enable appropriate cell responses.

This novel biomaterial is intended as a bone tissue engineered bone graft substitute, incorporating properties of excellent biocompatibility, osteoconductivity, and when cultured together with appropriate cell types, can result in new bone formation. These properties have been established through *in-vitro* and *in-vivo* studies. *In-vitro* culture of MSCs with the apatite microcarriers resulted in significantly better proliferation and viability over

polymeric microcarriers. Culturing of these cells on a three-dimensional, apatite substrate also elicited greater osteogenic potency over cells cultured via conventional monolayer culture, and this is believed to be attributed to the microcarrier's high surface roughness and presence of micropores, as well as phase pure apatite which mimics the cell's native microenvironment, thus delivering the appropriate biomolecular cues which facilitates and enhances osteogenic expression among the cells. In summary, *in-vitro* studies have successfully established that the apatite microcarriers are an effective platform for obtaining MSCs with high yield and osteogenic potency.

In-vivo studies of subcutaneously implanted MSC-loaded apatite microcarriers demonstrate ectopic new bone formation and evidence of neo-vascularisation. This is believed to be primarily attributed to the presence of highly viable and osteogenic donor MSCs, which were able to produce ECM and express factors that actively recruit host cells, thus contributing towards bone tissue formation, mineralisation and vascularisation. As such, this study has successfully validated the efficacy of using MSC-loaded apatite microcarriers to actively initiate, promote and facilitate new bone formation *in-vivo*.

To conclude, the objectives set out initially in this dissertation have been met. Furthermore, the information presented in this report thus far indicates that the use of apatite microcarriers in a single-step, non-invasive, injectable strategy for healing bone defects is highly promising. It is envisioned that such a biomaterial will have a significant impact in the orthopaedic field, thereby bringing the goal of bone regenerative therapy closer to clinical fruition.

Chapter 7

Future Work

7.1 Use of substituted apatite in the fabrication of microcarriers

Apatite has the potential to undergo chemical substitutions with different elements and chemical groups to produce a material with altered biological effects. For instance, Lim *et al.* has featured the synthesis of silver/silicon-cosubtituted apatite which incorporates enhanced bioactivity and antimicrobial properties[165]. The use of such a material in the fabrication of the microcarriers presents exciting opportunities for the use in clinical applications in which patients with severely diminished bone regenerative capacities are observed (i.e. Osteoporosis), or in cases of open wound trauma where risk of infection is of paramount concern.

7.2 Use of apatite microcarriers in dynamic bioreactors

The use of the apatite microcarriers as viable and efficient platform for stem cell expansion and osteogenic differentiation can be further explored in studies involving bioreactors. These bioreactors provide the dynamic conditions that optimise nutrient and waste exchange through fluid flow kinetics. In addition, shear forces created during fluid flow would impart mechanical stimuli on the attached cells, which has been suggested to further increase osteogenic potency via the mechanism of mechanotransduction[166]. This represents opportunities to further develop the microcarriers to incorporate properties that are relevant towards dynamic cell culture, as well as to investigate differences

between cell-material and cell-medium interactions so as to gain a deeper understanding of cell signalling pathways.

7.3 *In-vivo* evaluation of the healing of bone defects in medium to large sized animal models

Further *in-vivo* studies involving MSC-loaded apatite microcarriers implanted into bone defects in medium to large sized animals are proposed. This would simulate a more accurate environment in which the apatite microcarriers would be used. By implanting these microcarriers into larger sized animals, information that is more representative can be obtained with regard to the actual implantation procedure, as well as host immunological responses to the presence of the apatite microcarriers. In addition, creation of a bone defect at a weight bearing section of the bone (i.e. femur) would better recreate the *in-vivo* biomechanics that the apatite microcarriers would be exposed to, allowing for assessment of implant stability under loading, and subjecting the seeded cells with the appropriate biomechanical stimuli, which lead result in greater bone formation, and maturation of new bone. Finally, the process of defect site creation would result in the rupturing of blood vessels, allowing for hematoma formation, which is of great relevance towards simulating actual clinical conditions involving complex fractures or bone resection procedures. It would be interesting to investigate the performance of these apatite microcarriers under a more biologically and physiologically complex environment, so as to bring the development of this biomaterial closer to clinical acceptance.

References

[1] Desai BM. Osteobiologics. *American journal of orthopedics (Belle Mead, NJ)*. 2007;36:8-11.

[2] Mehta S, Nunley RM, Jahangir A, Sharan AD. Nanotechnology: From nano to micro to macro. May; 2007.

[3] Giannoudis PV, Dinopoulos H, Tsiridis E. Bone substitutes: an update. *Injury*. 2005;36:S20-S7.

[4] Laurencin C, Khan Y, El-Amin S. Bone graft substitutes. *Expert review of medical devices*. 2006;3:49.

[5] Toolan BC. Current concepts review: Orthobiologics. *Foot & ankle international*. 2006;27:561-6.

[6] Granero-Molto F, Weis JA, Longobardi L, Spagnoli A. Role of mesenchymal stem cells in regenerative medicine: application to bone and cartilage repair. *Expert Opin Biol Ther*. 2008;8:255-68.

[7] Horwitz EM, Prockop DJ, Fitzpatrick LA, Koo WWK, Gordon PL, Neel M, Sussman M, Orchard P, Marx JC, Pyeritz RE. Transplantability and therapeutic effects of bone marrow-derived mesenchymal cells in children with osteogenesis imperfecta. *Nature medicine*. 1999;5:309-13.

[8] Reddig PJ, Juliano RL. Clinging to life: cell to matrix adhesion and cell survival. *Cancer and Metastasis Reviews*. 2005;24:425-39.

[9] Griffiths B. Scale-up of suspension and anchorage-dependent animal cells. *Molecular Biotechnology*. 2001;17:225-38.

[10] DiGirolamo DJ, Clemens TL, Kousteni S. The skeleton as an endocrine organ. *Nature reviews rheumatology*. 2012;8:674-83.

[11] Rho JY, Kuhn-Spearing L, Zioupos P. Mechanical properties and the hierarchical structure of bone. *Medical engineering & physics*. 1998;20:92-102.

[12] Webster T, Ahn E. Nanostructured Biomaterials for Tissue Engineering Bone. In: Lee K, Kaplan D, editors. Tissue Engineering II: Springer Berlin Heidelberg; 2007. p. 275-308.

[13] Hutmacher DW. Scaffolds in tissue engineering bone and cartilage. *Biomaterials*. 2000;21:2529-43.

[14] Henkel J, Woodruff MA, Epari DR, Steck R, Glatt V, Dickinson IC, Choong PF, Schuetz MA, Hutmacher DW. Bone regeneration based on tissue engineering conceptions–a 21st century perspective. *Bone Research*. 2013;1:216-48.

[15] Voss K, Montavon PM. 13 - Fractures. In: Montavon PM, Voss K, S.J. Langley-HobbsA2 - P.M. Montavon KV, Langley-Hobbs SJ, editors. Feline Orthopedic Surgery and Musculoskeletal Disease. *Edinburgh*: W.B. Saunders; 2009. p. 129-52.

[16] Jilka RL. Biology of the basic multicellular unit and the pathophysiology of osteoporosis. *Medical and pediatric oncology*. 2003;41:182-5.

[17] Perren SM. Evolution of the internal fixation of long bone fractures. *JOURNAL OF BONE AND JOINT SURGERY-BRITISH VOLUME-*. 2002;84:1093-110.

[18] Bassett CAL, Herrmann I. Influence of oxygen concentration and mechanical factors on differentiation of connective tissues in vitro. 1961.

[19] Claes L, Recknagel S, Ignatius A. Fracture healing under healthy and inflammatory conditions. *Nature reviews rheumatology*. 2012;8:133-43.

[20] Dimitriou R, Jones E, McGonagle D, Giannoudis PV. Bone regeneration: current concepts and future directions. *BMC medicine*. 2011;9:66.

[21] Melnyk M, Henke T, Claes L, Augat P. Revascularisation during fracture healing with soft tissue injury. *Archives of orthopaedic and trauma surgery*. 2008;128:1159-65.

[22] Giannoudis PV, Einhorn TA, Marsh D. Fracture healing: the diamond concept. *Injury*. 2007;38:S3-S6.

[23] Einhorn TA. Clinical applications of recombinant human BMPs: early experience and future development. *The Journal of Bone & Joint Surgery*. 2003;85:82-8.

[24] Friedlaender GE, Perry CR, Cole JD, Cook SD, Cierny G, Muschler GF, Zych GA, Calhoun JH, LaForte AJ, Yin S. Osteogenic Protein-1 (Bone Morphogenetic Protein-7) in the Treatment of Tibial Nonunions A Prospective, Randomized Clinical Trial Comparing rhOP-1 with Fresh Bone Autograft*. *The Journal of Bone & Joint Surgery*. 2001;83:151-S8.

[25] Giannoudis PV, Tzioupis C. Clinical applications of BMP-7: the UK perspective. *Injury*. 2005;36:S47-S50.

[26] Harwood PJ, Giannoudis PV. Application of bone morphogenetic proteins in orthopaedic practice: their efficacy and side effects. *Expert opinion on drug safety*. 2005;4:75-89.

[27] Kain MS, Einhorn TA. Recombinant human bone morphogenetic proteins in the treatment of fractures. *Foot and ankle clinics*. 2005;10:639-50.

[28] Westerhuis R, Van Bezooijen R, Kloen P. Use of bone morphogenetic proteins in traumatology. *Injury*. 2005;36:1405-12.

[29] Fujita N, Matsushita T, Ishida K, Sasaki K, Kubo S, Matsumoto T, Kurosaka M, Tabata Y, Kuroda R. An analysis of bone regeneration at a segmental bone defect by controlled release of bone morphogenetic protein 2 from a biodegradable sponge composed of gelatin and β-tricalcium phosphate. *Journal of tissue engineering and regenerative medicine*. 2012;6:291-8.

[30] Burg KJL, Porter S, Kellam JF. Biomaterial developments for bone tissue engineering. *Biomaterials*. 2000;21:2347-59.

[31] Li RH, Wozney JM. Delivering on the promise of bone morphogenetic proteins. *Trends in Biotechnology*. 2001;19:255-65.

[32] Chen RR, Mooney DJ. Polymeric growth factor delivery strategies for tissue engineering. *Pharmaceutical research*. 2003;20:1103-12.

[33] Griffith LG, Naughton G. Tissue engineering--current challenges and expanding opportunities. *Science*. 2002;295:1009-14.

[34] Rouwkema J, Rivron NC, van Blitterswijk CA. Vascularization in tissue engineering. *Trends in Biotechnology*. 2008;26:434-41.

[35] Damien CJ, Parsons JR. Bone graft and bone graft substitutes: a review of current technology and applications. *Journal of Applied Biomaterials*. 1991;2:187-208.

[36] Feng J, Thian ES. Applications of nanobioceramics to healthcare technology. *Nanotechnology Reviews*. 2013;2:679-97.

[37] Burger EH, KLEIN-NULEND J. Mechanotransduction in bone—role of the lacuno-canalicular network. *The FASEB Journal*. 1999;13:S101-S12.

[38] Sikavitsas VI, Temenoff JS, Mikos AG. Biomaterials and bone mechanotransduction. *Biomaterials*. 2001;22:2581-93.

[39] Reich KM, Gay CV, Frangos JA. Fluid shear stress as a mediator of osteoblast cyclic adenosine monophosphate production. *Journal of cellular physiology*. 1990;143:100-4.

[40] Klein-Nulend J, Van der Plas A, Semeins C, Ajubi N, Frangos J, Nijweide P, Burger E. Sensitivity of osteocytes to biomechanical stress in vitro. *The FASEB Journal*. 1995;9:441-5.

[41] Johnson DL, McAllister TN, Frangos JA. Fluid flow stimulates rapid and continuous release of nitric oxide in osteoblasts. *American Journal of Physiology-Endocrinology And Metabolism*. 1996;34:E205.

[42] Klein-Nulend J, Helfrich M, Sterck J, MacPherson H, Joldersma M, Ralston S, Semeins C, Burger E. Nitric oxide response to shear stress by human bone cell cultures is endothelial nitric oxide synthase dependent. *Biochemical and Biophysical Research Communications*. 1998;250:108-14.

[43] Hervy M, Hoffman L, Beckerle MC. From the membrane to the nucleus and back again: bifunctional focal adhesion proteins. *Current opinion in cell biology*. 2006;18:524-32.

[44] Rhee S, Jiang H, Ho C-H, Grinnell F. Microtubule function in fibroblast spreading is modulated according to the tension state of cell–matrix interactions. *Proceedings of the National Academy of Sciences*. 2007;104:5425-30.

[45] Anselme K. Osteoblast adhesion on biomaterials. *Biomaterials*. 2000;21:667-81.

[46] Sheetz MP. Cell control by membrane–cytoskeleton adhesion. *Nature Reviews Molecular Cell Biology*. 2001;2:392-6.

[47] Hing KA. Bone repair in the twenty–first century: biology, chemistry or engineering? *Philosophical Transactions of the Royal Society of London Series A: Mathematical, Physical and Engineering Sciences*. 2004;362:2821-50.

[48] Salasznyk RM, Klees RF, Williams WA, Boskey A, Plopper GE. Focal adhesion kinase signaling pathways regulate the osteogenic differentiation of human mesenchymal stem cells. *Experimental cell research*. 2007;313:22-37.

[49] Banwart JC, Asher MA, Hassanein RS. Iliac crest bone graft harvest donor site morbidity: a statistical evaluation. *Spine*. 1995;20:1055-60.

[50] Goulet JA, Senunas LE, DeSilva GL, Greenfield MLV. Autogenous iliac crest bone graft: complications and functional assessment. *Clinical Orthopaedics and Related Research*. 1997;339:76-81.

[51] Clements JR, Carpenter BB, Pourciau JK. Treating segmental bone defects: a new technique. *The Journal of Foot and Ankle Surgery*. 2008;47:350-6.

[52] Williams DF. On the mechanisms of biocompatibility. *Biomaterials*. 2008;29:2941-53.

[53] Conn Jr J, Oyasu R, Welsh M, Beal JM. Vicryl (polyglactin 910) synthetic absorbable sutures. *The American Journal of Surgery*. 1974;128:19-23.

[54] Nandi S, Roy S, Mukherjee P, Kundu B, De D, Basu D. Orthopaedic applications of bone graft & graft substitutes: a review. *The Indian Journal of Medical Research*. 2010;132:15.

[55] Bose S, Tarafder S. Calcium phosphate ceramic systems in growth factor and drug delivery for bone tissue engineering: A review. *Acta Biomaterialia*. 2012;8:1401-21.

[56] Gold LI. The role for transforming growth factor-beta (TGF-beta) in human cancer. *Critical reviews in oncogenesis*. 1998;10:303-60.

[57] Turner N, Grose R. Fibroblast growth factor signalling: from development to cancer. *Nature Reviews Cancer*. 2010;10:116-29.

[58] O'Brien FJ. Biomaterials & scaffolds for tissue engineering. *Materials Today*. 2011;14:88-95.

[59] Meyers MA, Chen P-Y, Lin AY-M, Seki Y. Biological materials: Structure and mechanical properties. *Progress in Materials Science*. 2008;53:1-206.

[60] Bettinger CJ, Langer R, Borenstein JT. Engineering Substrate Topography at the Micro-and Nanoscale to Control Cell Function. *Angewandte Chemie International Edition*. 2009;48:5406-15.

[61] Kim HW, Song JH, Kim HE. Nanofiber generation of gelatin–hydroxyapatite biomimetics for guided tissue regeneration. *Advanced functional materials*. 2005;15:1988-94.

[62] Webster TJ, Ergun C, Doremus RH, Siegel RW, Bizios R. Specific proteins mediate enhanced osteoblast adhesion on nanophase ceramics. *Journal of Biomedical Materials Research*. 2000;51:475-83.

[63] Webster TJ, Siegel RW, Bizios R. Osteoblast adhesion on nanophase ceramics. *Biomaterials*. 1999;20:1221-7.

[64] Palin E, Liu H, Webster TJ. Mimicking the nanofeatures of bone increases bone-forming cell adhesion and proliferation. *Nanotechnology*. 2005;16:1828.

[65] Webster TJ, Ergun C, Doremus RH, Siegel RW, Bizios R. Enhanced functions of osteoblasts on nanophase ceramics. *Biomaterials*. 2000;21:1803-10.

[66] Habibovic P, Sees TM, van den Doel MA, van Blitterswijk CA, de Groot K. Osteoinduction by biomaterials—Physicochemical and structural influences. *Journal of Biomedical Materials Research Part A*. 2006;77A:747-62.

[67] Best S, Porter A, Thian E, Huang J. Bioceramics: past, present and for the future. *Journal of the European Ceramic Society*. 2008;28:1319-27.

[68] Thian E, Best S. Materials viewpoints in bone regenerative medicine: progress and prospects. *Materials Science and Technology*. 2008;24:1027-30.

[69] Habibovic P, de Groot K. Osteoinductive biomaterials—properties and relevance in bone repair. *Journal of tissue engineering and regenerative medicine*. 2007;1:25-32.

[70] Cheng L, Ye F, Yang R, Lu X, Shi Y, Li L, Fan H, Bu H. Osteoinduction of hydroxyapatite/β-tricalcium phosphate bioceramics in mice with a fractured fibula. *Acta Biomaterialia*. 2010;6:1569-74.

[71] Bohner M, Tadier S, van Garderen N, de Gasparo A, Döbelin N, Baroud G. Synthesis of spherical calcium phosphate particles for dental and orthopedic applications. *Biomatter*. 2013;3:e25103.

[72] Ramay HR, Zhang M. Biphasic calcium phosphate nanocomposite porous scaffolds for load-bearing bone tissue engineering. *Biomaterials*. 2004;25:5171-80.

[73] Arinzeh TL, Tran T, Mcalary J, Daculsi G. A comparative study of biphasic calcium phosphate ceramics for human mesenchymal stem-cell-induced bone formation. *Biomaterials*. 2005;26:3631-8.

[74] LeGeros RZ. Properties of osteoconductive biomaterials: calcium phosphates. *Clinical Orthopaedics and Related Research*. 2002;395:81-98.

[75] Galois L, Mainard D, Delagoutte J. Beta-tricalcium phosphate ceramic as a bone substitute in orthopaedic surgery. *International Orthopaedics*. 2002;26:109-15.

[76] LeGeros RZ. Calcium phosphate-based osteoinductive materials. *Chemical reviews*. 2008;108:4742-53.

[77] Samavedi S, Whittington AR, Goldstein AS. Calcium phosphate ceramics in bone tissue engineering: a review of properties and their influence on cell behavior. *Acta Biomaterialia*. 2013;9:8037-45.

[78] Huang Y, He J, Gan L, Liu X, Wu Y, Wu F, Gu Z-w. Osteoconductivity and osteoinductivity of porous hydroxyapatite coatings deposited by liquid precursor plasma spraying: in vivo biological response study. *Biomedical Materials*. 2014;9:065007.

[79] Zhou H, Lee J. Nanoscale hydroxyapatite particles for bone tissue engineering. *Acta Biomaterialia*. 2011;7:2769-81.

[80] Balçik C, Tokdemir T, Şenköylü A, Koç N, Timuçin M, Akin S, Korkusuz P, Korkusuz F. Early weight bearing of porous HA/TCP (60/40) ceramics in vivo: a longitudinal study in a segmental bone defect model of rabbit. *Acta Biomaterialia*. 2007;3:985-96.

[81] Porter A, Patel N, Brooks R, Best S, Rushton N, Bonfield W. Effect of carbonate substitution on the ultrastructural characteristics of hydroxyapatite implants. *Journal of Materials Science: Materials in Medicine*. 2005;16:899-907.

[82] LeGeros R, Hydroxyapatite JL, Kokubo T. Bioceramics and their clinical applications. *by T Kokubo, CRC Press, Boca Raton, Boston, New York, Washington, DC*. 2008:367.

[83] Ito A, Nakamura S, Aoki H, Akao M, Teraoka K, Tsutsumi S, Onuma K, Tateishi T. Hydrothermal growth of carbonate-containing hydroxyapatite single crystals. *Journal of crystal growth*. 1996;163:311-7.

[84] Bogdanoviciene I, Beganskiene A, Tõnsuaadu K, Glaser J, Meyer HJ, Kareiva A. Calcium hydroxyapatite, Ca10(PO4)6(OH)2 ceramics prepared by aqueous sol–gel processing. *Materials Research Bulletin*. 2006;41:1754-62.

[85] Saeri MR, Afshar A, Ghorbani M, Ehsani N, Sorrell CC. The wet precipitation process of hydroxyapatite. *Materials Letters*. 2003;57:4064-9.

[86] Thu B, Smidsrød O, Skjak-Brŧk G. Alginate gels — Some structure-function correlations relevant to their use as immobilization matrix for cells. In: R.H. Wijffels RMBCB, Tramper J, editors. Progress in Biotechnology: Elsevier; 1996. p. 19-30.

[87] Venkatesan J, Nithya R, Sudha PN, Kim S-K. Chapter Four - Role of Alginate in Bone Tissue Engineering. In: Se-Kwon K, editor. Advances in Food and Nutrition Research: Academic Press; 2014. p. 45-57.

[88] Challen I, Moorhouse R. Hydrocolloids in Restructured Foods. Hydrocolloids in Food Processing: Wiley-Blackwell; 2010. p. 165-214.

[89] Tipton PA. 8.12 - Synthesis of Alginate in Bacteria. In: Liu H-W, Mander L, editors. Comprehensive Natural Products II. *Oxford*: Elsevier; 2010. p. 423-41.

[90] BioPolymer F. Alginates / PGA / Functionality and Rheology. FMC; 2013.

[91] Draget KI, Taylor C. Chemical, physical and biological properties of alginates and their biomedical implications. *Food Hydrocolloids*. 2011;25:251-6.

[92] Grant GT, Morris ER, Rees DA, Smith PJ, Thom D. Biological interactions between polysaccharides and divalent cations: the egg-box model. *FEBS letters*. 1973;32:195-8.

[93] Salib N, El-Menshawy M, Ismail A. Utilization of sodium alginate in drug microencapsulation. *Pharm Ind*. 1978;40:1230-4.

[94] Matsumoto T, Mashiko K. Viscoelastic properties of alginate aqueous solutions in the presence of salts. *Biopolymers*. 1990;29:1707-13.

[95] Ribeiro C, Barrias C, Barbosa M. Calcium phosphate-alginate microspheres as enzyme delivery matrices. *Biomaterials*. 2004;25:4363-73.

[96] Poncelet D, Lencki R, Beaulieu C, Halle J, Neufeld R, Fournier A. Production of alginate beads by emulsification/internal gelation. I. Methodology. *Applied Microbiology and Biotechnology*. 1992;38:39-45.

[97] Chan L, Lee H, Heng P. Production of alginate microspheres by internal gelation using an emulsification method. *International journal of pharmaceutics*. 2002;242:259-62.

[98] Li R, Zhang X, Shi H. Effect of manufacturing parameters on the release profiles of casein-loaded alginate microspheres prepared by emulsification/internal gelation. *Journal of controlled release*. 2011;152:e154-e5.

[99] Xin R, Leng Y, Wang N. HRTEM Study of the Mineral Phases in Human Cortical Bone. *Advanced Engineering Materials*. 2010;12:B552-B7.

[100] Habibovic P, Barrere F, Blitterswijk CA, Groot K, Layrolle P. Biomimetic hydroxyapatite coating on metal implants. *Journal of the American Ceramic Society*. 2002;85:517-22.

[101] Choudhury P, Agrawal DC. 5 - Hydroxyapatite (HA) coatings for biomaterials. In: Webster TJ, editor. Nanomedicine: Woodhead Publishing; 2012. p. 84-127.

[102] Ferraz M, Mateus A, Sousa J, Monteiro F. Nanohydroxyapatite microspheres as delivery system for antibiotics: release kinetics, antimicrobial activity, and interaction with osteoblasts. *Journal of Biomedical Materials Research Part A*. 2007;81:994-1004.

[103] Oonishi H, Oonishi Jr H, Kim SC, Hench LL, Wilson J, Tsuji E, Fujita H, Oohashi H, Oomamiuda K. 27 - Clinical application of hydroxyapatite. In: Kokubo T, editor. Bioceramics and their Clinical Applications: Woodhead Publishing; 2008. p. 606-87.

[104] Bohner M, Galea L, Doebelin N. Calcium phosphate bone graft substitutes: Failures and hopes. *Journal of the European Ceramic Society*. 2012;32:2663-71.

[105] Reynolds MA, Aichelmann-Reidy ME, Branch-Mays GL, Gunsolley JC. The efficacy of bone replacement grafts in the treatment of periodontal osseous defects. A systematic review. *Annals of periodontology*. 2003;8:227-65.

[106] Oonishi H, Iwaki Y, Kin N, Kushitani S, Murata N, Wakitani S, Imoto K. Hydroxyapatite in revision of total hip replacements with massive acetabular defects: 4-to 10-year clinical results. *The Journal of bone and joint surgery British volume*. 1997;79:87-92.

[107] van Hemert WL, Willems K, Anderson PG, van Heerwaarden RJ, Wymenga AB. Tricalcium phosphate granules or rigid wedge preforms in open wedge high tibial osteotomy: a radiological study with a new evaluation system. *The Knee*. 2004;11:451-6.

[108] Chan CK, Kumar TS, Liao S, Murugan R, Ngiam M, Ramakrishnan S. Biomimetic nanocomposites for bone graft applications. 2006.

[109] Bohner M. Calcium orthophosphates in medicine: from ceramics to calcium phosphate cements. *Injury*. 2000;31:D37-D47.

[110] Botchwey E, Pollack S, Levine E, Laurencin C. Bone tissue engineering in a rotating bioreactor using a microcarrier matrix system. *Journal of Biomedical Materials Research*. 2001;55:242-53.

[111] Kunio I. Effects of Spherical Tetracalcium Phosphate on Injectability and Basic Properties of Apatitic Cement. *Key Engineering Materials*. 2002;240:369-72.

[112] Fischer E, Layrolle P, Van Blitterswijk C, De Bruijn J. Bone formation by mesenchymal progenitor cells cultured on dense and microporous hydroxyapatite particles. *Tissue Eng*. 2003;9:1179-88.

[113] Ikeda N, Kawanabe K, Nakamura T. Quantitative comparison of osteoconduction of porous, dense A–W glass–ceramic and hydroxyapatite granules (effects of granule and pore sizes). *Biomaterials*. 1999;20:1087-95.

[114] Zhang Z-Y, Teoh S-H, Hui JHP, Fisk NM, Choolani M, Chan JKY. The potential of human fetal mesenchymal stem cells for off-the-shelf bone tissue engineering application. *Biomaterials*. 2012;33:2656-72.

[115] Mauney JR, Volloch V, Kaplan DL. Role of adult mesenchymal stem cells in bone tissue engineering applications: current status and future prospects. *Tissue Eng*. 2005;11:787-802.

[116] Abbah S, Lu W, Peng S, Aladin D, Li Z, Tam W, Cheung K, Luk K, Zhou G. Extracellular matrix stability of primary mammalian chondrocytes and intervertebral disc cells cultured in alginate-based microbead hydrogels. *Cell transplantation*. 2008;17:10-1.

[117] Liu JY, Hafner J, Dragieva G, Burg G. High yields of autologous living dermal equivalents using porcine gelatin microbeads as microcarriers for autologous fibroblasts. *Cell transplantation*. 2006;15:445-51.

[118] Zangi L, Rivkin R, Kassis I, Levdansky L, Marx G, Gorodetsky R. High-yield isolation, expansion, and differentiation of rat bone marrow-derived mesenchymal stem cells with fibrin microbeads. *Tissue Eng*. 2006;12:2343-54.

[119] Johansson A, Nielsen V. Biosilon a new microcarrier. *Developments in biological standardization*. 1980;46:125.

[120] Cukierman E, Pankov R, Stevens DR, Yamada KM. Taking cell-matrix adhesions to the third dimension. *Science Signalling*. 2001;294:1708.

[121] Zhang Z-Y, Teoh SH, Teo EY, Khoon Chong MS, Shin CW, Tien FT, Choolani MA, Chan JKY. A comparison of bioreactors for culture of fetal mesenchymal stem cells for bone tissue engineering. *Biomaterials*. 2010;31:8684-95.

[122] Johansson S, Svineng G, Wennerberg K, Armulik A, Lohikangas L. Fibronectin-integrin interactions. *Front Biosci*. 1997;2:d126-d46.

[123] Jokinen J, Dadu E, Nykvist P, Kapyla J, White DJ, Ivaska J, Vehvilainen P, Reunanen H, Larjava H, Hakkinen L, Heino J. Integrin-mediated cell adhesion to type I collagen fibrils. *J Biol Chem*. 2004;279:31956-63.

[124] Hidalgo-Bastida LA, Cartmell SH. Mesenchymal stem cells, osteoblasts and extracellular matrix proteins: enhancing cell adhesion and differentiation for bone tissue engineering. *Tissue Eng Part B Rev*. 2010;16:405-12.

[125] Kandori K, Masunari A, Ishikawa T. Study on Adsorption Mechanism of Proteins Onto Synthetic Calcium Hydroxyapatites Through Ionic Concentration Measurements. *Calcified Tissue International*. 2005;76:194-206.

[126] Shen JW, Wu T, Wang Q, Pan HH. Molecular simulation of protein adsorption and desorption on hydroxyapatite surfaces. *Biomaterials*. 2008;29:513-32.

[127] Santos E, Farina M, Soares G, Anselme K. Surface energy of hydroxyapatite and b-tricalcium phosphate ceramics driving serum protein adsorption and osteoblast adhesion. *Journal of Materials Science: Materials in Medicine*. 2008;19:2307-16.

[128] Niemeyer P, Krause U, Fellenberg J, Kasten P, Seckinger A, Ho AD, Simank HG. Evaluation of mineralized collagen and α-tricalcium phosphate as scaffolds for tissue engineering of bone using human mesenchymal stem cells. *Cells Tissues Organs*. 2004;177:68-78.

[129] Melero-Martin JM, Dowling MA, Smith M, Al-Rubeai M. Expansion of chondroprogenitor cells on macroporous microcarriers as an alternative to conventional monolayer systems. *Biomaterials*. 2006;27:2970-9.

[130] HAUSCHKA EV, LIAN JB, COLE DEC, GUNDBERG CM. Osteocalcin and Matrix Gla Protein: Vitamin K-Dependent Proteins in Bone. *Physiological Reviews*. 1989;69:990-1047.

[131] Zhao F, Grayson WL, Ma T, Bunnell B, Lu WW. Effects of hydroxyapatite in 3-D chitosan–gelatin polymer network on human mesenchymal stem cell construct development. *Biomaterials*. 2006;27:1859-67.

[132] Britain G, Polkinghorne J. Review of the guidance on the research use of fetuses and fetal material: HM Stationery Office; 1989.

[133] Meinel L, Betz O, Fajardo R, Hofmann S, Nazarian A, Cory E, Hilbe M, McCool J, Langer R, Vunjak-Novakovic G. Silk based biomaterials to heal critical sized femur defects. *Bone*. 2006;39:922-31.

[134] Yoon E, Dhar S, Chun DE, Gharibjanian NA, Evans GR. In vivo osteogenic potential of human adipose-derived stem cells/poly lactide-co-glycolic acid constructs for bone regeneration in a rat critical-sized calvarial defect model. *Tissue Eng*. 2007;13:619-27.

[135] Jäger M, Degistirici Ö, Knipper A, Fischer J, Sager M, Krauspe R. Bone healing and migration of cord blood—derived stem cells into a critical size femoral defect after xenotransplantation. *Journal of Bone and Mineral Research*. 2007;22:1224-33.

[136] Chan J, Kumar S, Fisk NM. First trimester embryo-fetoscopic and ultrasound-guided fetal blood sampling for ex vivo viral transduction of cultured human fetal mesenchymal stem cells. *Human reproduction*. 2008;23:2427-37.

[137] Zhang ZY, Teoh SH, Chong MS, Schantz JT, Fisk NM, Choolani MA, Chan J. Superior osteogenic capacity for bone tissue engineering of fetal compared with perinatal and adult mesenchymal stem cells. *Stem Cells*. 2009;27:126-37.

[138] Guillot PV, De Bari C, Dell'Accio F, Kurata H, Polak J, Fisk NM. Comparative osteogenic transcription profiling of various fetal and adult mesenchymal stem cell sources. *Differentiation*. 2008;76:946-57.

[139] Kuznetsov SA, Krebsbach PH, Satomura K, Kerr J, Riminucci M, Benayahu D, Robey PG. Single-colony derived strains of human marrow stromal fibroblasts form bone after transplantation in vivo. *Journal of Bone and Mineral Research*. 1997;12:1335-47.

[140] Yoshikawa T, Ohgushi H, Tamai S. Immediate bone forming capability of prefabricated osteogenic hydroxyapatite. *Journal of Biomedical Materials Research*. 1996;32:481-92.

[141] Yamagiwa H, Endo N, Tokunaga K, Hayami T, Hatano H, Takahashi HE. In vivo bone-forming capacity of human bone marrow-derived stromal cells is stimulated by recombinant human bone morphogenetic protein-2. *Journal of bone and mineral metabolism*. 2001;19:20-8.

[142] Kruyt M, De Bruijn J, Wilson C, Oner F, Van Blitterswijk C, Verbout A, Dhert W. Viable osteogenic cells are obligatory for tissue-engineered ectopic bone formation in goats. *Tissue Eng*. 2003;9:327-36.

[143] Yang X, Tare RS, Partridge KA, Roach HI, Clarke NM, Howdle SM, Shakesheff KM, Oreffo RO. Induction of human osteoprogenitor chemotaxis, proliferation, differentiation, and bone formation by osteoblast stimulating factor-1/pleiotrophin: Osteoconductive biomimetic scaffolds for tissue engineering. *Journal of Bone and Mineral Research*. 2003;18:47-57.

[144] Al-Khaldi A, Eliopoulos N, Martineau D, Lejeune L, Lachapelle K, Galipeau J. Postnatal bone marrow stromal cells elicit a potent VEGF-dependent neoangiogenic response in vivo. *Gene therapy*. 2003;10:621-9.

[145] Levin D, Norman D, Zinman C, Rubinstein L, Sabo E, Misselevich I, Reis D, Boss J. Treatment of experimental avascular necrosis of the femoral head with hyperbaric oxygen in rats: histological evaluation of the femoral heads during the early phase of the reparative process. *Experimental and molecular pathology*. 1999;67:99-108.

[146] Carano RA, Filvaroff EH. Angiogenesis and bone repair. *Drug discovery today*. 2003;8:980-9.

[147] Pelissier P, Villars F, Mathoulin-Pelissier S, Bareille R, Lafage-Proust M-H, Vilamitjana-Amedee J. Influences of vascularization and osteogenic cells on heterotopic bone formation within a madreporic ceramic in rats. *Plastic and Reconstructive Surgery*. 2003;111:1932-41.

[148] Alves RD, Demmers JA, Bezstarosti K, van der Eerden BC, Verhaar JA, Eijken M, van Leeuwen JP. Unraveling the human bone microenvironment beyond the classical extracellular matrix proteins: A human bone protein library. *Journal of proteome research*. 2011;10:4725-33.

[149] Brunner M, Jurdic P, Tuckerman JP, Block MR, Bouvard D. Chapter One - New Insights into Adhesion Signaling in Bone Formation. In: Kwang WJ, editor. International Review of Cell and Molecular Biology: Academic Press; 2013. p. 1-68.

[150] Pataquiva-Mateus A, Wu HC, Lucchesi C, Ferraz M, Monteiro F, Spector M. Supplementation of collagen scaffolds with SPARC to facilitate mineralization. *Journal of Biomedical Materials Research Part B: Applied Biomaterials*. 2012;100:862-70.

[151] Krebsbach PH, Kuznetsov SA, Satomura K, Emmons RV, Rowe DW, Robey PG. Bone formation in vivo: comparison of osteogenesis by transplanted mouse and human marrow stromal fibroblasts. *Transplantation*. 1997;63:1059-69.

[152] Mankani MH, Kuznetsov SA, Fowler B, Kingman A, Gehron Robey P. In vivo bone formation by human bone marrow stromal cells: Effect of carrier particle size and shape. *Biotechnology and bioengineering*. 2001;72:96-107.

[153] Muraglia A, Martin I, Cancedda R, Quarto R. A nude mouse model for human bone formation in unloaded conditions. *Bone*. 1998;22:131S-4S.

[154] Woodard JR, Hilldore AJ, Lan SK, Park C, Morgan AW, Eurell JAC, Clark SG, Wheeler MB, Jamison RD, Wagoner Johnson AJ. The mechanical properties and osteoconductivity of hydroxyapatite bone scaffolds with multi-scale porosity. *Biomaterials*. 2007;28:45-54.

[155] Le Nihouannen D, Daculsi G, Saffarzadeh A, Gauthier O, Delplace S, Pilet P, Layrolle P. Ectopic bone formation by microporous calcium phosphate ceramic particles in sheep muscles. *Bone*. 2005;36:1086-93.

[156] Boden SD, Zdeblick TA, Sandhu HS, Heim SE. The use of rhBMP-2 in interbody fusion cages: definitive evidence of osteoinduction in humans: a preliminary report. *Spine*. 2000;25:376-81.

[157] Levine JP, Bradley J, Turk AE, Ricci JL, Benedict JJ, Steiner G, Longaker MT, McCarthy JG. Bone morphogenetic protein promotes vascularization and osteoinduction in preformed hydroxyapatite in the rabbit. *Annals of plastic surgery*. 1997;39:158-68.

[158] Kirker-Head C, Karageorgiou V, Hofmann S, Fajardo R, Betz O, Merkle H, Hilbe M, Von Rechenberg B, McCool J, Abrahamsen L. BMP-silk composite matrices heal critically sized femoral defects. *Bone*. 2007;41:247-55.

[159] Peterson B, Zhang J, Iglesias R, Kabo M, Hedrick M, Benhaim P, Lieberman JR. Healing of critically sized femoral defects, using genetically modified mesenchymal stem cells from human adipose tissue. *Tissue Eng*. 2005;11:120-9.

[160] Yu H, VandeVord PJ, Gong W, Wu B, Song Z, Matthew HW, Wooley PH, Yang SY. Promotion of osteogenesis in tissue-engineered bone by pre-seeding endothelial progenitor cells-derived endothelial cells. *Journal of orthopaedic research*. 2008;26:1147-52.

[161] Kwak BR, Mach F. Paracrine action accounts for marked protection of ischemic heart by Akt-modified mesenchymal stem cells. *Nature medicine*. 2005;11:367.

[162] Schuleri K, Boyle A, Hare J. Mesenchymal stem cells for cardiac regenerative therapy. Bone marrow-derived progenitors: Springer; 2007. p. 195-218.

[163] Phinney DG. Biochemical heterogeneity of mesenchymal stem cell populations. *Cell Cycle*. 2007;6:2884-9.

[164] Kinnaird T, Stabile E, Burnett M, Lee C, Barr S, Fuchs S, Epstein S. Marrow-derived stromal cells express genes encoding a broad spectrum of arteriogenic cytokines and promote in vitro and in vivo arteriogenesis through paracrine mechanisms. *Circulation research*. 2004;94:678-85.

[165] Lim PN, Tay BY, Chan CM, Thian ES. Synthesis and characterization of silver/silicon-cosubstituted nanohydroxyapatite. *Journal of Biomedical Materials Research Part B: Applied Biomaterials*. 2012;100:285-91.

[166] Mullender M, El Haj AJ, Yang Y, van Duin MA, Burger EH, Klein-Nulend J. Mechanotransduction of bone cellsin vitro: Mechanobiology of bone tissue. *Medical and Biological Engineering and Computing*. 2004;42:14-21.